Geological Society of America
Special Paper 419
2007

Exhumation of the Orocopia Schist and associated rocks of southeastern California: Relative roles of erosion, synsubduction tectonic denudation, and middle Cenozoic extension

Carl E. Jacobson
Department of Geological and Atmospheric Sciences, Iowa State University, Ames, Iowa 50011-3212, USA

Marty Grove
Department of Earth and Space Sciences and Institute of Geophysics and Planetary Physics, University of California, Los Angeles, California 90095-1567, USA

Ana Vućić
Department of Earth and Space Sciences, University of California, Los Angeles, California 90095-1567, USA

Jane N. Pedrick
Department of Geological and Atmospheric Sciences, Iowa State University, Ames, Iowa 50011-3212, USA

Kristin A. Ebert
Department of Earth and Space Sciences, University of California, Los Angeles, California 90095-1567, USA

ABSTRACT

The Orocopia Schist of the Orocopia Mountains is part of the regionally extensive Pelona-Orocopia-Rand Schist terrane, which is generally interpreted as a relict subduction complex underplated beneath southern California and southwestern Arizona during the latest Cretaceous–early Cenozoic Laramide orogeny. The schist in the Orocopia Mountains forms the lower plate of the Orocopia Mountains detachment fault and has an exposed structural thickness of ~1.5 km. Prograde metamorphism occurred in the albite-epidote amphibolite facies, although the upper half of the section exhibits a strong greenschist-facies retrograde overprint. A mylonite zone just a few meters thick is present at the top of the schist. The upper plate of the Orocopia Mountains detachment fault is divided into one mappable unit consisting of Proterozoic gneiss widely intruded by 76 Ma leucogranite and a second unit dominated by anorthosite-syenite with minor amounts of leucogranite. Both the leucogranite-gneiss and anorthosite-syenite units are locally cut by faults that may be genetically related to the Orocopia Mountains detachment fault. None of the rocks in the upper plate exhibit evidence of ductile deformation related to movement on the detachment fault.

Jacobson, C.E., Grove, M., Vućić, A., Pedrick, J.N., and Ebert, K.A., 2007, Exhumation of the Orocopia Schist and associated rocks of southeastern California: Relative roles of erosion, synsubduction tectonic denudation, and middle Cenozoic extension, *in* Cloos, M., Carlson, W.D., Gilbert, M.C., Liou, J.G., and Sorensen, S.S., eds., Convergent Margin Terranes and Associated Regions: A Tribute to W.G. Ernst: Geological Society of America Special Paper 419, p. 1–37, doi: 10.1130/2007.2419(01).

$^{40}Ar/^{39}Ar$ analysis of the schist yielded total gas ages of 54–50 Ma for hornblende, 52–34 Ma for muscovite, 33–14 Ma for biotite, and 25–24 Ma for K-feldspar. A single apatite fission track sample yielded an age of 16 Ma. The above results, combined with multidiffusion domain (MDD) analysis of K-feldspar, indicate two major episodes of cooling: one beginning at ca. 52–50 Ma, the other starting at ca. 24–22 Ma. The early Cenozoic phase of cooling is attributed to subduction refrigeration combined with erosional and tectonic denudation. The greenschist-facies retrogression of the schist probably occurred at this time. The middle Cenozoic cooling event is thought to be the result of normal-sense slip on the Orocopia Mountains detachment fault. The thin mylonite at the top of the schist probably formed in association with this structure. The early and middle Cenozoic events each appear to have contributed substantially to the 30–35 km of total exhumation required to bring the schist from its maximum depth of underthrusting to the surface.

Most $^{40}Ar/^{39}Ar$ ages from the upper plate fall into the following ranges: 76–69 Ma for hornblende, 75–56 Ma for biotite, and 78–42 Ma for K-feldspar. One apatite fission track age of 27 Ma was obtained from the anorthosite-syenite unit. MDD thermal histories for K-feldspar vary significantly with structural position, implying the presence of at least one major structural break within the upper plate. The distinctly old ages for the upper plate compared to the schist indicate that the former was exhumed to relatively shallow crustal levels by latest Cretaceous to early Cenozoic time. The upper plate was juxtaposed against the schist in the earliest Miocene by slip on the Orocopia Mountains detachment fault.

The two-stage cooling and exhumation history for the Orocopia Schist in the Orocopia Mountains is virtually identical to that inferred recently for the Gavilan Hills to the southeast based upon a similar thermochronologic analysis. Combined with preliminary investigations of several additional bodies of schist exposed along the Chocolate Mountains anticlinorium of southeastern California and southwestern Arizona, these data provide strong evidence for a major middle Cenozoic extensional event throughout the region. The inferred middle Cenozoic extensional faults are folded by the Chocolate Mountains anticlinorium. This contradicts a recent model for erosional unroofing of the Orocopia Schist, which predicts that the Chocolate Mountains anticlinorium developed primarily during the early Cenozoic.

Keywords: Pelona Schist, Rand Schist, argon, detachment fault, core complex.

INTRODUCTION

The Pelona, Orocopia, and Rand Schists and the schists of Portal Ridge and Sierra de Salinas (Fig. 1; to be referred to collectively as "the schist") have long been considered a key element of the Late Cretaceous to Cenozoic tectonic evolution of the southwesternmost United States and adjacent Sonora, Mexico (Grove et al., 2003, and references cited therein). These rocks have attracted attention because they comprise a relatively high-pressure eugeoclinal assemblage located well inboard of the continental margin. Although some disagreement persists (Barth and Schneiderman, 1996; Haxel et al., 2002), most workers interpret the schist as a broad correlative of the Franciscan Complex that was thrust beneath North American continental crust (the "upper plate") during low-angle, east-dipping subduction related to the Laramide orogeny (Yeats, 1968; Crowell, 1968, 1981; Burchfiel and Davis, 1981; Dickinson, 1981; May, 1986; Hamilton, 1987, 1988; Jacobson et al., 1988, 1996, 2002; Livaccari and Perry, 1993; Malin et al., 1995; Wood and Saleeby, 1997; Miller et al., 2000; Yin, 2002; Saleeby, 2003; Saleeby et al., 2007, this volume). Less certain, however, are the timing and nature of the processes involved in the exhumation of the schist. Elucidating the denudation history of the schist is critical to explaining many aspects of the geology of southern California and southwestern Arizona and can also shed light on more general debates regarding the mechanisms by which high-pressure rocks are brought to the surface (Cloos, 1982; Platt, 1986; Cloos and Shreve, 1988; Ring et al., 1999; Sedlock, 1999; Rubatto and Hermann, 2001; Yin, 2002).

As summarized by Ring et al. (1999), exhumation can occur by three processes: normal faulting, ductile thinning, and erosion. Until recently, most workers emphasized normal faulting as the primary mechanism for unroofing of the schist. This point of view grew out of the observation that the schist is typically separated from overlying North American basement by a series of retrograde to postmetamorphic low-angle faults exhibiting structural excision (Frost et al., 1981, 1982; Haxel et al., 1985, 2002;

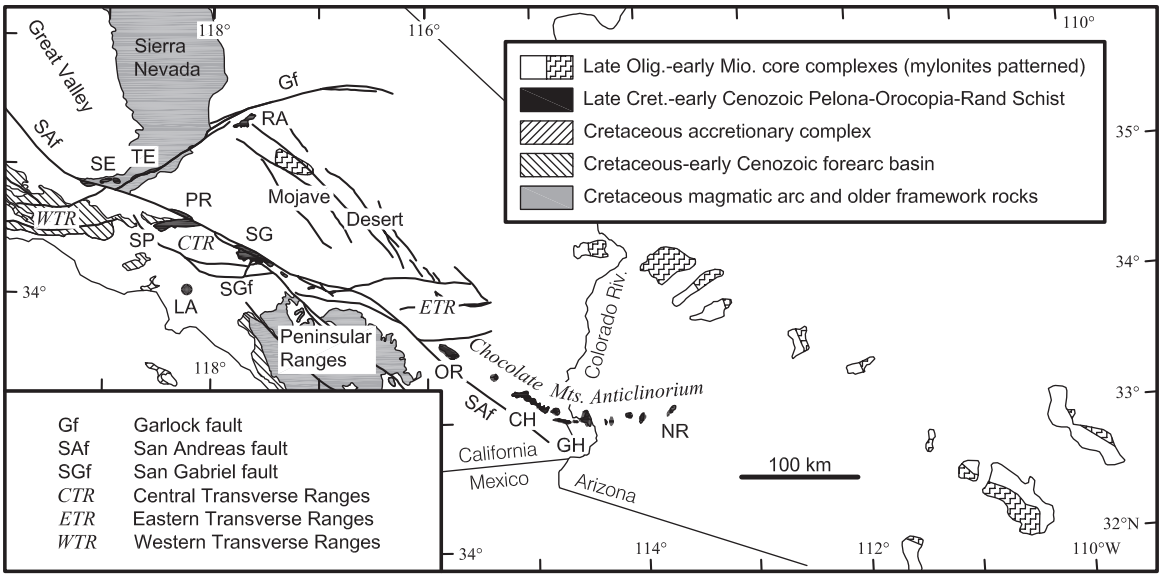

Figure 1. Distribution of the Pelona-Orocopia-Rand Schist and related rocks. Magmatic arc rocks of the Mojave Desert and southwestern Arizona omitted for clarity. Individual schist bodies referenced in text: CH—Chocolate Mountains; GH—Gavilan Hills; NR—Neversweat Ridge; OR—Orocopia Mountains; PR—Portal Ridge; RA—Rand Mountains; SE—San Emigdio Mountains; SG—San Gabriel Mountains; SP—Sierra Pelona; TE—Tehachapi Mountains. Additional schist bodies are present in the Gabilan Range and Sierra de Salinas of the Salinian terrane northwest of the map area. Modified from Jennings (1977), Dickinson (1991), and Glazner et al. (2002).

Silver and Nourse, 1986; Postlethwaite and Jacobson, 1987; Jacobson et al., 1988, 1996, 2002; Simpson, 1990; Malin et al., 1995; Oyarzabal et al., 1997; Wood and Saleeby, 1997; Saleeby et al., this volume). Some workers have argued that these faults are largely middle Cenozoic in age (Fig. 2A) (Frost et al., 1982, 1989; Hamilton, 1987, 1988; Bishop and Ehlig, 1990; Hendrix, 1993) and are temporally and genetically related to the detachment faults and core complexes distributed through much of the Cordillera (cf. Davis and Coney, 1979; Davis et al., 1986; Spencer and Reynolds, 1990, 1991; Dickinson, 1991). This interpretation has been put forth most widely for the bodies of Orocopia Schist exposed along the Chocolate Mountains anticlinorium, a regional structural high extending from the Orocopia Mountains in southeastern California to Neversweat Ridge at the southern end of the Tank Mountains in southwestern Arizona (Fig. 1). Other workers, however, have postulated that middle Cenozoic extension in the vicinity of the Chocolate Mountains anticlinorium was relatively modest (Sherrod and Tosdal, 1991; Spencer et al., 1995). In this context, it is important to note that most of the Chocolate Mountains anticlinorium is located over 100 km southwest of the well-known belt of extreme middle Cenozoic extension that runs from eastern California to south-central Arizona, and thence into Mexico (Fig. 1). Thus, if the schist exposures formed at the same time and by similar processes as the "classic" core complexes, then the extent of large-scale extension in the southwestern Cordillera is even greater than previously suspected.

An alternative view of the retrograde, low-angle faults atop the schist, and the one that we have favored, is that they are

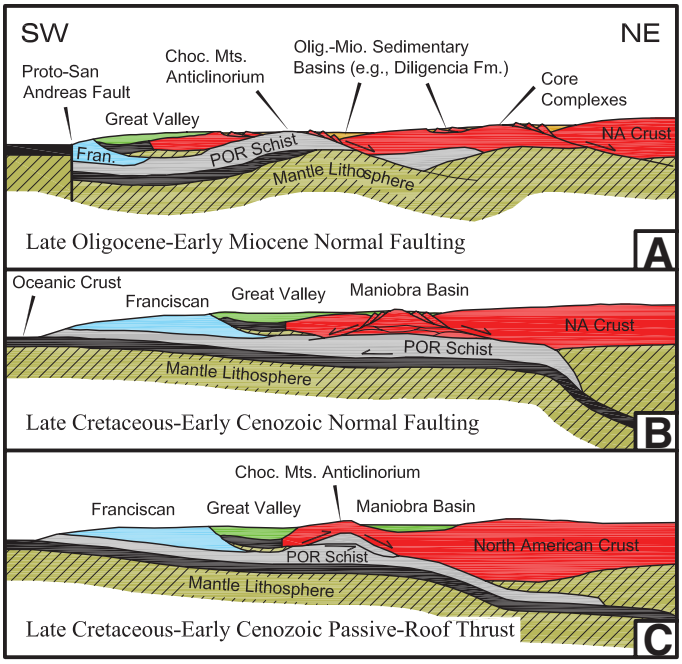

Figure 2. Models for the exhumation of the Pelona-Orocopia-Rand (POR) Schist. See text for explanation.

Late Cretaceous–early Cenozoic structures related to exhumation immediately following underthrusting and metamorphism (Fig. 2B) (May, 1986; Postlethwaite and Jacobson, 1987; Jacobson et al., 1988, 1996; Jacobson, 1990; Richard and Haxel, 1991; Malin et al., 1995; Oyarzabal et al., 1997; Wood and Saleeby, 1997; Saleeby, 2003; Saleeby et al., this volume). To a certain degree, this interpretation is motivated by analogy to models for the exhumation of the Franciscan Complex synchronous with subduction (Cloos, 1982; Platt, 1986; Jayko et al., 1987; Cloos and Shreve, 1988). More directly, it has been justified based upon K-Ar and $^{40}Ar/^{39}Ar$ thermochronologic studies that indicate significant cooling of the schist and upper plate in Late Cretaceous–early Cenozoic time (Evernden and Kistler, 1970; Armstrong and Suppe, 1973; Ehlig, 1981; Miller and Morton, 1980; Hoisch et al., 1988; Reynolds et al., 1988; Jacobson, 1990). In fact, Late Cretaceous–early Cenozoic ages have been obtained locally within the upper plate even for very low-temperature systems such as fission tracks and (U-Th)/He in apatite (Mahaffie and Dokka, 1986; Spotila et al., 1998; Blythe et al., 2000, 2002; Saleeby et al., this volume). These results have been used to infer that the schist was already at shallow crustal levels long before the initiation of middle Cenozoic extension.

Although the time of exhumation of the schist has long been a matter of controversy, it is only recently that the dominance of normal faulting has been questioned (Yin, 2002). Based on the thermochronologic data described above, Yin (2002) agreed that much of the unroofing of the schist occurred in Late Cretaceous–early Cenozoic time. However, he argued that the retrograde mylonitic contact between schist and upper plate, rather than being a normal fault, is a passive-roof thrust capping a duplex structure within the subduction zone (Fig. 2C). According to this model, the Chocolate Mountains anticlinorium, which most workers have assumed to be middle to late Cenozoic in age (Frost and Martin, 1983; Richard, 1989; Sherrod and Tosdal, 1991), is an early Cenozoic fault-bend fold above a ramp in the floor thrust of the duplex. The implication is that exhumation of the schist was driven predominantly by erosion of the topographic high defined by the anticlinorium.

Part of the problem in choosing between the above models is that past thermochronologic studies of the schist have been largely reconnaissance in nature. However, recent detailed analysis in the Gavilan Hills of southeasternmost California (Fig. 1) provides important new insight on this debate (Jacobson et al., 2002). In the Gavilan Hills, the Orocopia Schist is overlain along the retrograde, mylonitic Chocolate Mountains fault by a sheet of gneiss with maximum thickness of ~120 m (Haxel, 1977; Drobeck et al., 1986; Dillon et al., 1990; Simpson, 1990; Oyarzabal et al., 1997; Jacobson et al., 2002). The gneiss, in turn, is overlain along the low-angle Gatuna fault by low-grade metasedimentary and metavolcanic rocks of the Jurassic(?) Winterhaven Formation. $^{40}Ar/^{39}Ar$ thermal history results from the schist and gneiss reveal two distinct phases of cooling, one in the early Cenozoic, the other in the middle Cenozoic, indicating that exhumation is the result of multiple processes (Jacobson et al., 2002). The younger episode of cooling is attributed to slip on the Gatuna fault and demonstrates without doubt that this region *was* strongly affected by middle Cenozoic extension. On the other hand, the earlier phase of cooling implies that a significant amount of denudation also occurred simultaneously with low-angle subduction. Aspects of the data to be described below further suggest that at least some of the early cooling can be explained by normal-sense slip on the Chocolate Mountains fault. However, it is difficult to know how much of the early Cenozoic denudation was driven by this mechanism, as opposed to by erosion.

In this study, we extend our approach of the Gavilan Hills to investigate the exhumation history of the Orocopia Schist and upper plate in the Orocopia Mountains, which lie northeast of the San Andreas fault along the southern margin of the eastern Transverse Ranges (Figs. 1 and 3). This area is of interest for several reasons:

1. Preliminary $^{40}Ar/^{39}Ar$ analyses from more than a dozen schist bodies imply substantial variations in cooling history across the terrane (Jacobson, 1990; Grove et al., 2003); i.e., the detailed results from the Gavilan Hills may or may not be relevant to other areas.

2. The nature of the contact between schist and upper plate in the Orocopia Mountains has long been a matter of debate. This structure was originally interpreted as a thrust fault ("Orocopia thrust") along which the schist underwent tectonic burial and prograde metamorphism (Crowell and Walker, 1962), analogous to the Vincent thrust of the San Gabriel Mountains (Ehlig, 1958, 1981; Jacobson, 1983a, 1983b, 1997). However, Crowell and Walker (1962) and Crowell (1975) noted extensive brittle deformation within the upper plate, which led Crowell (1975) to suggest some reactivation of the thrust at shallow structural levels. Similar observations of cataclasis and hydrothermal alteration within the upper plate, as well as the recognition of retrograde mylonite at the top of the schist, prompted Jacobson et al. (1987, 1988, 1996) and Jacobson and Dawson (1995) to conclude that the present contact is largely an extensional fault. Based on the early Cenozoic cooling ages cited above (e.g., Jacobson, 1990), they suggested that most of the excision of the primary thrust took place during early Cenozoic exhumation, although they acknowledged that secondary movement could have occurred during the middle Cenozoic. In contrast, Goodmacher et al. (1989) and Robinson and Frost (1989, 1991) concluded that exhumation of the schist occurred primarily in middle Cenozoic time. They invoked movement along a system of anastomosing faults ("Orocopia Mountains detachment system"), including the contact between the schist and upper plate ("Orocopia Mountains detachment fault") and the Clemens Well fault to the northeast (Fig. 3). Subsequently, Robinson and Frost (1996) revised this view to take into account the evidence for early Cenozoic cooling of the schist (Jacobson, 1990). In this latter work, they interpreted the Orocopia Mountains detachment fault as an Eocene normal fault, with middle Cenozoic extension attributed principally to slip on the Clemens Well fault. Clearly, more work is needed to discriminate among these very different interpretations.

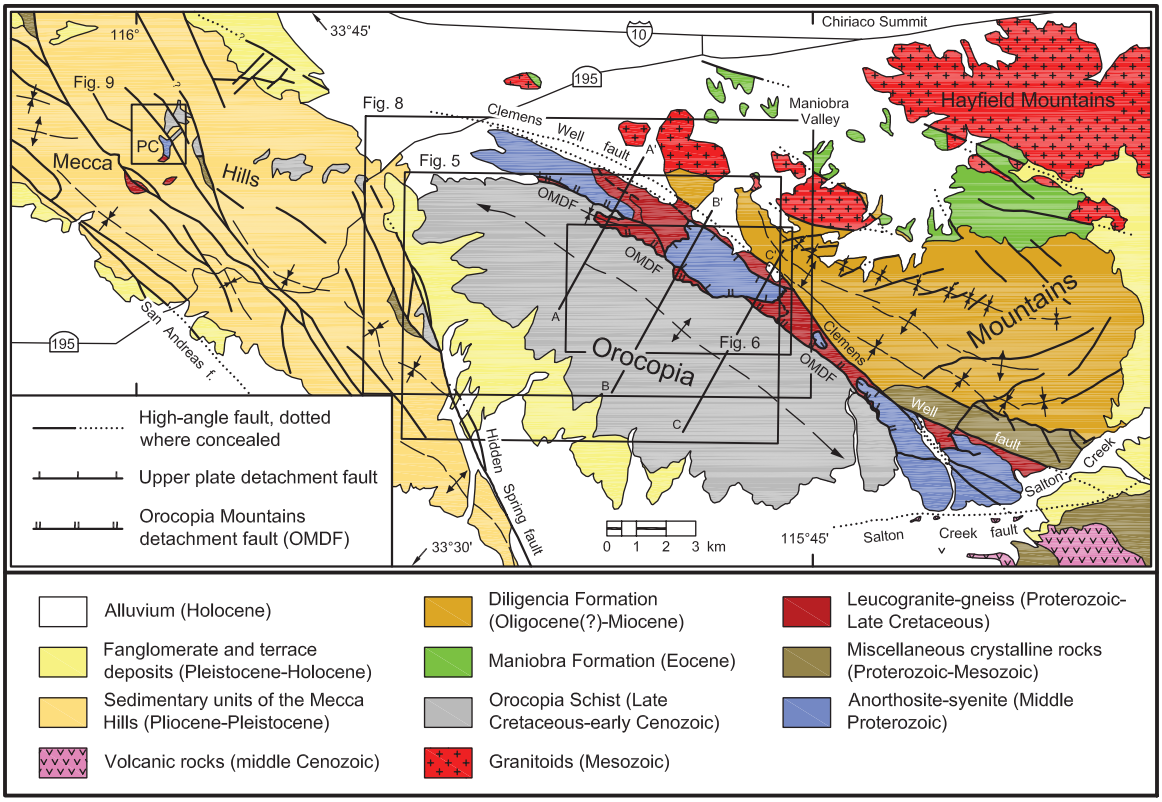

Figure 3. Geology of the Orocopia Mountains and vicinity (after Crowell, 1975). Contacts within the northwestern half of the upper plate of the Orocopia Mountains detachment fault were modified based on this study. Those in the southeastern half were modified based on the work of Ebert (2004). Lines A–A′ to C–C′ indicate locations of cross sections illustrated in Figure 4. PC—Painted Canyon.

3. The Orocopia Mountains detachment fault is folded by the Chocolate Mountains anticlinorium. Consequently, dating the fault provides a maximum age for the anticlinorium, which has implications for the passive-roof thrust model of Yin (2002).

To investigate the above issues, we performed $^{40}Ar/^{39}Ar$ step-heating experiments with hornblende, muscovite, biotite, and K-feldspar to constrain the temperature-time histories for both the schist and upper plate in the Orocopia Mountains. Additional control is provided by several apatite fission track ages, ion microprobe U-Pb dating of zircon from a Late Cretaceous leucogranite within the upper plate, and previous U-Pb dating of detrital zircon from the schist (Jacobson et al., 2000; Grove et al., 2003). The thermochronologic results were integrated with preexisting and new observations on the structural and metamorphic evolution of the schist and upper plate. As detailed below, these data reveal a two-stage exhumation history for the schist in the Orocopia Mountains very much like that found in the Gavilan Hills.

The present study concentrated on the western to northwestern part of the Orocopia Mountains (Fig. 3). A similar investigation has recently been conducted by Ebert et al. (2003), Ebert (2004), and Ebert and Yin (2004) in the southeastern part of the range. Our work focused more heavily on the contact between the schist and upper plate (Orocopia Mountains detachment fault) and placed a greater emphasis on relating thermochronologic results to fabric elements within the schist. In contrast, Ebert et al. (2003), Ebert (2004), and Ebert and Yin (2004) focused on detailed mapping within the upper plate and analysis of the Clemens Well fault.

Whereas the vast majority of the new data obtained in this study come from the Orocopia Mountains, we also report $^{40}Ar/^{39}Ar$ step-heating results for three new samples of K-feldspar from the Orocopia Schist of the Gavilan Hills. These new data were collected to facilitate comparisons of thermal history between the two regions.

REGIONAL BACKGROUND

The Orocopia Schist of the Orocopia Mountains is exposed in a northwest-trending, postmetamorphic antiform that defines the northernmost culmination of the Chocolate Mountains anticlinorium (Figs. 3 and 4). Proterozoic to Cretaceous igneous and metamorphic rocks of the upper plate crop out in a narrow belt that sits above the schist along the Orocopia Mountains detachment fault. The structure, metamorphism, and thermochronology of the schist and upper plate are described in detail below.

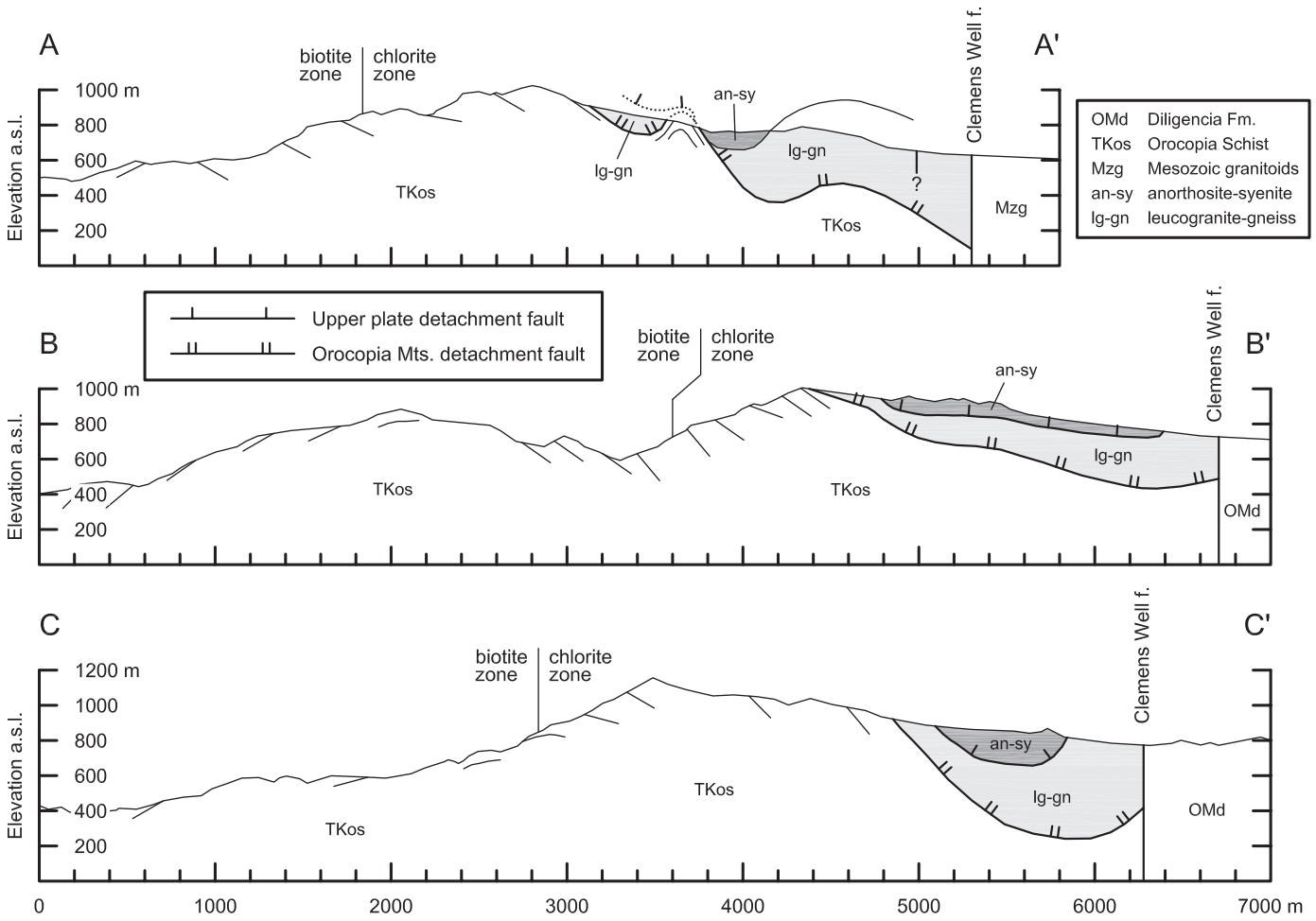

Figure 4. Cross sections through the western Orocopia Mountains (see Fig. 3 for locations of the section lines). Form lines in the Orocopia Schist are based on field measurements of the attitude of foliation. In cross section A–A′, the lines above the present level of the ground surface at a distance of ~3.5 km from the left edge of the figure represent the inferred locations of the Orocopia Mountains detachment fault and upper plate detachment fault. The surface trace of the boundary between the biotite and chlorite zones is indicated in each section.

The Orocopia Schist and upper plate are bounded to the northeast by the brittle, steeply dipping Clemens Well fault. Crystalline rocks are exposed directly northeast of the Clemens Well fault (Fig. 3), but differ from those to the southwest in terms of both lithology (Crowell and Walker, 1962; Ebert, 2004) and cooling history (Ebert, 2004). In the northwestern part of the range, Crowell (1962, 1975) and Crowell and Walker (1962) mapped two branches of the Clemens Well fault. Only the northeastern branch is a major lithologic break (Figs. 3 and 4). As described in more detail below, we infer that the southwestern branch formed by reactivation of a low-angle fault within the upper plate. The Clemens Well fault has been interpreted as a branch of the San Andreas system (Crowell, 1962, 1975; Powell, 1981, 1993) or as a major middle Cenozoic detachment fault with top-east displacement (Goodmacher et al., 1989; Robinson and Frost, 1989, 1991, 1996).

Whereas the western half of the Orocopia Mountains is underlain primarily by crystalline rock, the eastern part of the range is dominated by two Cenozoic sedimentary units (Fig. 3). The older of these is the lower Eocene marine Maniobra Formation (Crowell and Susuki, 1959; Crowell, 1975; Advocate et al., 1988). The Maniobra Formation, which is depositional upon Mesozoic granitoids, defines the easternmost limit of an extensive marine incursion into southern California during Late Cretaceous and early Cenozoic time (Grove, 1993). The younger unit is the latest Oligocene(?) to early Miocene nonmarine Diligencia Formation, which locally includes basaltic volcanic rocks (Crowell, 1975; Spittler and Arthur, 1982; Squires and Advocate, 1982; Law et al., 2001; Ebert, 2004). The Diligencia Formation is commonly thought to record an important phase of middle Cenozoic extension, but the exact relation of sedimentation to currently exposed faults, such as the Orocopia Mountains detachment fault or Clemens Well fault, is unclear. Neither the Maniobra nor the Diligencia Formation contains detritus of Orocopia Schist.

The Orocopia Mountains are flanked to the west and northwest by Pliocene-Pleistocene nonmarine sedimentary rocks of the Mecca Hills, which are exposed in a transpressional uplift

located immediately northeast of the San Andreas fault (Crowell, 1975; Sylvester and Smith, 1975, 1976). Orocopia Schist and upper-plate rocks crop out in the floors of several canyons incised into the sedimentary units (Fig. 3). These exposures are significant, because they are located on the southwest limb of the main antiform of Orocopia Schist, and thus have the potential to place constraints on the geometry of the Orocopia Mountains detachment fault. Note, however, that the present contact between the upper plate and Orocopia Schist in this area is a strand of the San Andreas fault (Ehlig and Crowell, 1975; Sylvester and Smith, 1976). Despite this complexity, thermochronology was conducted on several samples from the inlier of schist and upper plate within Painted Canyon (denoted "PC" in Fig. 3).

A major ambiguity in interpreting the geology of the Orocopia Mountains stems from the fact that the eastern Transverse Ranges may have undergone significant clockwise vertical-axis rotation related to transform motion on the San Andreas system (Luyendyk et al., 1985; Carter et al., 1987; Dickinson, 1996). The two paleomagnetic sites nearest to the schist and upper plate, within the Diligencia Formation, have yielded apparent clockwise rotations of 107° ± 9° and 164° ± 11° (Carter et al., 1987). These values are substantially higher than the ~40° apparent rotations typical of most of the eastern Transverse Ranges and have been attributed to local deformation along the Clemens Well fault (Carter et al., 1987). No paleomagnetic data are available for the fault-bounded block that includes the Orocopia Schist and upper plate. Correcting present-day structural orientations in the western Orocopia Mountains to pre-Neogene trends is thus problematic.

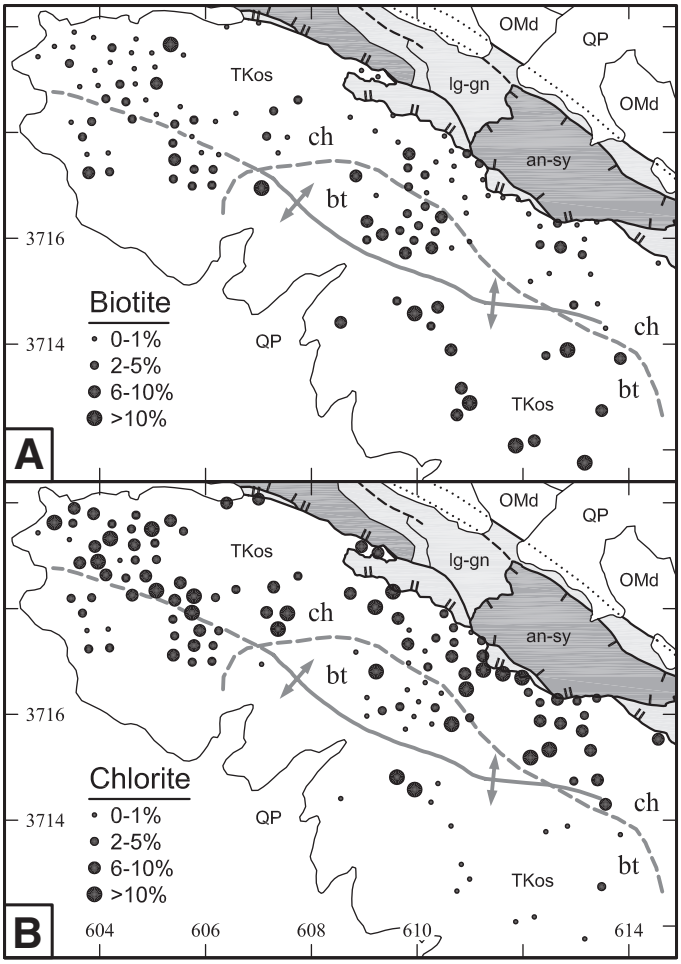

Figure 5. Abundances of biotite and chlorite in metagraywacke from the Orocopia Schist estimated visually from thin sections. The relatively few samples with K-feldspar were excluded, as these involve a different reaction path than those without K-feldspar (Ernst, 1963). Heavy gray lines indicate boundary between biotite (bt) and chlorite (ch) zones and hinge line of postmetamorphic domal structure of schist. Unit abbreviations as in Figure 4, with the addition that "QP" indicates sedimentary deposits of Pliocene to Holocene age. See Figure 3 for location. Two-kilometer UTM grid ticks shown.

STRUCTURE AND METAMORPHISM

Orocopia Schist

The schist of the Orocopia Mountains exhibits a complex structural and metamorphic history reflecting the combined processes of underthrusting and exhumation (Raleigh, 1958; Crowell, 1975; Dawson, 1987; Jacobson et al., 1987, 1988, 1996; Robinson and Frost, 1989, 1996; Jacobson and Dawson, 1995). By far, the most abundant rock type is metagraywacke. Metabasite, the second most abundant unit, constitutes no more than ~1% of the section and occurs mostly as a series of meter-scale bands that can be traced along the length of the range within the upper part of the section. Metachert, marble, and serpentinite are rare but distinctive lithologies typically associated with the metabasite.

Mineral assemblages within the metagraywacke provide evidence for an important petrologic boundary. Deep in the structural section, the metagraywacke exhibits prograde mineral assemblages of albite-epidote amphibolite facies, with relatively little evidence of retrograde overprinting (Jacobson and Dawson, 1995). The dominant minerals are quartz, albite, muscovite, and biotite. Lesser prograde phases are epidote, garnet, calcite, calcic amphibole, and microcline. Retrograde chlorite after biotite and/or garnet is widespread but generally not abundant. We refer to this lower part of the section as the "biotite zone" (Figs. 4 and 5). In contrast, metagraywacke within approximately the upper half of the exposed section shows extensive retrograde replacement of biotite and garnet by chlorite ("chlorite zone"; Figs. 4 and 5). Ignoring the relatively minor amount of garnet, this mineralogic transformation is attributed to the reaction phengite-poor muscovite + biotite + quartz + $H_2O \Leftrightarrow$ phengite-rich muscovite + chlorite (Ernst, 1963; see also Jacobson et al., 2002).

A retrograde origin for the chlorite zone is confirmed by electron microprobe analyses of calcic amphibole from metabasite (Fig. 6; data from Jacobson and Dawson, 1995). All samples are from the upper part of the section, reflecting the limited distribution of this rock type. Amphibole cores are relatively aluminous (hornblende to tschermakitic hornblende), with rims high in Si

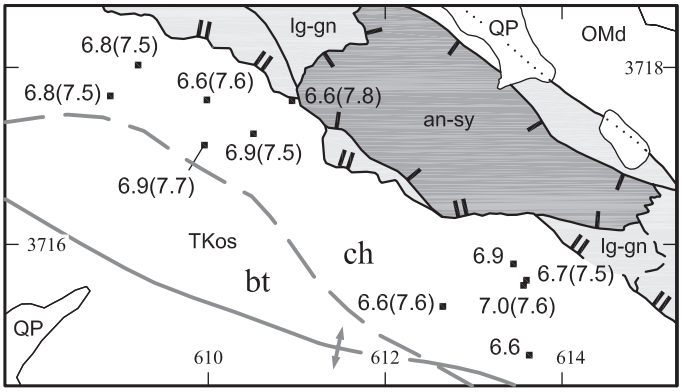

Figure 6. Silicon contents of amphibole (per 23 oxygen atoms) in mafic Orocopia Schist. First number indicates average core composition. Second number (in parentheses) indicates average Si content of actinolitic rims wide enough to be analyzed. Unit abbreviations and other symbols as in Figures 4 and 5. See Figure 3 for location. Two-kilometer UTM grid ticks shown.

(actinolite). Elsewhere in the schist terrane, aluminous amphibole is characteristic of the albite-epidote amphibolite facies or higher grades of metamorphism (Jacobson, 1995). Thus, the presence of relict hornblende in this area requires that metamorphic grade in the upper part of the section was originally significantly higher than indicated by the chlorite-rich (greenschist-facies) assemblages now found in the metagraywacke. Widespread metastable persistence of hornblende during greenschist-facies retrogression is compatible with observations from other bodies of schist and upper plate (Jacobson, 1997; Jacobson et al., 2002). Development of the actinolite rims on hornblende was presumably coeval with the growth of chlorite in the metagraywacke. A retrograde origin for the chlorite zone is also consistent with the observation that prograde metamorphism of the Pelona-Orocopia-Rand Schist typically produced relatively high-temperature assemblages in the upper part of the structural section (i.e., inverted metamorphic zonation; Ehlig, 1958, 1981; Graham and England, 1976; Jacobson, 1983a, 1995; Graham and Powell, 1984; Peacock, 1988), opposite to the case here.

Despite the strong retrogression in the upper half of the section, textures from this region are overwhelmingly crystalloblastic rather than mylonitic; i.e., rocks of the chlorite zone do not generally exhibit significant grain-size reduction or development of porphyroclasts. The exception to this is the presence of a mylonitic to ultramylonitic fabric within the uppermost several meters of schist. Microfabrics within the mylonite indicate dominantly top-northeast to top-east sense of shear (Simpson, 1986; Robinson and Frost, 1989, 1996; Jacobson and Dawson, 1995; Ebert, 2004).

Folds in the Orocopia Schist have been grouped into two generations (Jacobson and Dawson, 1995). Earlier folds are potentially related to underthrusting, whereas younger structures have been attributed to exhumation. Folds in both sets range from open to isoclinal. The earlier fold axes trend northeast-southwest, whereas the younger ones are oriented northwest-southeast to north-south. The earlier folds display no consistent sense of vergence. The younger ones verge consistently northeast to east.

Upper Plate

The oldest unit within the upper plate is quartzofeldspathic to mafic gneiss (Crowell and Walker, 1962; see the GSA Data Repository[1] for more detailed descriptions of rock units in the upper plate). The gneiss is intruded by a suite of plutonic rocks including gabbro, anorthosite, syenite, and various intermediate compositions. The anorthosite-syenite suite is correlated with rocks in the San Gabriel Mountains (Crowell and Walker, 1962; Carter, 1980, 1987) having an intrusive age of 1190 Ma (Silver et al., 1963; Barth et al., 1995). Gneiss adjacent to the anorthosite-syenite intrusion underwent contact metamorphism to granulite facies but was later retrogressed to amphibolite facies. Quartz within the retrogressed granulite gneiss is commonly blue to violet. Both the anorthosite-syenite suite and the retrogressed granulite gneiss are characterized by hairline mesoperthite. Felsic end members of both units locally include K-feldspar as a separate phase in addition to that present as lamellae in the mesoperthite. The youngest unit in the upper plate is a leucogranite (alaskite of Crowell and Walker, 1962) of Late Cretaceous age (ca. 76 Ma; below) that occurs as dikes to small stocks. It is much more abundant in the gneiss than in the anorthosite-syenite.

Anorthosite-syenite and gneiss are locally intermingled, presumably reflecting an original intrusive relation. At the map scale, however, there is a clear distinction between areas dominated by gneiss and those composed largely of anorthosite-syenite. To some degree, this could reflect a relatively sharp initial boundary to the anorthosite-syenite pluton. However, it is also clear that the primary contact between anorthosite-syenite and gneiss has been modified by several episodes of faulting, which could have excised a broader zone of transition between the two. Some of the faulting is brittle and probably related to the Orocopia Mountains detachment fault or younger events. However, other contacts between anorthosite-syenite and gneiss are ductile shear zones marked by strong foliations parallel to the contact in both units. The latter style of contact is locally intruded by the leucogranite.

Crowell and Walker (1962) and Crowell (1975) mapped the gneiss and leucogranite as separate units. However, these rock types are so intimately associated that we have combined them as a single map unit (leucogranite-gneiss of Fig. 3 and subsequent figures). Leucogranite also intrudes the anorthosite-syenite, but generally not in abundance. One exception occurs in the area directly above Orocopia Schist adjacent to cross section line B–B′ on Figure 3. Here, the sliver mapped as leucogranite-gneiss is composed of subequal leucogranite and anorthosite-syenite. In general, leucogranite dikes in the anorthosite-syenite are most

[1]GSA Data Repository item 2007066, Rock descriptions, sample lists, and ion microprobe and $^{40}Ar/^{39}Ar$ step-heating results, is available on the Web at http://www.geosociety.org/pubs/ft2007.htm. Requests may also be sent to editing@geosociety.org.

abundant adjacent to contacts with the leucogranite-gneiss and scarce to absent within the interior of the unit. In some cases, the marginal zone of leucogranite-bearing anorthosite-syenite appears to have been faulted out, and anorthosite-syenite devoid of dikes is in direct contact with leucogranite-gneiss.

Both the leucogranite-gneiss and anorthosite-syenite are locally in contact with the Orocopia Schist along the Orocopia Mountains detachment fault. Nowhere do any of the upper-plate units exhibit a ductile fabric related to this contact. To the contrary, rocks at the base of the upper plate typically are highly fractured and display pervasive signs of low-temperature alteration, such as the replacement of feldspar by clay minerals. It is these features that led previous workers to view this contact as an exhumation structure (Jacobson et al., 1987, 1988, 1996; Goodmacher et al., 1989; Robinson and Frost, 1989, 1991, 1996; Jacobson and Dawson, 1995).

Our interpretation of structural relations within the upper plate is illustrated in the cross sections of Figure 4. These sections are highly interpretive, owing to uncertainties in mapping that result from the inherent complexity of the contacts, rugged topography, extensive debris cover, and strong desert varnish. Nonetheless, the sections illustrate that anorthosite-syenite tends to sit above leucogranite-gneiss. This is in part a primary intrusive relation and in part a low-angle fault contact, which we refer to as the "upper plate detachment fault." This fault was noted locally by Crowell and Walker (1962) and Crowell (1975), but we have also mapped it in places where they considered the contact to be intrusive. Related to this is our interpretation of the fault along the northeast side of the anorthosite-syenite body crossed by section lines B–B′ and C–C′ (Fig. 3). Crowell and Walker (1962) and Crowell (1975) considered this structure to be a branch of the Clemens Well fault. Although the fault is generally steeply dipping, we believe the present orientation to be the result of deformation of the low-angle upper plate detachment fault. The latter fault is exceptionally well exposed along the northwest end of the anorthosite-syenite body. There, the anorthosite-syenite clearly sits above the leucogranite-gneiss along a subhorizontal zone of gouge, a relationship noted by Crowell and Walker (1962) and Crowell (1975). This same distinctive structure can be traced along the southwest side of the anorthosite-syenite, where it dips moderately to steeply northeastward. We have not been able to clearly delineate the fault along the southeast margin of the anorthosite-syenite body. However, we have recognized a "pseudostratigraphy" within the anorthosite-syenite defined by a zone of leucogranite dikes that can be traced continuously around the southeast nose to the northeast side of the body. These relations taken together imply that the anorthosite-syenite occurs as a flat sheet exposed in the core of a synform (Fig. 4).

We suggest that broadly similar contact relations between the anorthosite-syenite and leucogranite-gneiss are also present along section line A–A′, although there the contact along the northeast side of the anorthosite-syenite may be intrusive (Figs. 3 and 4). Also distinctive in this area is the thin synformal keel of leucogranite-gneiss that projects northwestward on top of the Orocopia Schist. This feature, mapped by Crowell and Walker (1962) and Crowell (1975), demonstrates unequivocal folding of the Orocopia Mountains detachment fault, consistent with our view that the entire upper plate is folded. A synformal structure for the upper plate has also been mapped by Ebert (2004) and Ebert and Yin (2004) immediately southeast of the area covered here.

Few asymmetric fabrics were observed in the gouge along either the upper plate detachment fault or the Orocopia Mountains detachment fault. Furthermore, where present, they provide only qualitative information about transport direction, as slickenlines are not well developed. The limited data are consistent with slip of the upper plate broadly to the east or northeast.

Based on our field studies and the observations of Ebert (2004) and Ebert and Yin (2004) to the southeast, we suspect that the part of the upper plate investigated here may include important low-angle, brittle faults in addition to the upper plate detachment fault. Results of the thermochronologic analysis presented below appear to support this view. However, because of the difficulties of mapping already described, the details remain obscure.

LEUCOGRANITE U-Pb ZIRCON CRYSTALLIZATION AGE

The leucogranite is considered to be part of a belt of Laramide-age peraluminous intrusives in southeastern California and southern Arizona (Keith and Wilt, 1986). Keith and Wilt (1986) postulated that such plutons were derived by melting of underplated Orocopia Schist. Alternatively, these bodies could represent a mix of mantle and crustal melts emplaced above the zone of penetration of the Farallon plate into the asthenosphere (Coney and Reynolds, 1977; Dickinson and Snyder, 1978). In the latter scenario, underthrusting of the schist would have occurred later, after the Farallon plate had attained an even shallower angle of descent. In any case, the Orocopia Schist of the Orocopia Mountains shows modest peak temperature of metamorphism and no evidence of partial melting. Thus, whatever the regional significance of the peraluminous intrusives, the age of the leucogranite in the Orocopia Mountains provides a maximum bound for both underthrusting and exhumation of the schist in this area.

We analyzed a total of 88 zircon grains from eight individual samples of leucogranite (Fig. 7; see Appendix 1 for a description of the ion microprobe analysis protocol employed). Ages range from 1.78 Ga to 70 Ma, indicating significant inheritance. Detailed interpretation is hindered by the difficulty of testing for concordance owing to the low precision of the $^{207}Pb/^{235}U$ ages. Nonetheless, a large proportion of the $^{206}Pb/^{238}U$ ages fall in the range 80–70 Ma (Fig. 7), which we take to bracket the time of crystallization. The weighted mean for this group of results is 76.3 ± 0.6 Ma. This is comparable to a conventional U-Pb zircon age of 79 Ma obtained for a similar leucogranite in the Chocolate Mountains (Robinson and Frost, 1996, p. 282; E.G. Frost, 2005, personal commun.). The large number of Jurassic and Middle to

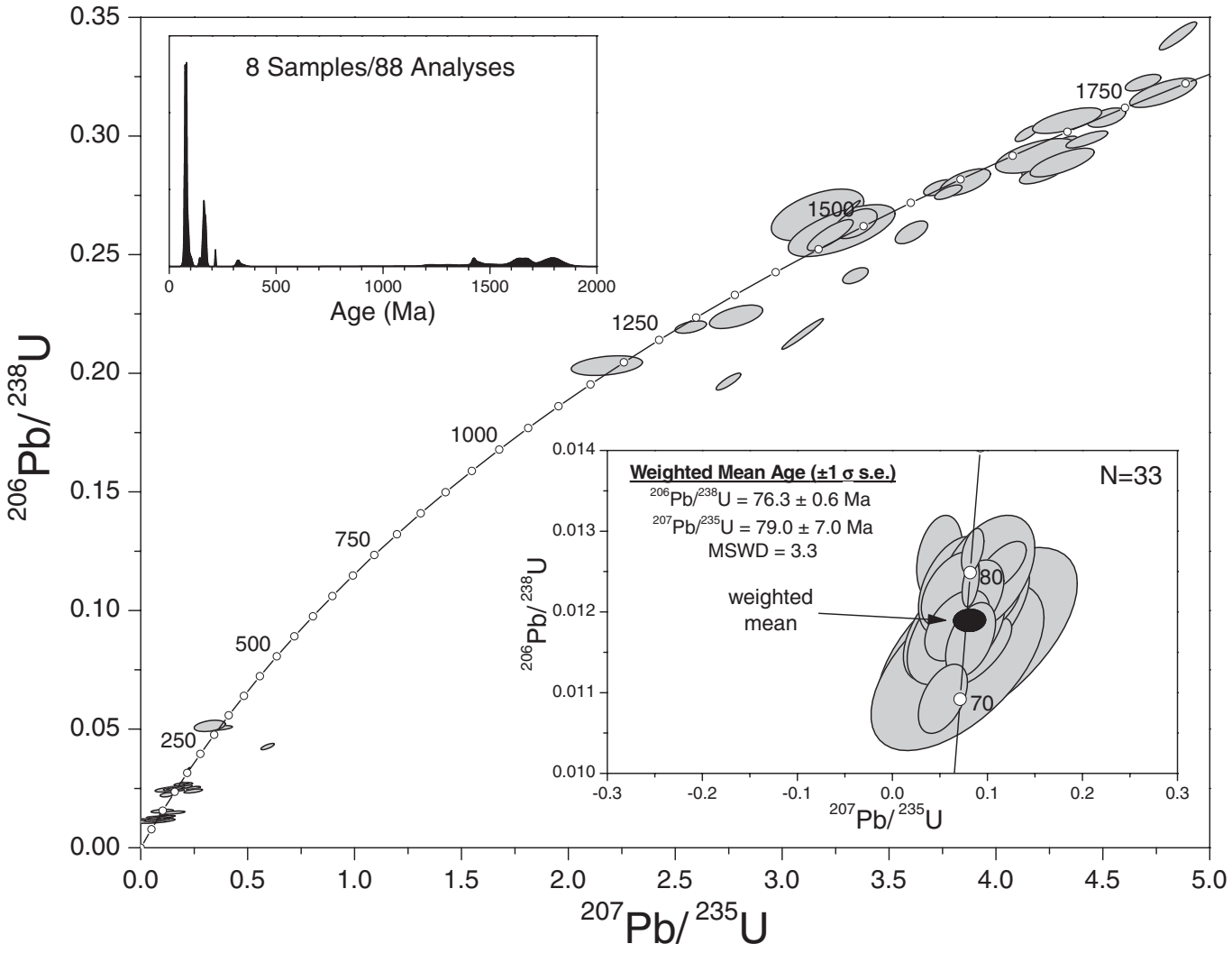

Figure 7. U-Pb concordia diagram of leucogranite zircon ages obtained by ion microprobe analysis. Ellipses represent errors of one standard deviation. Inset in lower right shows expanded view of the youngest ages, which are considered to indicate the time of igneous crystallization. Inset in upper left shows probability distribution plot of the analyses. $^{206}Pb/^{238}U$ and $^{207}Pb/^{206}Pb$ ages are used for grains younger and older than 1.0 Ga, respectively.

late Early Proterozoic inherited grains is consistent with known ages of basement rocks in southeastern California (references cited in Grove et al., 2003).

$^{40}Ar/^{39}Ar$ THERMOCHRONOLOGY

$^{40}Ar/^{39}Ar$ thermochronology performed on minerals with varying retentivities for radiogenic argon ($^{40}Ar^*$) is a powerful technique for constraining the thermal histories of crustal rocks (e.g., McDougall and Harrison, 1999; see Appendix 1 for a description of analytical methods). Unfortunately, our ability to interpret quantitatively the form of age spectra measured from hydrous phases such as hornblende, muscovite, and biotite suffers from the fact that argon release occurs in vacuo outside of their stability fields (i.e., dehydroxylation and incongruent melting affect these materials during our measurements; see McDougall and Harrison, 1999, and references cited therein). Because of the potential for homogenization of diffusion gradients during in vacuo degassing of hydrous minerals (Gaber et al., 1988; Lee et al., 1991; McDougall and Harrison, 1999), we have generally limited our interpretation of results from hydrous phases to consideration of total gas model ages that are calculated from the step-heating results. We believe that these model ages provide the best measure of thermal history, as they are expected to correspond most closely to the time of bulk $^{40}Ar^*$ closure (see discussion in Jacobson et al., 2002), which we assume to have occurred at ~525 ± 50 °C, ~400 ± 50 °C, and ~350 ± 50 °C for hornblende, muscovite, and biotite, respectively (McDougall and Harrison, 1999). Although bulk closure depends upon a variety of factors (notably, effective diffusion dimension, diffusion geometry, and cooling rate), we consider that the experimental basis upon

which closure temperatures are calculated from hydrous phases remains too poorly established to allow more detailed estimates. However, although it is unwise to interpret age gradients from hydrous phases quantitatively, their form may allow qualitative interpretation of cooling history, and we comment on this where appropriate. Finally, note that in calculating total gas ages from hornblende, we have excluded low-temperature steps (<950 °C) in which Ar release was predominantly from low-Ca/K regions that we believe to be intergrown with less-retentive K-rich phases (see McDougall and Harrison, 1999).

In contrast to the situation for the hydrous phases, quantitative information about thermal histories can be obtained from K-feldspar step-heating data using the multidiffusion domain (MDD) technique outlined in Lovera et al. (1991, 1997, 2002). The amenability of K-feldspar to this approach appears to be related in poorly understood ways to the rich array of microstructures that typify basement feldspar (Lovera et al., 1993). Regardless of the nature of the intracrystalline controls, K-feldspar has been empirically demonstrated to be capable of recording continuous thermal history information from ~350 to ~150 °C (Lovera et al., 1997, 2002, and references cited therein; Parsons et al., 1999, offer a dissenting opinion). We have followed the criteria and procedures outlined in Lovera et al. (2002) to identify appropriate samples for detailed study (see Appendix 1).

Bulk closure age constraints from the hydrous phases and continuous MDD thermal histories from K-feldspar can be utilized to elucidate the cooling histories of the Orocopia Schist and upper plate and determine the slip history of the Orocopia Mountains detachment fault. In an attempt to achieve this goal, we performed $^{40}Ar/^{39}Ar$ step-heating analyses on 98 samples of hornblende, muscovite, biotite, and K-feldspar from the Orocopia Schist and upper plate. Most samples were collected from the main body of the Orocopia Mountains, although several were selected from the inlier of schist and upper plate in Painted Canyon within the Mecca Hills (Fig. 3). Individual release spectra and data tables for all samples are included in the GSA Data Repository. Ages for most of these samples, along with two prior results from Jacobson (1990), are listed in Table 1 and plotted in map view on Figure 8 for samples from the main body of the Orocopia Mountains and on Figure 9 for those from Painted Canyon. Note, however, that we omit from these and subsequent figures two samples of hornblende (OR373 and OR374A) and two of K-feldspar (OR340A and OR344) showing evidence of severe contamination with excess $^{40}Ar^*$ ($^{40}Ar_E$). Based upon the cross sections of Figure 4, we have plotted the total gas ages as a function of structural depth (Fig. 10). Note that our confidence in assigning structural "elevations" to samples in Figure 10 is highest for the lower plate and somewhat tenuous for portions of the upper plate.

Release spectra for hornblende, muscovite, and biotite are presented in composite plots in Figures 11 and 12, with the exception of two samples of biotite and one of hornblende from the anorthosite-syenite unit that show anomalously old ages; these are illustrated separately in Figure 13. Release spectra and the results of MDD modeling for the K-feldspar samples are shown in Figure 14 (excluding samples OR340A and OR344). In addition to the samples from the Orocopia Mountains, Figure 14 includes the three new K-feldspar results for the Gavilan Hills that we generated in order to compare thermal histories for the Orocopia Schist from the two areas (see also Table 2).

Hornblende

Hornblendes were analyzed from five metabasite samples from the Orocopia Schist, all from the chlorite zone. Although the total gas ages calculated from these samples are tightly clustered at 54–50 Ma (Table 1; Fig. 8B), each sample exhibits a significant age gradient from a little less than 40 Ma to ca. 60 Ma (Fig. 11A), which complicates interpretation of the results. Note that we discount steps released at <950 °C, as noted above, and a few anomalous high-temperature steps with ages of ca. 70 Ma. In addition, all of the samples tend to be relatively unradiogenic (43%–76% $^{40}Ar^*$; Table 1). For many metamorphic hornblendes that exhibit age gradients, such variation is associated with gradients in Ca/K that imply intergrowths with fine-grained, less-retentive, K-rich phases (McDougall and Harrison, 1999). However, with the exception of steps released at less than 950 °C, this behavior is not clearly manifested by the hornblendes from the Orocopia Schist (see Fig. DR1). The lack of correspondence between age and Ca/K, coupled with the fact that the release spectra are all so similar, indicates that the total gas ages are probably geologically meaningful and suggests protracted equilibration at temperatures within the partial ^{40}Ar retention zone for hornblende (~525 °C; McDougall and Harrison, 1999).

Age spectra were determined for seven samples of hornblende from the upper plate in the main body of the Orocopia Mountains, four from the leucogranite-gneiss (including one sample from Jacobson, 1990) and three from the anorthosite-syenite. Six of the seven samples exhibit very similar flat spectra, with the exception of a minimal number of anomalous steps (Fig. 11B). Total gas ages for these six well-behaved samples range from 76 to 69 Ma (excluding one ca. 100 Ma step from sample OR349). Thus, even the youngest hornblende age from the upper plate (69 Ma) is significantly older than the oldest age from the schist (54 Ma). Furthermore, there is essentially no overlap even of individual step ages between the schist and upper plate (Figs. 11A and 11B). Overlap is limited to a few anomalous low-temperature steps with low Ca/K from the upper plate that are of similar age to the high-temperature steps from the schist. The flatter age spectra for upper-plate hornblendes compared to those from the schist suggest more rapid cooling through hornblende Ar closure.

One sample from the anorthosite-syenite (OR342) yielded an exceptionally old total gas age (117 Ma) and is plotted separately from the others (Fig. 13). This sample is problematic in two respects. First, its saddle-shaped spectrum implies the presence of $^{40}Ar_E$ (McDougall and Harrison, 1999). In addition, other samples from the upper plate have Ca/K ratios in the range of ~10–30. The much lower ratio for this sample suggests extensive contamination with biotite.

TABLE 1. SUMMARY OF $^{40}Ar/^{39}Ar$ AGES FROM THE OROCOPIA MOUNTAINS

Orocopia Schist				Upper plate			
Sample	Age ± 1σ (Ma)	$^{40}Ar^{*\dagger}$	Zone‡	Sample	Age (Ma)	$^{40}Ar^{*\dagger}$	Zone§
Hornblende				Hornblende			
OR32	50.2 ± 0.7	62.9	chl	OR211	74.5 ± 0.3	80.2	lg-gn (deep)
OR79	51.9 ± 0.5	53.7	chl	OR235A#	74.3 ± 0.8	90.0	lg-gn (deep)
OR109	54.2 ± 1.3	42.5	chl	OR294	71.3 ± 0.2	84.1	lg-gn (deep)
OR171	50.4 ± 0.5	75.5	chl	OR329	72.2 ± 0.7	76.9	lg-gn (deep)
OR303B	53.8 ± 1.4	47.2	chl	OR342	117.0 ± 0.4	96.9	an-sy
				OR349	76.4 ± 0.6	79.3	an-sy
Muscovite				OR356	68.9 ± 0.7	78.0	an-sy
OR15	43.2 ± 0.3	91.5	chl				
OR17	43.7 ± 0.3	91.9	chl	Muscovite			
OR30	41.1 ± 0.3	91.1	chl	OR306	49.4 ± 0.6	79.7	lg-gn (deep)
OR49	47.4 ± 0.1	91.9	chl	OR371	97.3 ± 0.8	95.3	pc
OR68B	47.3 ± 0.3	88.8	chl				
OR70	48.8 ± 0.3	91.9	chl	Biotite			
OR77B	44.6 ± 0.1	92.8	chl	OR251G	63.0 ± 0.3	81.9	lg-gn (deep)
OR83	42.6 ± 0.1	91.4	chl	OR317	69.6 ± 0.3	71.7	an-sy
OR94A	44.3 ± 0.4	88.6	chl	OR322	67.0 ± 0.3	84.7	lg-gn (shallow)
OR113	34.5 ± 0.2	91.2	bio	OR328	65.9 ± 0.5	84.9	lg-gn (deep)
OR130	43.7 ± 0.2	91.2	bio	OR332A	67.7 ± 0.3	89.5	lg-gn (shallow)
OR148	41.9 ± 0.2	89.6	bio	OR333A	66.6 ± 0.4	81.9	lg-gn (deep)
OR164	40.5 ± 0.1	92.8	chl	OR339	65.3 ± 0.3	86.5	lg-gn (shallow)
OR178#	42.7 ± 0.6	52.5	chl	OR348A	65.4 ± 0.3	89.8	an-sy
OR213	42.5 ± 0.3	86.9	myl	OR353	64.8 ± 0.3	84.3	lg-gn (deep)
OR213A	51.7 ± 0.4	87.0	myl	OR361	158.0 ± 0.5	94.7	an-sy
OR224B	41.8 ± 0.3	89.3	chl	OR364	65.6 ± 0.6	87.8	lg-gn (shallow)
OR232A	49.3 ± 0.2	90.5	myl	OR365	75.1 ± 0.3	91.4	an-sy
OR246	48.7 ± 0.3	89.3	myl	OR366	69.1 ± 0.4	85.7	lg-gn (shallow)
OR307	41.7 ± 0.1	89.5	chl	OR368	73.5 ± 0.4	87.7	an-sy
OR308	43.5 ± 0.1	91.3	chl	OR374	67.1 ± 2.0	86.2	pc
OR312A	34.3 ± 0.6	79.8	bio	OR404	55.7 ± 2.1	60.9	an-sy
OR314	42.1 ± 0.1	92.0	bio	OR410	67.1 ± 0.5	73.4	an-sy
OR337	45.3 ± 0.3	86.5	chl	OR411	71.5 ± 2.7	91.0	an-sy
OR351	42.5 ± 0.3	85.6	chl	OR412	98.1 ± 0.8	88.4	an-sy
OR358	43.3 ± 0.3	86.1	chl	OR418	66.8 ± 0.4	90.8	an-sy
OR359	43.9 ± 0.3	86.1	myl	OR420A	64.4 ± 0.3	89.5	lg-gn (shallow)
OR372	42.7 ± 0.6	86.1	chl	OR423	69.4 ± 0.2	91.2	lg-gn (shallow)
MRD35	44.0 ± 0.3	89.7	bio	OR425A	66.4 ± 0.4	92.2	lg-gn (shallow)
MRD132	38.5 ± 0.3	87.7	bio	OR426	59.1 ± 0.5	82.3	lg-gn (shallow)
				OR427	65.3 ± 0.3	90.9	lg-gn (shallow)
Biotite							
OR18	20.3 ± 0.5	39.7	bio	K-feldspar			
OR49	25.9 ± 0.2	38.9	chl	OR316	59.0 ± 0.4	84.8	an-sy
OR68B	23.4 ± 0.5	36.2	chl	OR350B	43.8 ± 2.5	83.9	lg-gn (deep)
OR83	18.8 ± 0.5	26.5	chl	OR352A	41.7 ± 0.4	77.7	lg-gn (deep)
OR113	21.3 ± 0.2	77.2	bio	OR363	78.1 ± 1.7	81.4	an-sy
OR130	29.0 ± 0.7	47.9	bio	OR367	52.0 ± 0.5	75.6	lg-gn (shallow)
OR148	25.0 ± 0.3	62.0	bio	OR371	42.7 ± 1.5	90.8	pc
OR164	23.8 ± 0.1	73.3	chl	OR420A	60.6 ± 0.4	78.5	lg-gn (shallow)
OR292	27.8 ± 0.3	39.0	myl	OR422	54.9 ± 0.4	86.9	lg-gn (shallow)
OR308	33.0 ± 0.5	57.6	chl	OR426	55.3 ± 0.5	72.3	lg-gn (shallow)
OR312A	25.3 ± 0.1	71.3	bio	OR427	61.7 ± 0.3	87.9	lg-gn (shallow)
OR314	23.7 ± 0.1	69.1	bio	OR428	48.7 ± 0.5	73.6	lg-gn (deep)
OR337	22.5 ± 0.6	30.1	chl				
MRD132	14.3 ± 0.4	29.8	bio				
K-feldspar							
OR17	25.3 ± 1.0	62.5	chl				
MRD35	24.2 ± 0.5	72.0	bio				

†Percent of total measured ^{40}Ar derived from decay of ^{40}K.

‡Indicates whether sample of Orocopia Schist is from the biotite (bio), chlorite (chl), or mylonite (myl) zone.

§Indicates whether sample of upper plate is from the deep or shallow part of the leucogranite-gneiss unit (lg-gn) or the anorthosite-syenite unit (an-sy) in the main body of the Orocopia Mountains or from Painted Canyon (pc).

#From Jacobson (1990).

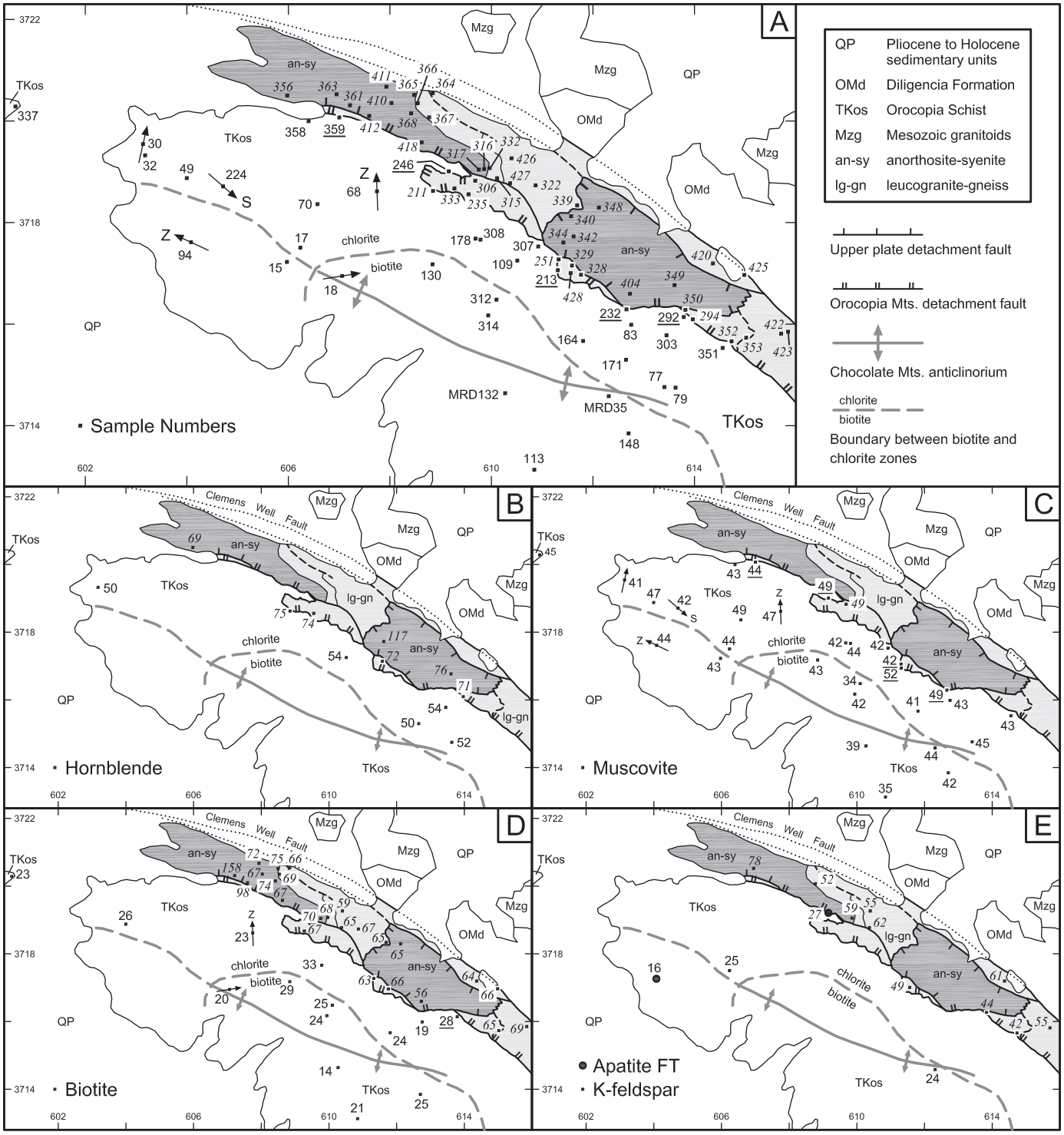

Figure 8. Sample numbers (A) and $^{40}Ar/^{39}Ar$ total gas ages and fission track ages in Ma (B–E). Sample numbers with prefix "MRD" were collected by Dawson (1987). Sample numbers without a prefix belong to the "OR" suite and were collected by the authors (Table 1). For these samples, the "OR" prefix has been omitted to reduce clutter. For the same reason, we do not show letter suffixes to sample numbers, which reflect multiple samples collected at a single locality (e.g., Table 1). Ages from the Orocopia Schist indicated in plain text, those from the upper plate shown in italics. Mylonite samples underlined. Arrows indicate trends of fold hinges. Sense of asymmetry ("S" or "Z") for fold hinges shown where determined. See Figure 3 for location. Two-kilometer UTM grid ticks shown.

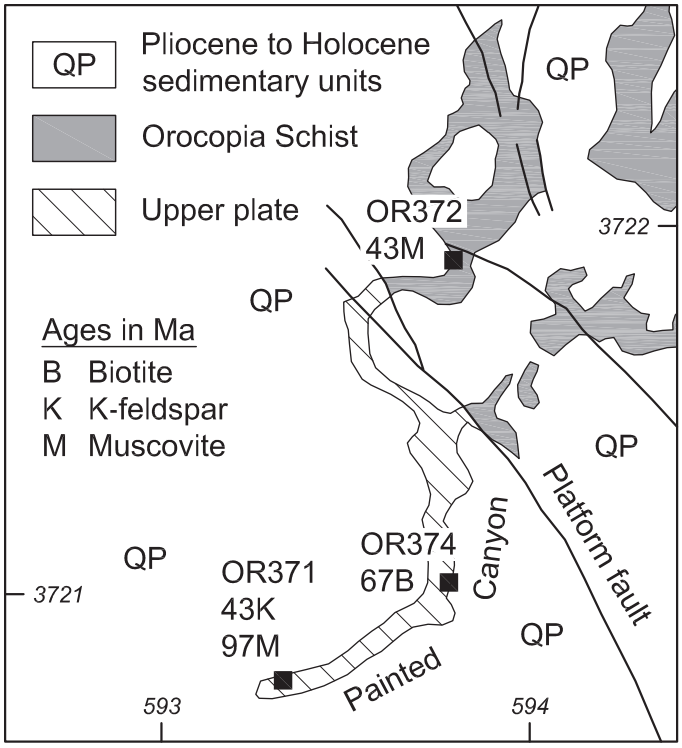

Figure 9. Muscovite (M), biotite (B), and K-feldspar (K) $^{40}Ar/^{39}Ar$ total gas ages from Painted Canyon in the Mecca Hills. Geology from Sylvester and Smith (1976). See Figure 3 for location. One-kilometer UTM grid ticks shown.

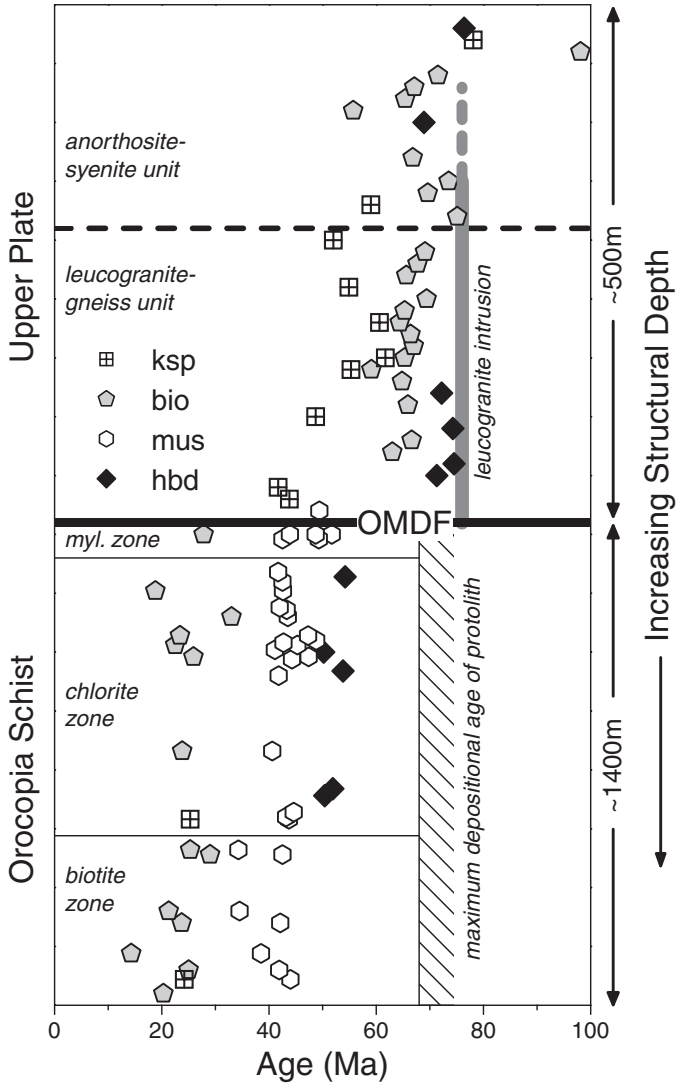

Figure 10. Distribution of $^{40}Ar/^{39}Ar$ total gas ages versus structural position for the Orocopia Schist and upper plate. Vertical scale is highly diagrammatic. For example, note that the scale for the upper plate is greatly exaggerated relative to that for the schist and that the thickness of the mylonite zone in the schist is highly expanded compared to the chlorite and biotite zones.

Two hornblendes were analyzed from the upper plate in Painted Canyon. Unfortunately, both were too strongly contaminated with $^{40}Ar_E$ to be interpretable (samples OR373 and OR374A; see Fig. DR1).

Muscovite

Muscovites were analyzed from 30 samples representing all structural levels within the schist (Fig. 8C). Samples were divided into three groups: (1) biotite-zone samples from deep in the section, (2) chlorite-zone samples from high in the section, and (3) mylonites from the structurally highest few meters of schist. Four of the chlorite-zone samples are from tight fold hinges that we interpret to belong to the younger generation with northeastward to eastward vergence (above; see also Jacobson and Dawson, 1995). Muscovite within these fold hinges shows textures indicative of recrystallization synchronous with or subsequent to folding. Muscovite in the mylonites occurs both as newly recrystallized sericitic matrix and as relict "fish"-shaped porphyroclasts (Jacobson and Dawson, 1995). Although the porphyroclast size fraction was analyzed, recrystallized mica occurs along the margins of these grains.

Overall, total gas ages measured for muscovites from the schist span a range from 52 to 34 Ma (Table 1; Figs. 8C and 10). Ages from fold hinges are compatible with those from nearby normally foliated samples. Release spectra generally show moderate age gradients within about the first 20% of ^{39}Ar released, followed by relatively level plateaus (Figs. 12A–12C). However, muscovites from some mylonites exhibit monotonically increasing ages with high-temperature outgassing. Muscovites from the mylonites yielded the oldest total gas ages (average of 47 Ma). Average total gas ages for the chlorite and biotite zones are progressively younger at 44 and 40 Ma, respectively. Within each of the three groups, plateaus and total gas ages show a range of ~10 m.y. Figures 8B and 10 indicate that much of this spread occurs even for samples located quite close to one another, so

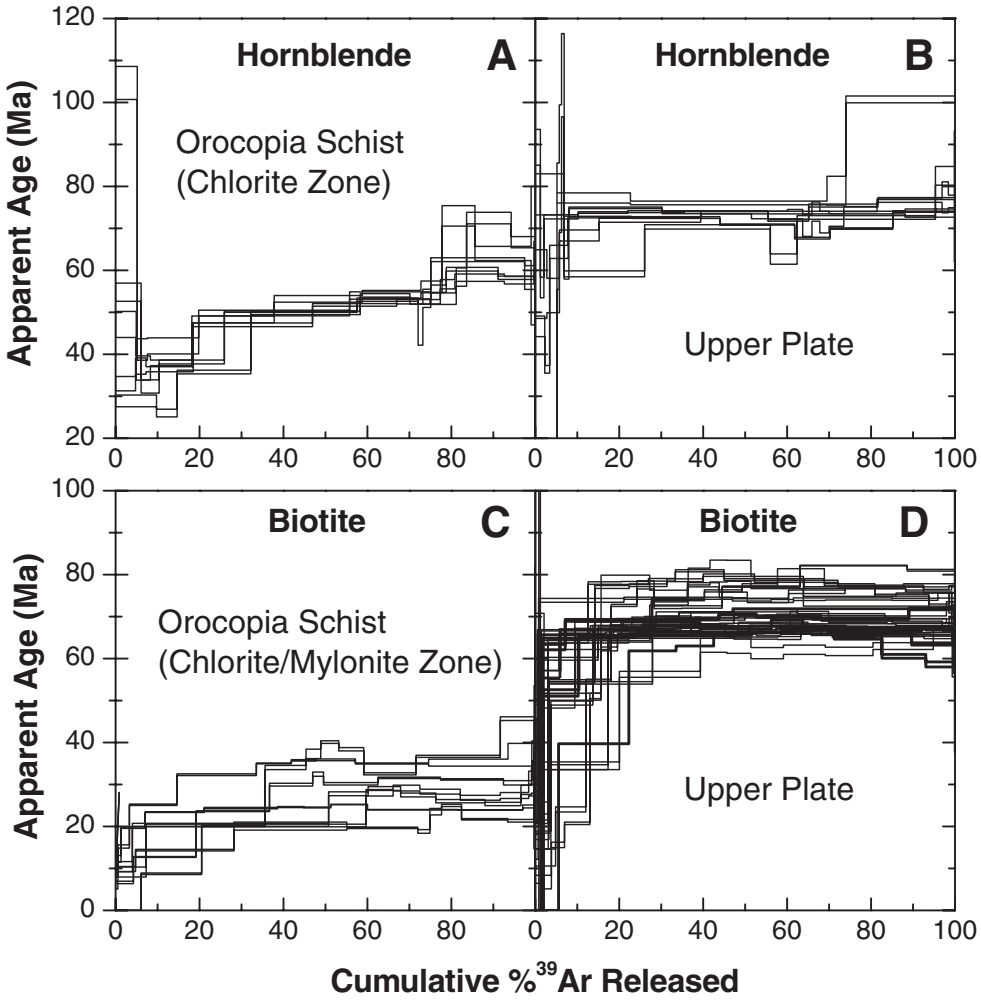

Figure 11. Incremental argon release spectra for hornblende and biotite from the upper plate of the Orocopia Mountains detachment fault and the structurally high part of the Orocopia Schist (chlorite and mylonite zones). Does not include the one hornblende and two biotite samples from the upper plate that yielded anomalously old ages (see Fig. 13). Errors shown are ±1σ analytical uncertainties.

it cannot be explained solely by structural position at the scale of each group. Given the setting, it is likely that recrystallization related to deformation and variation in the degree of hydrothermal alteration or weathering have been factors.

We include in our data set for the schist one muscovite from Jacobson (1990) (sample OR178; see Table 1). A second schist muscovite from that study (sample OR230B) has been omitted, because a significant number of the high-temperature steps are anomalously old, with ages up to nearly 80 Ma. Steps that old were not reproduced in any of the 29 new samples of schist muscovite analyzed here.

Muscovite is rare in the upper plate, except as a minor retrograde phase. Only two samples were analyzed, both of which yielded results that are difficult to interpret. One, sample OR306 (Fig. DR2, part 2) has a total gas age of 49 Ma, which is anomalously young compared to the biotite ages for the upper plate. This sample shows a very pronounced age gradient from 55 to 20 Ma, so the young age may reflect low retentivity of argon due to strong recrystallization. In contrast, an anomalously old age of 97 Ma was obtained for a sample from Painted Canyon (OR371; Fig. 9). The release spectrum for this sample exhibits an unusual hump within the low-temperature steps (Fig. DR2, part 3).

Biotite

Biotite was analyzed from 14 samples of schist. Total gas ages range from 33 to 14 Ma (Fig. 10). Because the biotites tend to be quite unradiogenic (Table 1), their total gas ages are less well determined than those for muscovite. Consequently, in a given part of the structural section, biotites exhibit a much larger spread in age than do corresponding muscovites (Figs. 12A versus 12D, and 12B versus 12E). This is probably due partly to

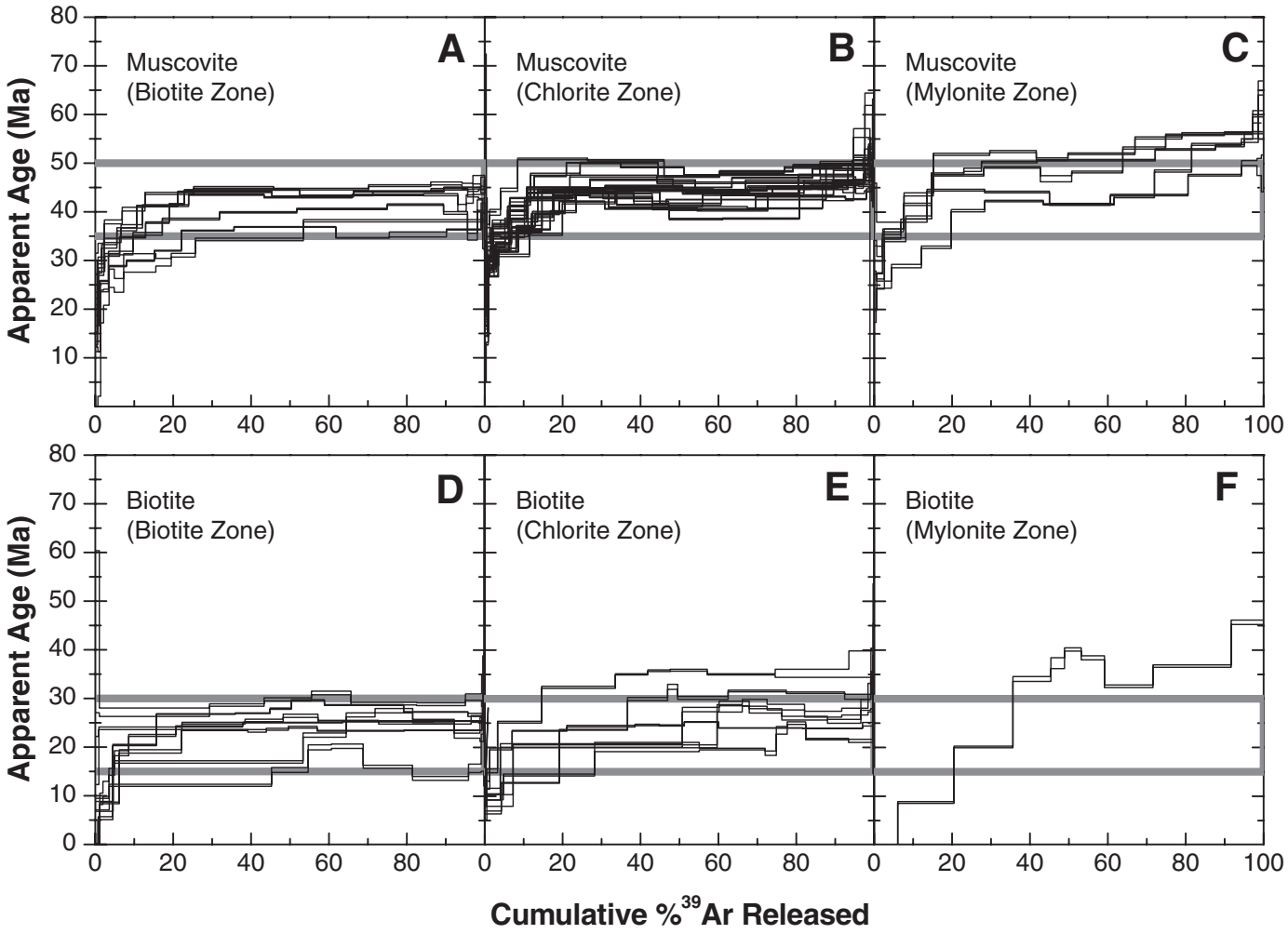

Figure 12. Incremental argon release spectra of muscovite and biotite from the biotite, chlorite, and mylonite zones of the Orocopia Schist in the Orocopia Mountains. Thick gray lines are references for comparing ages from the different zones. Errors shown are ±1σ analytical uncertainties.

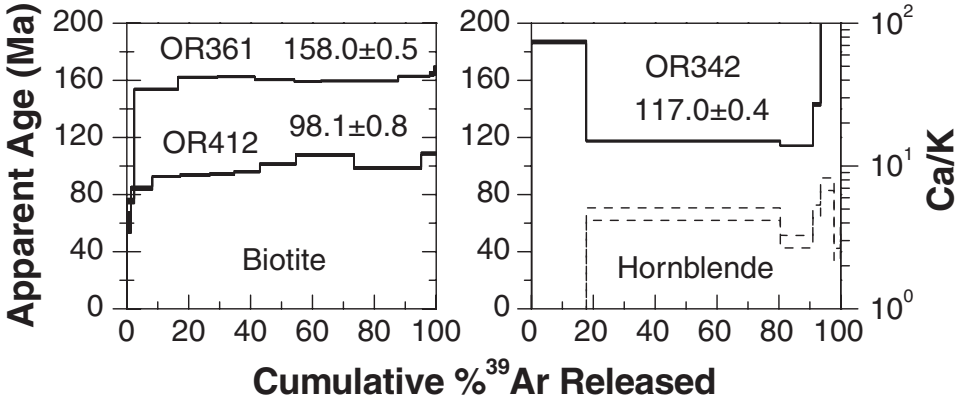

Figure 13. Incremental argon release spectra (solid pattern) for hornblende and biotite and Ca/K (dashed lines) for hornblende for three anomalously old samples from the anorthosite-syenite unit. Numeric values are total gas ages (for hornblende, steps released at less than 950 °C are excluded). Errors shown are ±1σ analytical uncertainties.

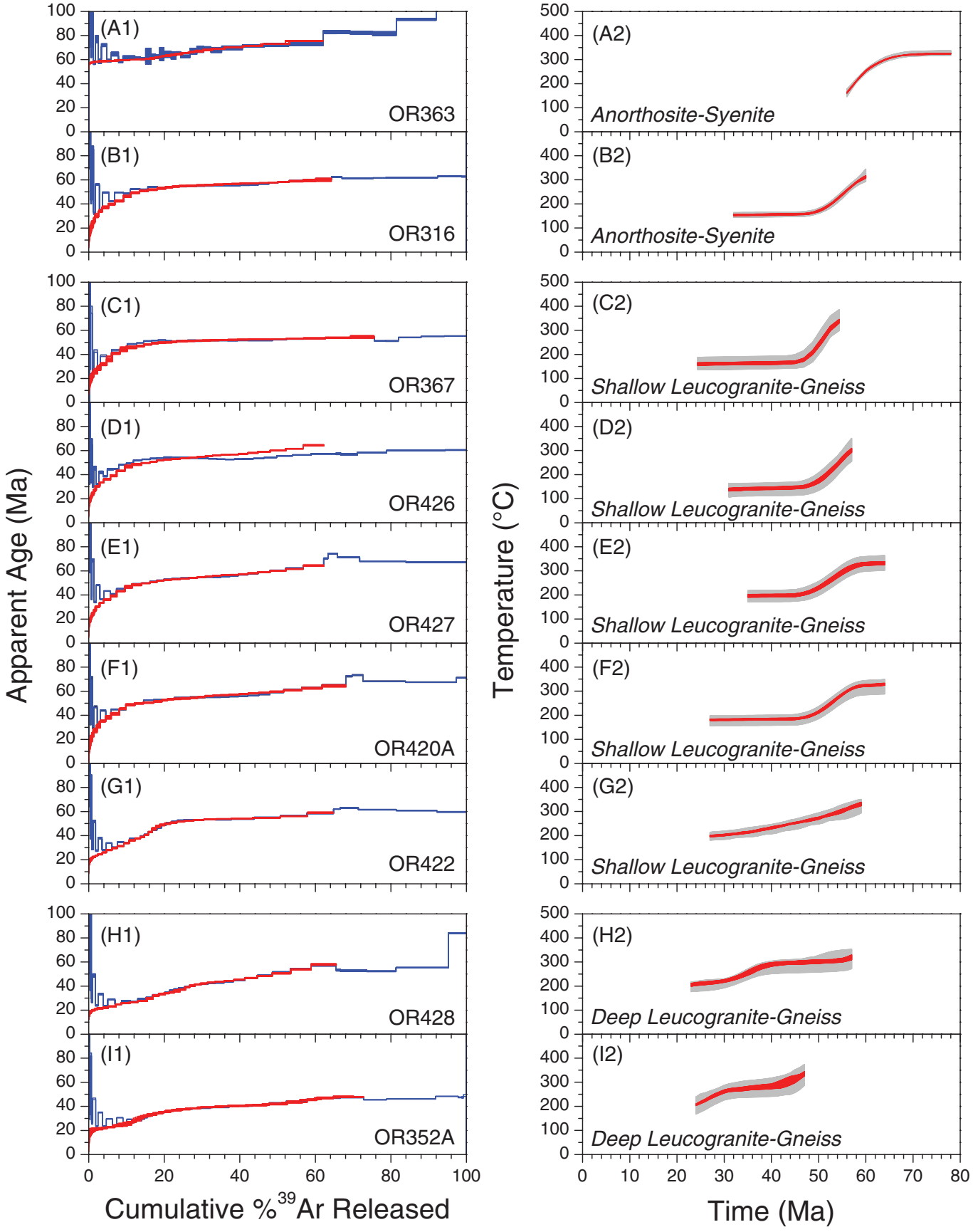

Figure 14 (*on this and following page*). Thermal history results for K-feldspar, excluding problematic samples OR340A and OR344 described in text. Plots in left column show measured (blue) and modeled (red) age spectra. Errors for measured spectra indicate ±1σ analytical uncertainties. Modeled spectra represent 50 best-fit solutions determined from multidiffusion domain (MDD) analysis. Right column shows calculated monotonic cooling histories. Red and gray bands indicate 90% confidence intervals for median and overall distributions, respectively (see text).

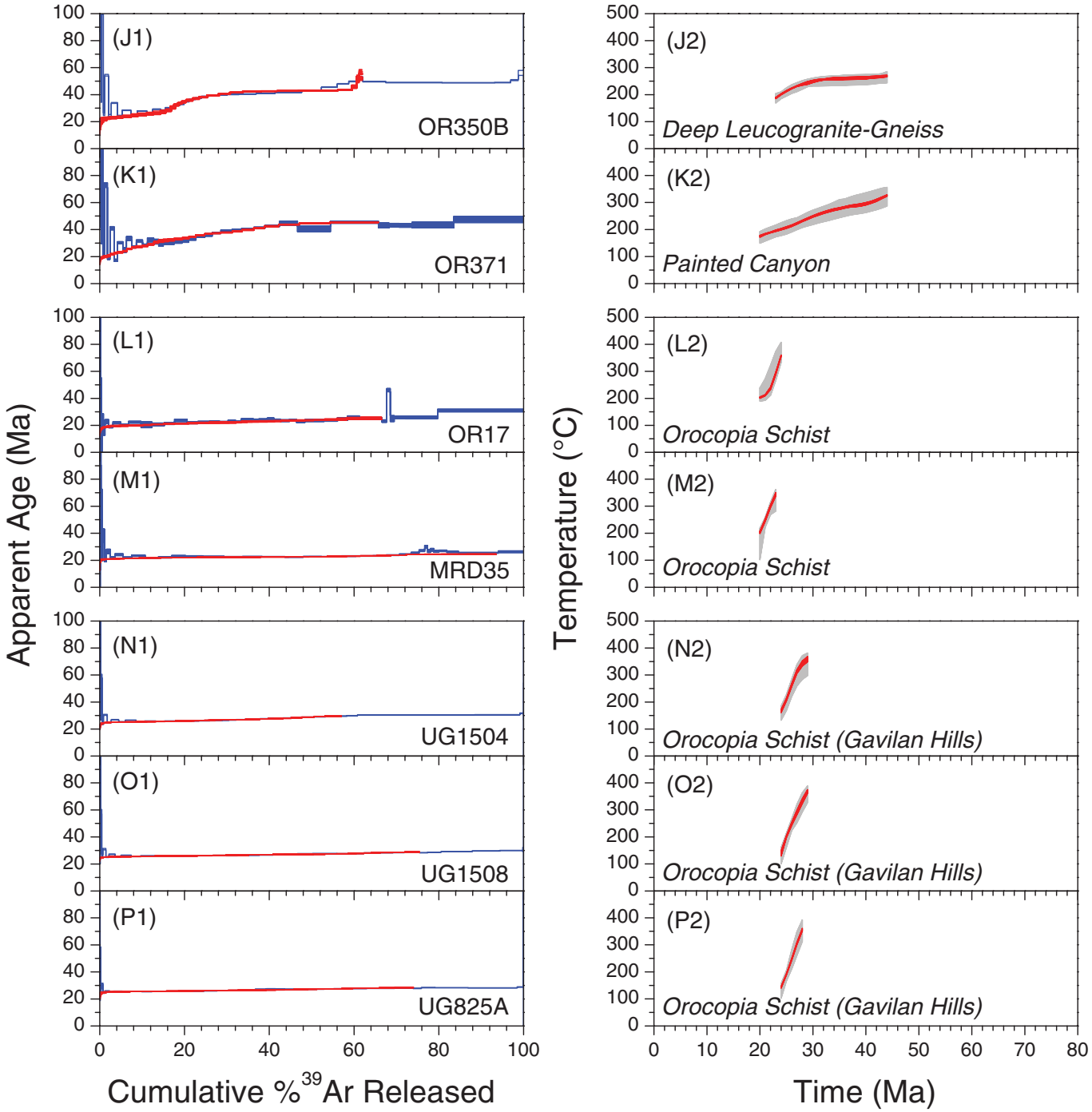

Figure 14 (*continued*).

retrograde alteration to chlorite, which occurs to some extent even in the most pristine samples. It is likely also the result of weathering, which is much more prominent in biotite than muscovite (as indicated by limonitic staining and anomalous interference colors). In any case, whereas we consider that the overall young ages for biotite are significant, any individual analysis may have relatively high error. In particular, we discount the youngest age of 14 Ma (sample MRD132; Table 1). The ^{40}Ar from this sample is only 30% radiogenic, and the age is a distinct outlier compared to the next younger age of 19 Ma (sample OR83). An age of 14 Ma also seems incompatible with the results from K-feldspar (below). In addition, even the 19 Ma age just cited is itself likely to be unreliable. Although it is not significantly younger than another biotite age of 20 Ma (sample

TABLE 2. SUMMARY OF K-FELDSPAR $^{40}Ar/^{39}Ar$ AGES FROM THE GAVILAN HILLS

Sample	Age ± 1σ (Ma)	$^{40}Ar^{*\dagger}$
UG825A	27.4 ± 0.6	87.8
UG1504	28.9 ± 0.4	87.4
UG1508	28.0 ± 0.4	92.9

†Percent of total measured ^{40}Ar derived from decay of ^{40}K.

OR18), sample OR83 yielded the least radiogenic argon of any biotite analyzed (27%) and has an age inconsistent with those from nearby samples of biotite.

Despite the above complications, biotite from the schist does appear to show a slight decrease in age structurally downward. The average total gas ages of biotite from the chlorite and biotite zones are 26 and 24 Ma respectively. Only one biotite was sampled from the mylonite zone (Fig. 10). As is the case for muscovite, the porphyroclast size fraction of this biotite exhibits a strong age gradient, with the high-temperature steps being among the oldest obtained from any of the samples (Figs. 12D–12F).

Two of the samples of schist biotite were collected from fold hinges, one each from the early and late generations. The ages of both are similar to those derived from the rest of the samples (Fig. 8D).

Twenty-two upper-plate biotites were analyzed, including one from Painted Canyon. Total gas ages range from 75 to 59 Ma (Table 1; Figs. 8D, 9, and 10), with the exception of one relatively young age (56 Ma) from the least radiogenic sample (sample OR404) and two anomalously old results (158 Ma from sample OR361 and 98 Ma from sample OR412; Fig. 13). Biotite ages are thus markedly older in the upper plate than in the schist (Figs. 10, 11C, and 11D).

While many of the biotite samples from the upper plate show distinct age gradients, others exhibit essentially flat age spectra (Fig. 11D; see also Fig. DR2). Because there is no systematic difference in total gas age between these two groups, we conclude that the difference in behavior is an artifact of variable homogenization during in vacuo step heating (e.g., Vedder and Wilkins, 1969).

Biotites from the upper plate generally appear to be much less altered in thin section than those from the schist. Another indication of their more pristine condition is that they are much more radiogenic than the lower-plate biotites (Table 1).

K-Feldspar

Release Spectra and Total Gas Ages

Fifteen K-feldspars from the Orocopia Mountains were selected for analysis in this study, including one from Painted Canyon (Table 1). In addition, we ran three samples from the Gavilan Hills to facilitate comparison of results from the two areas. Age spectra for all samples, excluding two that did not provide usable results, are illustrated in Figure 14.

Four K-feldspars were analyzed from the two separate bodies of the anorthosite-syenite unit within the study area. Three of these (samples OR340A, OR344, and OR363) come from relatively shallow positions in the unit. These samples are transitional in composition between anorthosite, gabbro, and syenite and contain K-poor alkali feldspar that exhibits complex exsolution textures. They were collected from close to the two biotites and one hornblende that show anomalously old total gas ages (Fig. 13). In similar fashion, the K-feldspars from these rocks also appear relatively old. The samples exhibit variable contamination by both low- and high-temperature $^{40}Ar_E$ (see Lovera et al., 2002), consistent with the evidence of $^{40}Ar_E$ in the anomalously old hornblende (Fig. 13). In two of the cases (samples OR340A and OR344), the levels of $^{40}Ar_E$ were high enough to render the samples uninterpretable (Fig. DR3). The third sample, however, is not so severely affected (OR363; Fig. 14A1). The fourth sample from the anorthosite-syenite (OR316) was obtained from a leucogranite intrusion near the base of the unit. Its release spectrum is well behaved (Fig. 14B1), and its total gas age falls within the range of those obtained from the leucogranite-gneiss unit (Table 1).

Eight samples were analyzed from the leucogranite-gneiss unit. Five of these (OR367, OR420A, OR422, OR426, and OR427) were collected from relatively shallow levels within the unit based upon the projected position of the Orocopia Mountains detachment fault in the subsurface. All of these samples yielded similar total gas ages (62–52 Ma; Table 1) and typically exhibited ^{40}Ar loss profiles from <25 Ma to >55 Ma (Figs. 14C1–14G1). The remaining three samples (OR350B, OR352A, and OR428) were collected from positions close to the Orocopia Mountains detachment fault, i.e., from the deep levels of the unit. These yielded younger total gas ages (49–52 Ma; Table 1) and age spectra with younger maximum ages (typically younger than 50 Ma; Figs. 14H1–14J1).

The one sample from Painted Canyon (OR371), from a pegmatite vein, yielded results similar to those from the three samples of leucogranite close to the Orocopia Mountains detachment fault (Table 1; Fig. 14K1). The significance of this similarity is not clear, however, because the Orocopia Schist and upper plate in Painted Canyon are separated by a Neogene high-angle fault, and rock types and associations within the upper plate in Painted Canyon differ somewhat from those in the main body of the Orocopia Mountains. In other words, it is difficult to correlate structural positions of upper-plate rocks between the Orocopia Mountains and Painted Canyon.

K-feldspar is not common within the Orocopia Schist of the Orocopia Mountains, and we managed to analyze only two samples from this unit (OR17 and MRD35). Although widely separated in map view, both samples are from near the boundary between the biotite and chlorite zones, i.e., from the middle of the exposed section. Both yielded similar total gas ages (25 and 24 Ma, respectively) comparable to the youngest reliable biotite ages from the schist. In stark contrast to the results from the upper plate, these K-feldspars exhibit distinctly flatter age spectra (Figs. 14L1 and 14M1) indicative of much more rapid cooling.

The final three samples we examined come from the Orocopia Schist of the Gavilan Hills. K-feldspar is relatively abundant

in this area due to the moderately high grade of metamorphism (oligoclase amphibolite facies). All three samples show remarkably flat age spectra, analogous to the schist samples from the Orocopia Mountains (Figs. 14N1–14P1). Total gas ages, however, are slightly older (29–27 Ma; Table 2) than for the schist samples from the Orocopia Mountains.

Multidiffusion Domain Modeling

Robust thermal histories can be obtained from MDD analysis provided that ^{39}Ar diffusion properties deduced from hours of heating in the laboratory adequately mimic ^{40}Ar* loss profiles that reflect millions of years of crustal residence (Lovera et al., 1997, 2002, and references cited therein). The key to evaluating a sample for suitability for detailed thermal history analysis is to look for self-consistent behavior between the age spectrum (the expression of natural ^{40}Ar* loss) and a similarly scaled representation of the laboratory diffusion properties (the log r/r_o spectrum; see Richter et al., 1991). Results for the two samples from the anorthosite-syenite unit that we have already cited as problematic (OR340A and OR344) are relatively poorly correlated. In addition to both low- and high-temperature $^{40}Ar_E$ contamination, the samples exhibit intermediate age maxima that are inconsistent with volume diffusion in MDD materials characterized by a single value of activation energy (*E*). The remaining samples all yield reasonably well-correlated age and log r/r_o spectra and appear to be amenable to thermal history analysis. One sample, however, exhibits a minor intermediate age maximum, which degrades the quality of the thermal history results that can be obtained from it (sample OR426; Fig. 14D1).

The most important MDD parameter is activation energy (*E*). Variations in *E* of 1 kcal/mol typically result in shifts in calculated temperature of ~15 °C (Lovera et al., 1997). Unfortunately, it can be difficult to determine *E* accurately from step-heating experiments, because the low-temperature Arrhenius array from which this parameter is traditionally estimated is expected to define a slope proportional to *E* only when the domains contributing ^{39}Ar have been outgassed by less than ~60% (see Lovera et al., 1997, for a discussion of factors complicating estimation of *E*). Isothermal duplicate measurements to correct for low-temperature Cl-correlated $^{40}Ar_E$ (see Harrison et al., 1994) frequently reveal that rapid outgassing of small domains leads to inaccurate estimates of *E*. To mitigate against this problem, we adopted the practice of Grove et al. (2003) of assuming an average value of *E* (46 kcal/mol) that is based upon analysis of more than 100 basement K-feldspars (Lovera et al., 1997). In an attempt to ensure that our samples are adequately described by this value, we assigned a standard deviation of 3 kcal/mol to this constant value of *E* and calculated ten equivalent best-fit domain distribution sets by randomly selecting values of *E* from a normal distribution defined by the indicated uncertainty. From these results, we calculated 50 best-fit solutions to the age spectra. Because the geologic setting within the Orocopia Mountains indicates the likelihood of monotonic cooling subsequent to the time of leucogranite intrusion at 76 Ma, we allowed only solutions that preclude transient heating (Figs. 14A2–14P2). In addition, we show only the portions of the calculated temperature-time histories that are well constrained by readily interpreted segments of the ^{40}Ar/^{39}Ar spectra.

Monotonic cooling histories calculated for the 16 samples amenable to MDD analysis are shown in Figures 14A2–14P2 (more complete results of the MDD analyses are presented in Figure DR3). Sample OR363 from the anorthosite-syenite unit represents the shallowest structural level examined. Its calculated thermal history indicates that it began to cool below 300 °C at ca. 70 Ma, with peak cooling approaching 20 °C/m.y. at ca. 60 Ma (Fig. 15). The structurally deeper leucogranite sample within the anorthosite-syenite unit (OR316) exhibits a compatible thermal history (Fig. 14B2), with most rapid cooling (maximum of 17 °C/m.y.) centered around 55 Ma (Fig. 15). Note that while an

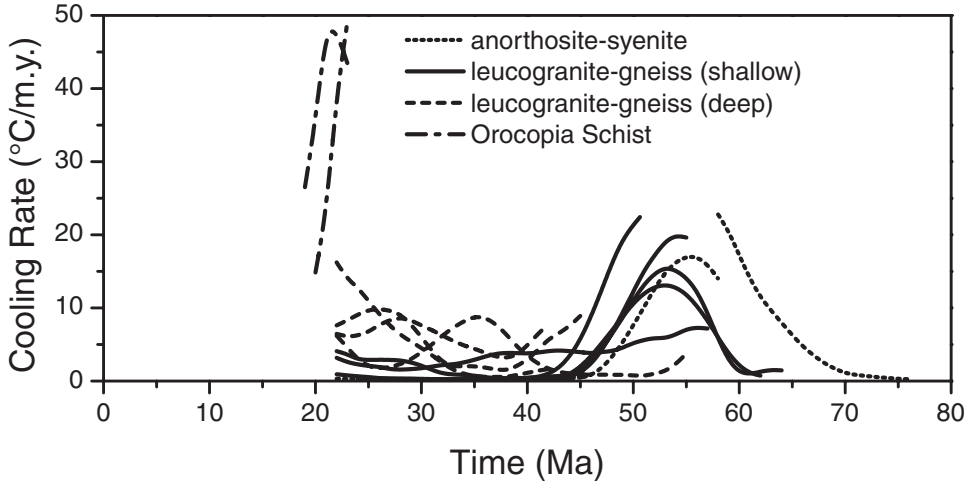

Figure 15. Inferred cooling rates versus time for K-feldspar samples from the Orocopia Mountains. Rates calculated by differentiating temperature-time plots in right column of Figure 14.

apparent offset exists between the time of peak cooling exhibited by samples OR363 and OR316, this could simply be an artifact resulting from difficulty in resolving $^{40}Ar_E$ in the low-temperature portion of the release spectrum of sample OR363 (i.e., the time of rapid cooling is much better constrained in sample OR316).

Most K-feldspars from the shallow levels of the underlying leucogranite-gneiss unit exhibit remarkably similar thermal histories (Figs. 14C2–14G2), with most rapid cooling (up to 20 °C/m.y.) occurring between 55 and 53 Ma and much slower cooling after 45 Ma (Fig. 15). Sample OR422 (Fig. 14G2) is an exception in that it indicates more continuous, slower cooling and appears to behave in a manner transitional to the samples collected from positions near the Orocopia Mountains detachment fault (i.e., the deep samples; Figs. 14H2–14J2). The deep samples, as well as the sample from Painted Canyon, are all similar in that none exhibit the pulse of rapid cooling between 55 and 53 Ma indicated by the shallow samples (Fig. 15), and all show higher temperatures at a given time compared to the shallow samples (Fig. 14). However, there is not much indication that the shallow and deep samples of leucogranite were at different depths prior to 60 Ma, as biotite ages yielded by both groups are similar (mostly 69–59 Ma). Finally, most of the deep K-feldspars appear to have cooled most rapidly (up to 10–15 °C/m.y.) after ca. 25 Ma. Hence results from virtually all upper-plate K-feldspar samples are consistent with tectonic quiescence at 45–30 Ma (Fig. 15).

The two K-feldspar results from the Orocopia Schist in the Orocopia Mountains are strikingly different from those obtained from the upper plate in that they record >350 °C conditions in the footwall prior to 24 Ma (Figs. 14L2 and 14M2) and very rapid cooling (up to 50 °C/m.y.) between 23 and 22 Ma (Fig. 15). Very similar middle Cenozoic temperatures and cooling rates were obtained from all three samples of Orocopia Schist from the Gavilan Hills, although the time of peak cooling occurred several million years earlier in the latter area (Figs. 14N2–14P2).

DISCUSSION

Most workers believe that the Pelona-Orocopia-Rand Schist comprises a subduction complex accreted beneath North America during the Laramide orogeny (Yeats, 1968; Crowell, 1968, 1981; Burchfiel and Davis, 1981; Dickinson, 1981; May, 1986; Hamilton, 1987, 1988; Jacobson et al., 1988, 1996, 2002; Livaccari and Perry, 1993; Malin et al., 1995; Wood and Saleeby, 1997; Miller et al., 2000; Yin, 2002; Saleeby, 2003; Saleeby et al., this volume). Initially, virtually all contacts between schist and upper plate were viewed as remnants of the original subduction thrust (Ehlig, 1968, 1981; Haxel and Dillon, 1978; Dillon et al., 1990), although it is now recognized that most of these faults are exhumation structures (Frost et al., 1981, 1982; Haxel et al., 1985, 2002; Silver and Nourse, 1986; Postlethwaite and Jacobson, 1987; Jacobson et al., 1988, 1996, 2002; Robinson and Frost, 1989, 1991, 1996; Oyarzabal et al., 1997; Saleeby et al., this volume). Less clear, however, is what proportion of the exhumation occurred in Late Cretaceous or early Cenozoic time synchronously with subduction versus how much was associated with middle Cenozoic regional extension and detachment faulting (Fig. 2). Thermochronologic analysis is ideally suited to answer this question, but until our recent work in the Gavilan Hills (Jacobson et al., 2002), too few data were available to provide definitive constraints. Aggregating the results for the Gavilan Hills and the new analyses obtained here, we now have an exceptional data set for addressing this issue. Particularly when considered in conjunction with other recent geochronologic investigations (Grove et al., 2003), our combined results provide a remarkably clear and consistent picture pertaining to the development of the Orocopia Schist along a significant extent of the Chocolate Mountains anticlinorium.

Integrated Thermal History of the Gavilan Hills

Results from the Gavilan Hills have been discussed previously by Jacobson et al. (2002) but are reviewed here for comparison with the data for the Orocopia Mountains. In this context, it is important to bear in mind a critical difference in basic geologic relations between the Orocopia Mountains and Gavilan Hills. As emphasized above, the contact between the schist and upper plate in the Orocopia Mountains (i.e., the Orocopia Mountains detachment fault) must have formed at relatively shallow crustal levels. This is indicated by the abundant evidence of brittle deformation and hydrothermal alteration along the fault, as well as by the complete absence of ductile fabrics in the base of the upper plate related to the contact. In contrast, the boundary between the schist and upper plate in the Gavilan Hills (the Chocolate Mountains fault) is clearly a deeper-level structure, as evidenced by the fact that both the schist and upper plate adjacent to the fault exhibit mylonitic textures and greenschist-facies retrograde metamorphism (Jacobson et al., 2002). The Chocolate Mountains fault in the Gavilan Hills is overlain by a second major structure, the Gatuna fault, which separates the upper plate from the low-grade Winterhaven Formation. It is the Gatuna fault that most resembles the Orocopia Mountains detachment fault in terms of having been active at a relatively shallow structural level.

Figure 16A illustrates our previous $^{40}Ar/^{39}Ar$ data for the schist and upper plate in the Gavilan Hills (Jacobson et al., 2002), along with the three new K-feldspar results obtained here. As explained earlier, we employ MDD thermal history results for K-feldspar but use total gas ages to represent the bulk Ar closure for hydrous phases (hornblende, muscovite, and biotite). Additional controls on the youngest stages of evolution of the region are provided by two apatite fission track ages from the schist and one from the upper plate (Oyarzabal et al., 1997) and by the occurrence of clasts of schist in the conglomerate of Bear Canyon, which is loosely dated as Miocene in age (Dillon, 1976; Hughes, 1993). At the other extreme, limits on the age of deposition and underthrusting of the schist protolith are available from recent analysis of detrital zircons (Grove et al., 2003). In that study, U-Pb ages were measured for 66 zircons from two samples of metagraywacke from the Gavilan Hills and one from the adja-

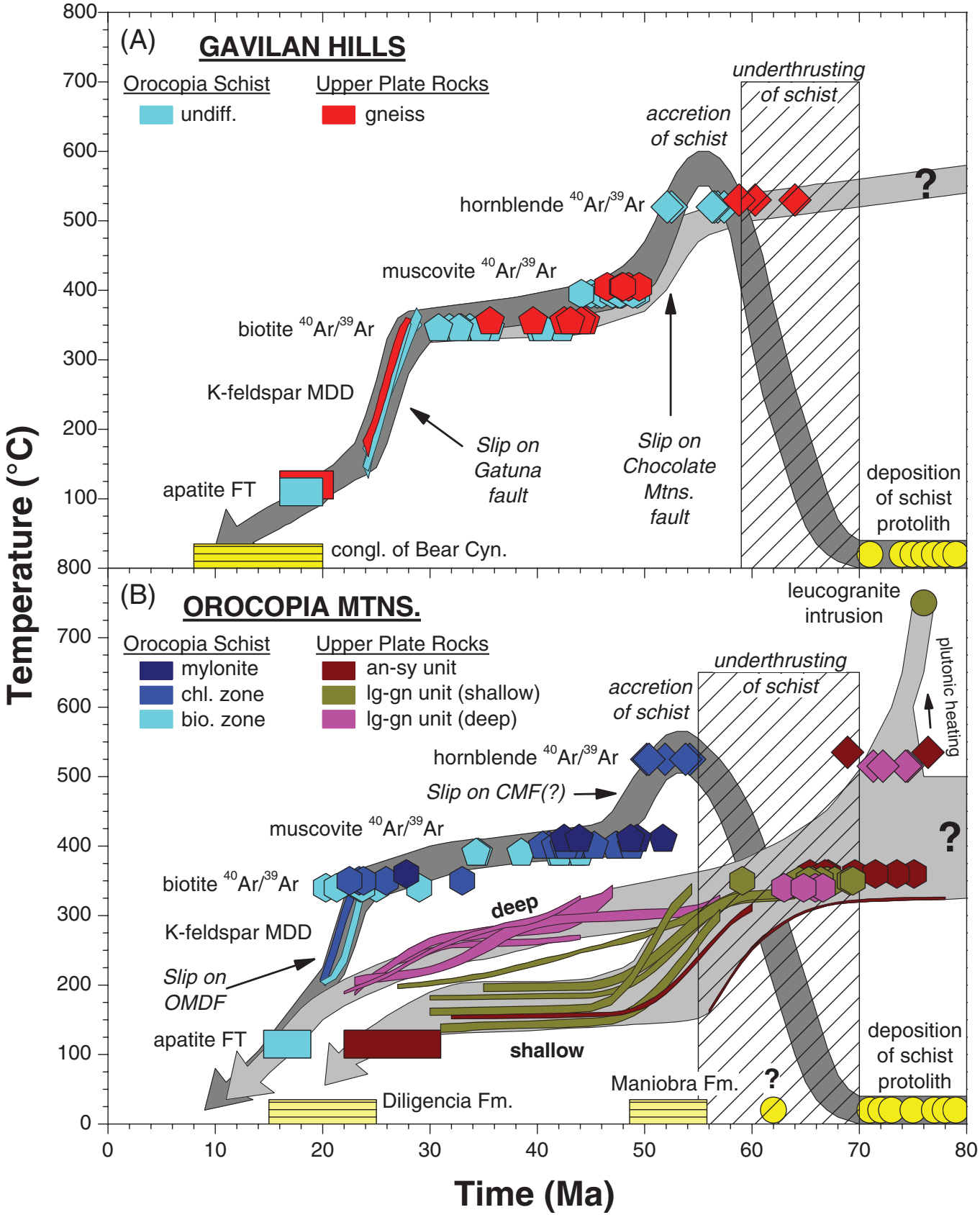
(A)
GAVILAN HILLS
Orocopia Schist
undiff.
Upper Plate Rocks
gneiss
underthrusting of schist
accretion of schist
hornblende 40Ar/39Ar
muscovite 40Ar/39Ar
biotite 40Ar/39Ar
K-feldspar MDD
apatite FT
Slip on Gatuna fault
Slip on Chocolate Mtns. fault
deposition of schist protolith
congl. of Bear Cyn.
?
(B)
OROCOPIA MTNS.
Orocopia Schist
mylonite
chl. zone
bio. zone
Upper Plate Rocks
an-sy unit
lg-gn unit (shallow)
lg-gn unit (deep)
leucogranite intrusion
plutonic heating
underthrusting of schist
accretion of schist
hornblende 40Ar/39Ar
Slip on CMF(?)
muscovite 40Ar/39Ar
biotite 40Ar/39Ar
K-feldspar MDD
deep
Slip on OMDF
apatite FT
shallow
deposition of schist protolith
Maniobra Fm.
Diligencia Fm.
Temperature (°C)
Time (Ma)
0
100
200
300
400
500
600
700
800
0
10
20
30
40
50
60
70
80

cent Peter Kane Mountain area. The light and dark gray bands in Figure 16A show temperature-time paths for the upper plate and schist, respectively, inferred from the above data. The peak temperature for the schist (~575 °C) is constrained by garnet-hornblende thermometry (Oyarzabal, 1996; see also Graham and Powell, 1984).

Based on the detrital zircons, the depositional age of the schist protolith must be less than ca. 70 Ma (Fig. 16A). The hornblende $^{40}Ar/^{39}Ar$ total gas ages, some as old as 57 Ma, indicate a time window of no more than ~13 m.y. between sedimentation and underplating of this eugeoclinal assemblage beneath North American crust. Peak metamorphism was followed immediately by a phase of rapid cooling that lasted until ca. 50 Ma. A second period of rapid cooling is indicated at 28–24 Ma.

For the upper plate, ages for most minerals closely track those from the schist (Fig. 16A). The one exception is hornblende, which is slightly older in the upper plate (64–59 Ma) than in the schist (57–52 Ma). This indicates that the schist and upper plate were brought together along the Chocolate Mountains fault at ca. 52–50 Ma (i.e., the time at which the cooling paths for the schist and upper plate become coincident) and that the fault has remained essentially dormant since. In addition, the fact that hornblende ages are younger in the schist than in the upper plate suggests that the fault separates formerly deeper structural levels below from shallower levels above, i.e., that the Chocolate Mountains fault has a normal sense of displacement (cf. Wheeler and Butler, 1994; Ring et al., 1999). In other words, we hypothesize that the Chocolate Mountains fault is an exhumation structure that overprinted the original subduction thrust. Furthermore, because the Chocolate Mountains fault is only slightly younger than the peak metamorphism of the schist, we conclude that underplating and exhumation were driven by the same basic mechanism, i.e., subduction.

The early Cenozoic event that caused cooling of the schist and juxtaposition with the upper plate in the Gavilan Hills was followed by a period of quiescence during which the schist and upper plate remained at temperatures appropriate to mid-crustal levels. Renewed rapid cooling beginning at ca. 28 Ma denotes the time at which the schist and upper plate, as a unit, were brought to near-surface levels. Jacobson et al. (2002) attributed this event to extension along the Gatuna fault.

Integrated Thermal History of the Orocopia Mountains

The thermal history of the Orocopia Mountains (Fig. 16B) is constrained by (1) $^{40}Ar/^{39}Ar$ data obtained in this study, (2) one apatite fission track age each from the schist and upper plate (Table 3; analyses performed by S.S. Boettcher, 1996, personal commun.; see Table DR1 for details of the analytical results), and (3) U-Pb analyses of over 100 detrital zircon grains from ten samples of metagraywacke (Grove et al., 2003). Note that results from the various thermochronometers in Figure 16B are color-coded to indicate different domains within the lower and upper plates of the Orocopia Mountains detachment fault, i.e., biotite zone, chlorite zone, and mylonites in the schist and leucogranite-gneiss (deep versus shallow) and anorthosite-syenite units in the upper plate. Although quantitative thermometry has not been performed on the schist in the Orocopia Mountains, a reasonable estimate of peak temperature of metamorphism (~550 °C) can be made by comparison to results obtained from other schist bodies of epidote amphibolite facies (Graham and Powell, 1984; Jacobson, 1995).

Thermal Evolution of the Schist

Figure 16 indicates that the thermal evolution of the schist in the Orocopia Mountains is remarkably similar to that in the Gavilan Hills. As in the Gavilan Hills, the depositional age of the graywacke protolith is clearly less than ca. 70 Ma and may be as young as 62 Ma. However, Grove et al. (2003) suggested

Figure 16. Generalized temperature-time paths for Orocopia Schist (dark gray) and upper-plate rocks (light gray) in the Gavilan Hills (A) and Orocopia Mountains (B). Paths based upon K-feldspar MDD analysis (lines), apatite fission track data (rectangles), and hornblende (diamonds), muscovite (pentagons), and biotite (hexagons) bulk closure ages. Note that divergent paths have been indicated for upper-plate rocks present within the Orocopia Mountains depending upon their proximity to the Orocopia Mountains detachment fault. While structurally highest rocks of the anorthosite-syenite unit appear to define yet another path, insufficient data are available to constrain it. MDD paths for K-feldspar reflect 90% confidence interval for the median distribution shown in Figure 14. Bulk closure temperatures for argon diffusion are assumed to be 525 ± 50 °C for hornblende, 400 ± 50 °C for muscovite, and 350 ± 50 °C for biotite (McDougall and Harrison, 1999). Some symbols are shifted up or down from these temperatures in order to reduce overlap. Analytical error for bulk closure ages (±1σ; Table 1) is typically smaller than the width of the symbol. Some anomalous biotite and hornblende ages from the upper plate of ca. 100 Ma or older (Fig. 13) have been excluded (see text). Muscovite ages from the upper plate also not shown. Boxes for apatite fission track ages constructed using ±1σ error for age and a closure temperature of 115 ± 20 °C. These boxes are constrained by only a single analysis each for the schist in the Orocopia Mountains and the upper plate in both areas (Table 3) (Oyarzabal et al., 1997) and by two analyses for the schist in the Gavilan Hills (Oyarzabal et al., 1997). Detrital zircon ages from Grove et al. (2003). Age of the conglomerate of Bear Canyon after Dillon (1976), Sherrod and Tosdal (1991), and Hughes (1993). Age of the Maniobra Formation from Advocate et al. (1988). Age of the Diligencia Formation based on Spittler and Arthur (1982), Frizzell and Weigand (1993), Law et al. (2001), and Ebert (2004). an-sy—anorthosite-syenite; CMF—Chocolate Mountains fault; lg-gn—leucogranite-gneiss; MDD—multidiffusion domain; OMDF—Orocopia Mountains detachment fault.

TABLE 3. POOLED APATITE FISSION TRACK AGES OF SAMPLES FROM THE OROCOPIA MOUNTAINS

Sample	Number of grains	Rock unit	Age ± 1σ (Ma)
OR97	20	Orocopia Schist	16.2 ± 1.7
OR245	25	anorthosite-syenite	26.5 ± 4.5

Note: Analyst, S.S. Boettcher, University of Texas, Austin.

that the 62 Ma result could reflect metamorphic zircon growth, so we ignored this analysis when constructing the temperature-time path. Accretion of the schist beneath the Orocopia Mountains must have occurred by 60–55 Ma, as indicated by the oldest consistently reproduced hornblende $^{40}Ar/^{39}Ar$ step ages (Fig. 11A).

The schist in the Orocopia Mountains exhibits the same two-stage cooling history as that in the Gavilan Hills. One obvious difference, however, is that final closure of muscovite in the schist occurred somewhat later in the Orocopia Mountains than in the Gavilan Hills. Biotite ages from the schist are also younger in the Orocopia Mountains than in the Gavilan Hills. In part, this may be evidence for somewhat different amounts of early Cenozoic exhumation in the two areas. In addition, these discrepancies may reflect the much greater structural thickness of schist exposed in the Orocopia Mountains (~1.5 km) than in the Gavilan Hills (~300 m), as both areas do show a younging of cooling ages with structural depth (Fig. 10 of this paper vs. Fig. 4 of Jacobson et al., 2002). Also note that the second phase of cooling in the Orocopia Mountains did not initiate until ca. 24 Ma (Fig. 16B), compared to ca. 28 Ma in the Gavilan Hills (Fig. 16A).

Thermal Evolution of the Upper Plate

In stark contrast to the very similar temperature-time paths exhibited by the schist in the Orocopia Mountains and Gavilan Hills, upper-plate rocks from the two areas were clearly subjected to entirely different thermal histories (Fig. 16). The two most obvious disparities are the much older biotite ages yielded by upper-plate rocks in the Orocopia Mountains (mostly 75–63 Ma) relative to those from the Gavilan Hills (45–36 Ma) and the sharply divergent K-feldspar MDD results. While not quite so striking, hornblende ages in the Orocopia Mountains (mostly 76–69 Ma) are ~10 m.y. older on average than those from the Gavilan Hills (64–59 Ma). These data strongly imply that the upper plate within the Orocopia Mountains was at much shallower crustal depths (less than 12 km) during Late Cretaceous time than the upper plate within the Gavilan Hills (greater than 15–20 km). By the same token, the schist and upper plate in the Orocopia Mountains were also clearly at different structural levels throughout most of the Cenozoic.

As already noted, K-feldspars from the shallow and deep parts of the leucogranite-gneiss unit within the Orocopia Mountains exhibit differing MDD paths (Fig. 16B). The K-feldspars in the shallow region show a pronounced cooling event in the early Cenozoic that coincides with the early temperature drop exhibited by the Orocopia Schist. From 45 to 24 Ma, this part of the leucogranite-gneiss remained at temperatures ~200–250 °C lower than those recorded by the schist. In contrast, biotite total gas ages and K-feldspar MDD paths from samples within the structurally deep part of the leucogranite-gneiss show no evidence for the early Cenozoic cooling event. Temperatures in this part of the leucogranite-gneiss differ from those in the schist by only ~100–125 °C for the period 45–24 Ma. The above contrasts imply that the leucogranite-gneiss must include at least two separate structural slices. It is perplexing, however, that the deep part of the unit fails to show any sign of the early Cenozoic cooling event, particularly considering that deep and shallow samples exhibit only a minor difference in their average biotite ages (Fig. 16B). Perhaps refrigeration of the upper plate during initial underthrusting of the schist caused biotite to close over a broad depth range so that only less-retentive K-feldspar remained sensitive to depth-dependent temperature variation.

An additional major structural break may be indicated within the northwestern body of anorthosite-syenite unit by the K-feldspar with total gas age of 78 Ma (sample OR363; Figs. 8A and 8E) and the two biotites with ages of 98 and 158 Ma (samples OR412 and OR361; Figs. 8A and 8D). Furthermore, rock types at these sample sites appear to correlate with those at locality OR342 in the southeastern body of anorthosite-syenite, which yielded the poorly constrained but relatively old hornblende age of 117 Ma (Figs. 8A and 8B). Note, however, that we have not been able to delineate continuous fault contacts between these restricted areas of anomalously old samples and the rest of the section (Figs. 8B and 8D), although this is not surprising considering the difficulties in mapping described above. Conversely, note that some clear structural discontinuities within the upper plate are not accompanied by significant contrasts in $^{40}Ar/^{39}Ar$ ages (e.g., compare biotite ages on either side of the fault at the northwest end of the southeast body of anorthosite-syenite in Fig. 8D).

Finally, the anomalously young muscovite age of 49 Ma obtained from sample OR306 (Table 1), which is located very close to the base of the upper plate (Fig. 8C), may provide evidence for yet another, very deep, structural slice within the upper plate. However, as noted above, the young age of this sample could also be due to low retentivity of Ar.

It is clear from previous mapping and analysis (Crowell, 1962, 1975; Crowell and Walker, 1962; Goodmacher et al., 1989; Robinson and Frost, 1989, 1991, 1996), results produced in this study (Fig. 7), and regional relationships (Powell, 1993; Barth et al., 2001) that the Late Cretaceous magmatic arc was firmly established in the area of the Orocopia Mountains at 80–70 Ma. Transient heating associated with the intrusion of voluminous granitic material must have had a significant impact upon the thermal structure of the crust. Consequently, one possibility, and the option assumed in Figure 16B, is that the relative uniformity of hornblende $^{40}Ar/^{39}Ar$ ages from the structurally lower portions of the upper plate reflects homogenization due to heating produced by intrusion of the ubiquitous 76 Ma leucogranites, rather than high background temperatures (>525 °C) appropriate for the deeper (15–20 km) Cretaceous crustal levels that appear to characterize the upper plate within the Gavilan Hills (Fig. 16A). Alternatively, the rapid cooling event indicated for the upper plate in the Orocopia Mountains at the end of the Cretaceous could be due to exhumation, perhaps related to extensional faulting, as has been called upon to explain latest Cretaceous hornblende and biotite ages in a number of ranges within the eastern Mojave Desert (Foster et al., 1992; Wells et al., 2002, 2005).

Tectonic Implications

In contrast to the situation for the Gavilan Hills, in the Orocopia Mountains the thermal histories of the schist and upper plate do not merge until earliest Miocene time. This relationship requires the Orocopia Mountains detachment fault to be much younger than the Chocolate Mountains fault. Indeed, these data provide clear evidence that the contact between schist and upper plate in the Orocopia Mountains is a major middle Cenozoic detachment fault, as previously inferred by Robinson and Frost (1989, 1991). Furthermore, based on the structural style and thermal history data (Fig. 16B), we consider it highly likely that the various demonstrated and hypothesized low-angle faults *within* the upper plate are related to this same event. Following Goodmacher et al. (1989) and Robinson and Frost (1989, 1991), we adopt the name "Orocopia Mountains detachment system" to refer to this entire set of structures. In addition, our limited data from Painted Canyon (Fig. 9) indicate that the cooling histories for the schist and upper plate in that area are broadly similar to those for the equivalent units within the main body of the Orocopia Mountains. This implies that similar structural levels of schist and upper plate are exposed in both areas, which leads us to conclude that the Orocopia Mountains detachment system is domed by the Chocolate Mountains anticlinorium. Finally, note that our conclusions regarding the age and origin of faults between the schist and upper plate and within the upper plate in the northwestern Orocopia Mountains are identical to those reached by Ebert (2004) and Ebert and Yin (2004) for the southeastern part of the range.

Our interpretation that the Orocopia Mountains detachment fault formed at a relatively shallow level in middle Cenozoic time suggests that its origin is analogous to that of the Gatuna fault of the Gavilan Hills. A corollary to this observation is that a ductile structure corresponding to the early Cenozoic Chocolate Mountains fault of the Gavilan Hills does not appear to be present within the Orocopia Mountains. However, because the early Cenozoic cooling history of the schist in the Orocopia Mountains is so similar to that in the Gavilan Hills, we suspect that an equivalent fault was present but has been excised by the Orocopia Mountains detachment fault (see also below).

It is important to note that the most compelling evidence for middle Cenozoic slip along the Orocopia Mountains detachment fault comes from biotite and K-feldspar (Fig. 16B). Previous thermochronologic studies of the Pelona-Orocopia-Rand Schist focused on hornblende and muscovite, which give Late Cretaceous to early Cenozoic ages (Ehlig, 1981; Jacobson, 1990). It was this emphasis on higher-temperature thermochronology that led some authors to stress the early cooling of the schists, while downplaying the role of middle Cenozoic detachment faults (Jacobson, 1990; Jacobson and Dawson, 1995; Oyarzabal et al., 1997; Wood and Saleeby, 1997; Law et al., 2001; Glazner et al., 2002). Now that lower-temperature thermochronology from biotite and K-feldspar is available, the local importance of middle Cenozoic exhumation has been dramatically confirmed and cannot be ignored.

Relative Magnitudes of Early and Middle Cenozoic Exhumation

Various geobarometers applied to peak metamorphic assemblages in the schist yield pressure estimates mostly in the range of 800–900 MPa (Graham and Powell, 1984; Jacobson, 1995). This implies that early and middle Cenozoic exhumation together must account for ~30–35 km of unroofing of the schist (assuming an average crustal density of 2.7 g/cm^3). Our thermal history data can be utilized to make a rough estimate of the amount of exhumation associated with each of the two events. Figure 16 indicates that schist in both the Orocopia Mountains and Gavilan Hills was at a temperature of ~350 °C at the onset of middle Cenozoic detachment faulting. If we assume a surface temperature of 20 °C and a geothermal gradient of 20–30 °C/km, which lies at the middle to low end of various estimates for this region in late Oligocene–early Miocene time (Dickinson, 1991; Spencer and Reynolds, 1991; Foster and John, 1999; Wong and Gans, 2003), this implies that middle Cenozoic extension and younger events accommodated ~11–17 km of denudation. It is likely that the middle Cenozoic extension alone can account for most of this total, because (1) the limited apatite fission track results from the Orocopia Mountains and Gavilan Hills imply that the schist was already below 100 °C by ca. 19–16 Ma and (2) on a regional scale, the schist was widely exposed by middle Miocene time, as indicated by its presence as detritus in alluvial sediments (Ehlig et al., 1975; Dillon, 1976; Goodman and Malin, 1992; Hughes, 1993). Note, however, that the youngest sedimentary rocks containing clasts of schist in the immediate vicinity of the Orocopia Mountains are Pliocene in age (Sylvester and Smith, 1975).

It is useful to compare the inferred depth and temperature conditions for the Orocopia Schist immediately prior to middle Cenozoic extension to those for the core complexes to the northeast (Fig. 1). Based on regional stratigraphic and structural reconstructions and on thermobarometry of synextensional mylonitic rocks, the core complexes are typically estimated to have been exhumed from depths of ~10–15 km (Anderson, 1988; Dickinson, 1991; Ketcham, 1996; Foster and John, 1999), similar to the case suggested above for the schist. In contrast, many of the core complexes appear to have been at temperatures of 500 °C or even greater during the initial stages of detachment faulting (Anderson, 1988; Dickinson, 1991; Spencer and Reynolds, 1991), considerably above the temperatures indicated for the Orocopia Schist at the onset of middle Cenozoic extension (Fig. 16). The implication is that either preextensional thermal gradients were higher in the area of the core complexes than in the schist belt or we have overestimated the amount of denudation that occurred along the Orocopia Mountains detachment fault and Gatuna fault. Estimates of horizontal extension across the core complex belt commonly range from ~40 km to over 80 km (Dickinson, 1991; Spencer and Reynolds, 1991; Foster and John, 1999; Glazner et al., 2002). Inasmuch as the amount of denudation of the schist may have been less than that associated with the core complexes, we consider 20–40 km to be a conservative first-order approxi-

mation for the magnitude of horizontal extension that occurred across the schist belt in the middle Cenozoic.

In light of the above discussion, our inference of ~11–17 km of middle to late Cenozoic exhumation of the Orocopia Schist must be considered highly approximate. Furthermore, our estimate of ~30–35 km for the original depth of underthrusting of the schist is, itself, subject to large error. Nonetheless, it is clear that a substantial amount (perhaps ~12–25 km) of the overall denudation of the schist must have occurred prior to the onset of middle Cenozoic extension. The comparatively small temperature drop (~125–175 °C; Fig. 16) associated with the early Cenozoic exhumation is taken as evidence for below-normal geothermal gradients induced by "subduction refrigeration" (cf. Dumitru et al., 1991; Grove and Lovera, 1996). Moreover, because of the subdued temperature variation within the crust that results from this process, exhumation can occur without leaving much of an imprint in the cooling record and not be detectable with our methods. Thus, whereas it is tempting to visualize that the bulk of the early Cenozoic exhumation was confined to the narrow interval of rapid cooling at ca. 54–48 Ma (Fig. 16), denudation of refrigerated rocks could well have continued undetected into the period of slow cooling that began at 48 Ma.

Origin of the Retrograde Fabrics within the Orocopia Schist

The Orocopia Schist of the Orocopia Mountains exhibits several features indicative of retrograde metamorphism and fabric overprinting that presumably relate to exhumation history. The most prominent of these is the chlorite zone within the upper part of the structural section (Figs. 4 and 5). The lack of stratigraphic markers makes it difficult to estimate the precise thickness of this zone, but the cross sections of Figure 4 imply a conservative minimum estimate of 700 m. As summarized earlier, the development of chlorite at the expense of biotite involved extensive recrystallization of muscovite. Thus, the widespread and highly consistent early Cenozoic $^{40}Ar/^{39}Ar$ ages derived from muscovite within the chlorite zone (Fig. 8C) provide strong evidence that this retrograde sequence is related to the early Cenozoic phase of exhumation of the schist, not to the current contact between schist and upper plate (i.e., the Orocopia Mountains detachment fault). Note that the chlorite zone is very similar mineralogically and texturally to a greenschist-facies zone of retrograde metamorphism within the upper 150 m of the Orocopia Schist in the Gavilan Hills (Oyarzabal et al., 1997; Jacobson et al., 2002). Muscovites from the retrograde zone in the Gavilan Hills likewise yield early Cenozoic $^{40}Ar/^{39}Ar$ ages (Jacobson et al., 2002).

Although the chlorite zone does not appear to be genetically related to the Orocopia Mountains detachment fault, the occurrence of this thick retrograde feature at the top of the section implies that the present fault contact was preceded by an earlier shear zone above the schist. Further evidence for this hypothesized structure is provided by the widespread folds within the chlorite zone with northeastward to eastward vergence (Jacobson and Dawson, 1995). As noted, muscovites from four such fold hinges also yield early Cenozoic $^{40}Ar/^{39}Ar$ ages (Fig. 8C). Based on the age relations, we correlate the proposed shear zone with the Chocolate Mountains fault of the Gavilan Hills.

A second distinctive retrograde element within the schist of the Orocopia Mountains is the thin mylonite zone directly beneath the upper plate. Quartz in the mylonite shows pervasive evidence of ductile flow and recrystallization (Jacobson and Dawson, 1995, Fig. 10C therein), which suggests that deformation occurred at temperatures of 300 °C or greater (Sibson, 1982). One possibility is that this zone of deformation is coeval with and transitional to the retrograde fabrics within the much broader chlorite zone. However, the mylonite, although only a few meters thick, is remarkably persistent along the length of the contact between the schist and upper plate. Considering the large amount of slip that must have occurred on this contact during the middle Cenozoic, it seems highly improbable that this feature would be so well preserved if it were a relic of the early Cenozoic phase of exhumation and retrograde metamorphism. Instead, we conclude that the mylonite indicates a minor amount of ductile deformation within the schist during middle Cenozoic extension. This is compatible with the ~350 °C temperature for the lower plate immediately prior to initiation of slip on the Orocopia Mountains detachment fault (Fig. 16B). This is hot enough to allow plastic flow and recrystallization of quartz, but not so hot that temperature would have stayed above the brittle-ductile transition for long once extension began. Deformation at this time could also account for the partial argon loss exhibited by muscovite and biotite porphyroclasts within the mylonite (Figs. 12C and 12F).

As noted earlier, the mylonite at the top of the schist in the Orocopia Mountains shows dominantly top-northeast to top-east sense of shear (Simpson, 1986; Robinson and Frost, 1989, 1996; Jacobson and Dawson, 1995), which is the same transport direction indicated by the asymmetric folds in the schist (Jacobson and Dawson, 1995). If our assignment of an early Cenozoic age for the folds, but a middle Cenozoic age for mylonite, is correct, then the common transport direction must be coincidental. This could be explained by both phases of deformation having an extension direction roughly perpendicular to the strike of the continental margin. However, such arguments are difficult to constrain because of the uncertainty regarding Neogene rotations in the Orocopia area (Luyendyk et al., 1985; Carter et al., 1987; Dickinson, 1996; Law et al., 2001).

The above discussion suggests that the Orocopia Schist exhibits at most a minor retrograde overprint related to middle Cenozoic extension. This contrasts strongly with relations in much of the core complex belt, where mylonitic textures are commonly developed over structural thicknesses of hundreds of meters to several kilometers beneath detachment faults (Anderson, 1988; Davis et al., 1986; Glazner et al., 2002). This is consistent with our previous inference that average extension across the schist belt, while significant, was probably less than that associated with the core complexes.

Mechanism of Early Cenozoic Exhumation

A variety of factors, including the extreme middle Cenozoic cooling indicated for the Orocopia Schist (Fig. 16), the obvious structural breaks represented by the Orocopia Mountains detachment fault (above) and Gatuna fault (Jacobson et al., 2002), and the regional setting (Davis and Coney, 1979; Davis et al., 1986; Spencer and Reynolds, 1990, 1991; Dickinson, 1991; Glazner et al., 2002), provide compelling evidence that extensional faulting played the dominant role in exhuming the Orocopia Schist during the middle Cenozoic. However, determining whether the early Cenozoic cooling and exhumation were due predominantly to tectonic denudation (Fig. 2B) (May, 1986; Postlethwaite and Jacobson, 1987; Jacobson et al., 1988, 1996; Jacobson, 1990; Richard and Haxel, 1991; Malin et al., 1995; Oyarzabal et al., 1997; Wood and Saleeby, 1997; Saleeby, 2003) or erosion (Fig. 2C) (Yin, 2002) remains a problem. We have already argued that some normal slip occurred along the Chocolate Mountains fault in the Gavilan Hills and a postulated correlative fault in the Orocopia Mountains. In addition, structures similar to the Chocolate Mountains fault are widely recognized in southeasternmost California and southwesternmost Arizona (Dillon, 1976; Haxel, 1977; Haxel et al., 1985, 2002; Drobeck et al., 1986; Sherrod and Tosdal, 1991; Uselding et al., 2001; Jacobson et al., 2002) and may also be of early Cenozoic age (Grove et al., 2003). However, even if faulting accounted for some of the early Cenozoic unroofing of the schist, erosion may also have contributed to denudation, or even have been the dominant mechanism. For example, the parallelism of the cooling curves for the schist and the shallow part of the leucogranite-gneiss unit from ca. 53 to 25 Ma could indicate that both structural levels were moving toward the surface at the same rate, implying no major faulting or flow within the bulk of the crust. On the other hand, this interpretation does not readily explain the lack of evidence for early Cenozoic cooling in the deep part of the leucogranite-gneiss. Clearly, more work is needed to elucidate this issue.

Consideration of sedimentation history also does not appear to resolve the ambiguity. Deposition of the marine Maniobra Formation coincided with the early phase of cooling of the schist (Fig. 16B), suggesting some form of genetic relationship. However, various authors have cited the Maniobra Formation as evidence in favor of either tectonic (Fig. 2B) (Robinson and Frost, 1996) or erosional (Fig. 2C) (Yin, 2002) denudation of the schist. For the northwestern part of the schist terrane, Wood and Saleeby (1997, p. 981) argued against erosion as the primary mechanism of exhumation based on the paucity of nearby sediments of appropriate age. On the other hand, recent studies of detrital zircons from the Pelona-Orocopia-Rand Schist indicate that a significant amount of the material eroded from southern California and adjoining areas in the latest Cretaceous to early Cenozoic was likely carried to the continental margin, where it was subducted (Grove et al., 2003). Thus, it is difficult to use mass-balance arguments to constrain the mechanisms of denudation, a point made in general by Ring et al. (1999).

In summary, thermochronologic evidence suggests that the Orocopia Schist underwent a large amount of exhumation in the early Cenozoic, concurrent with shallow subduction. Some proportion of this unroofing is likely to have occurred along the Chocolate Mountains and similar faults, but the exact amount of denudation produced by tectonic versus erosional processes remains unresolved.

Passive-Roof Thrust Model for Exhumation of the Orocopia Schist and the Role of the Chocolate Mountains Anticlinorium

Yin (2002) has made a major contribution to discussions of the Pelona-Orocopia-Rand Schist by stressing the potential importance of erosional exhumation. We agree completely that previous workers, ourselves included, have unjustly discounted this mechanism. Nonetheless, as developed below, we disagree with several of Yin's (2002) propositions. In particular, we see difficulties with his passive-roof thrust model and the associated inference that the Chocolate Mountains anticlinorium is early Cenozoic in age.

Passive versus Conventional Roof Thrusts

Yin's (2002) passive-roof thrust model for synsubduction exhumation of the schist involves a duplex structure within the top of the accretionary wedge (Fig. 2C). The duplex is folded above a ramp in the floor thrust, with the fold extending to the surface as the Chocolate Mountains anticlinorium. According to this view, exhumation of the schist results primarily from erosion of the anticlinorium. Yin's (2002) model can be compared to the idealized geometry of both "conventional" and passive-roof thrusts. In the conventional case, the roof and floor thrusts merge both down- and updip of the duplex, and both faults have the same sense of displacement (e.g., Fig. 19 in Boyer and Elliot, 1982). In contrast, for the situation of the passive-roof thrust, neither fault extends updip of a "frontal tip line" (e.g., Fig. 7 in Banks and Warburton, 1986). In this geometry, the structural unit between the floor and roof thrusts acts as a wedge driving the forward propagation of both faults. A consequence of the indenting motion of the wedge is that roof and floor thrusts exhibit opposite senses of displacement.

At first glance, an appealing aspect of the passive-roof thrust model is that it appears to explain a long-noted anomaly of the Chocolate Mountains fault system, i.e., that it exhibits top-northeast to top-east sense of displacement (Haxel and Dillon, 1978; Dillon et al., 1990; Simpson, 1990; Oyarzabal et al., 1997; Jacobson et al., 2002), opposite to the transport direction of the subducting Farallon plate. However, close inspection of Yin's (2002) model (Fig. 2C) indicates that the inferred geometry is actually that of a conventional duplex system, *not* a passive-roof thrust. In fact, this point is recognized implicitly by Yin (2002, p. 185), who proposed two potential causes for westward extrusion of the schist other than the inherent geometry of a passive-roof thrust: (1) ductile flow of thickened lower crust beneath the

Maria fold belt to the northeast and (2) return flow of buoyant, water-rich schist along the subduction channel (cf. Cloos, 1982; Cloos and Shreve, 1988; Chemenda et al., 2000). However, by definition, these are both mechanisms of tectonic rather than erosional denudation. In our view, they do not differ substantially from exhumation models proposed previously by Jacobson et al. (1996, 2002) and Oyarzabal et al. (1997), particularly in terms of attributing the anomalous sense of movement along the Chocolate Mountains fault to subduction return flow. Therefore, in certain respects, there is less difference among these interpretations than might appear to be the case. That said, however, it should be pointed out that a fault between schist and upper plate in the Rand Mountains, which Postlethwaite and Jacobson (1987) and Nourse (1989) interpreted as a Late Cretaceous–early Cenozoic normal fault analogous to the Chocolate Mountains fault, shows top-southwest transport. This leads us to envision a component of symmetric collapse of North American crust in response to underplating of schist, in addition to any component of flow of schist up the dip of the subduction zone (Fig. 2B; see also Malin et al., 1995; Wood and Saleeby, 1997; Saleeby, 2003).

Is There Evidence for Late Cretaceous–Early Cenozoic Extension in Southern California?

Yin (2002) pointed out that models for synsubduction exhumation of the schist by normal faulting typically imply a significant amount of extension of North American crust (e.g., Fig. 2B), and he argued that such interpretations are inconsistent with field evidence. A detailed examination of geologic relations throughout southern California bearing on this controversy is beyond the scope of this paper. However, we would simply reiterate that our thermochronologic data provide direct evidence for early Cenozoic extensional structures in the form of the Chocolate Mountains fault. In addition, we note that inferences of Late Cretaceous–early Cenozoic low-angle normal faulting within southern California and southwestern Arizona, made independently of any consideration of the Pelona-Orocopia-Rand Schist, are common (Ballard, 1990; Carl et al., 1991; Applegate and Hodges, 1995; Beyene et al., 2000; Boettcher et al., 2002; Wells et al., 2002, 2005). Furthermore, Late Cretaceous–early Cenozoic extension may be difficult to recognize because of overprinting by middle Cenozoic and younger deformation. For example, along the length of the Chocolate Mountains anticlinorium, rocks that could represent middle to lower North American crust are either completely absent or present in sections with structural thicknesses of only a few hundred meters (Dillon, 1976; Haxel, 1977; Haxel et al., 1985, 2002; Drobeck et al., 1986; Sherrod and Tosdal, 1991); i.e., rocks that might preserve evidence of synsubduction normal faulting are simply not well exposed.

It is also important to consider that tectonic denudation of schist at deep crustal levels need not be expressed by normal faulting within the shallow crust. For example, as noted above and by Yin (2002), exhumation of the schist could have occurred by updip flow within the subduction channel or by ductile thinning and lateral flow restricted to the base of overlying North American crust (cf. Clark and Royden, 2000). Figure 2B illustrates one possible expression of lower crustal flow involving extrusion of crustal lenses bounded by anastomosing, low-angle shear zones (flow could also have been more homogeneous). Such deformation is independent of whether normal faults extend to the surface.

Yin (2002) has further argued against synsubduction extension based on the apparent absence of early Cenozoic detachment-related sediments. However, if exhumation occurred largely by ductile flow in the deep crust, then the impact on sedimentation may have been subtle. Furthermore, we suggest that uppermost Cretaceous to lower Eocene sediments, such as the Maniobra Formation of the Orocopia Mountains or the San Francisquito Formation of the central Transverse Ranges (Kooser, 1982; Grove, 1993), could represent exactly the predicted record of synextensional sedimentation (Fig. 2B; see also Robinson and Frost, 1996). These units indicate a major marine embayment at the latitude of southern California and were considered by Grove (1993) to have been deposited in fault-bounded basins.

Age of the Chocolate Mountains Anticlinorium

According to the model of Yin (2002), erosional denudation of the schist in early Cenozoic time was driven by the topographic high of the Chocolate Mountains anticlinorium (Fig. 2C). The anticlinorium is central to the model in that it is used to infer the presence of the passive-roof thrust, which, in turn, is called upon to explain the top-northeast to top-east sense of transport on the Chocolate Mountains fault. However, a number of workers have argued that the Chocolate Mountains anticlinorium is middle to late Cenozoic in age (Frost and Martin, 1983; Richard, 1989; Sherrod and Tosdal, 1991; Ebert, 2004; Girty et al., 2005). In light of the great lateral extent of this feature (Fig. 1), its age of inception is of considerable interest, irrespective of its bearing on the passive-roof thrust model.

The Chocolate Mountains anticlinorium is cored by domes of Orocopia Schist extending from the Orocopia Mountains to Neversweat Ridge (Fig. 1). In the Orocopia Mountains, the antiform of schist clearly folds the Orocopia Mountains detachment fault (Figs. 3 and 4; see also Ebert, 2004), indicating that the antiform must have formed after ca. 24 Ma. Thus, at least in this range, the Chocolate Mountains anticlinorium is too young to have developed in the manner suggested by Yin (2002). The exact age of the structure, however, is ambiguous. Robinson and Frost (1996) considered that doming of the schist was coeval with middle Cenozoic detachment faulting. This is a reasonable inference, because synextensional folds, with axes both parallel to and at a high angle to the transport direction, are a common feature of detachment faults (Spencer, 1982, 1984). On the other hand, it is noteworthy that the axis of the schist antiform is parallel to kilometer-scale folds in the adjacent Pliocene-Pleistocene sediments of the Mecca Hills on the west and the Oligocene(?)-Miocene Diligencia Formation to the east (Fig. 3). Even the outcrops of Mesozoic granite and Eocene Maniobra Formation north of the Diligencia Formation appear to be controlled by the same structural trend. This parallelism of fold axes might indicate a common origin related to Neogene transpres-

sion. However, the folds in the Orocopia Schist and units to the east must be older than those in the Mecca Hills for two reasons: (1) The Pliocene-Pleistocene sediments of the Mecca Hills sit unconformably upon the breached dome of the Orocopia Schist (Fig. 3), and (2) the folded Diligencia Formation in the eastern to northeastern Orocopia Mountains is overlain depositionally by flat-lying Pliocene-Pleistocene terrace gravels that may correlate with the folded sediments in the Mecca Hills (Spittler and Arthur, 1982; Law et al., 2001).

Folds in the Diligencia Formation were recently discussed by Law et al. (2001; see also Spittler and Arthur, 1982). They emphasized the parts of the basin where hinges trend approximately east-west and considered this deformation to be related to regional north-south contraction in the Mojave Desert (e.g., Bartley et al., 1990; Glazner et al., 2002). Law et al. (2001) suggested that northwest-southeast fold axes in the western Diligencia basin were the result of rotation adjacent to the Clemens Well fault. In contrast, we argue that northwest-southeast trends represent the fundamental structural grain within the region of the western Orocopia Mountains (Fig. 3).

Although the Chocolate Mountains anticlinorium in the Orocopia Mountains must be younger than earliest Miocene, the above discussion indicates that the structure in this area could be the result of transpression along the San Andreas fault and thus not representative of the anticlinorium as a whole. However, as already noted, middle Cenozoic exhumation in the Gavilan Hills is thought to have occurred along the Gatuna fault, which is also folded by the Chocolate Mountains anticlinorium (Jacobson et al., 2002). Consequently, the anticlinorium in the Gavilan Hills must likewise be middle to late Cenozoic in age. Furthermore, faults considered to be equivalent to the Gatuna fault, and which are folded by the Chocolate Mountains anticlinorium, can be traced for over 100 km from the southern Chocolate Mountains to the eastern end of the anticlinorium (Fig. 1) (Dillon, 1976; Haxel, 1977; Haxel et al., 1985, 2002; Drobeck et al., 1986; Sherrod and Tosdal, 1991; Uselding et al., 2001; Jacobson et al., 2002). A middle to late Cenozoic age for the Chocolate Mountains anticlinorium has also been inferred by Richard (1989), Sherrod and Tosdal (1991), and Girty et al. (2005) based on facies patterns of early Miocene volcanic rocks and reversals in dip of these units and overlying sedimentary rocks on opposing limbs of the anticlinorium.

In summary, it does not appear that the present-day Chocolate Mountains anticlinorium can be invoked as evidence for a topographic high above the Orocopia Schist in the early Cenozoic. This does not disprove the role of topography and erosion in bringing about the early exhumation of the schist, but shows that any such topography must have been generated by other mechanisms.

Relationship of the Diligencia Formation to Middle Cenozoic Exhumation of the Orocopia Schist

The Diligencia Formation has long been viewed as part of a larger group of upper Oligocene(?) to lower Miocene sedimentary and volcanic sequences in southern California attributed to regional extension (Bohannon, 1975; Crowell, 1981; Spittler and Arthur, 1982; Law et al., 2001). Robinson and Frost (1989, 1991, 1996) inferred that the deposition of the Diligencia Formation was directly related to slip on the Orocopia Mountains detachment fault and/or Clemens Well fault. However, whereas some detritus in the lower part of the Diligencia Formation was derived from the south to southwest (i.e., from the vicinity of the current exposures of the Orocopia Mountains detachment fault and Clemens Well fault), most of the sediment had a northerly source (Spittler and Arthur, 1982; Law et al., 2001; Ebert, 2004). This led Law et al. (2001) to downplay the role of the Clemens Well fault in controlling deposition of the Diligencia Formation. On the other hand, we have argued that relations in Painted Canyon (this study; Crowell, 1962, 1975; Crowell and Walker, 1962) require that the Orocopia Mountains detachment fault (and potentially the Clemens Well fault if it is also part of the larger detachment system) is folded over the range. In this case, the breakaway zone of the detachment system would have been situated to southwest, beyond the present-day trace of the San Andreas fault. Thus, the Diligencia Formation, itself, may have formerly continued a considerable distance to the southwest. If so, coarse, southwest-derived sediment may have been present in this no-longer-exposed part of the section.

Geographic Extent of Middle Cenozoic Exhumation

The results of this study, Jacobson et al. (2002), and Grove et al. (2003) provide evidence for a major extensional event affecting the Orocopia Schist along the length of the Chocolate Mountains anticlinorium. However, the degree to which middle Cenozoic extension contributed to exhumation within other parts of the schist belt remains uncertain. For example, in the northwesternmost part of the terrane (Portal Ridge, San Emigdio Mountains, Sierra de Salinas, Tehachapi Mountains; Fig. 1), preliminary thermochronologic studies of the schist and associated deep levels of the upper plate have yielded biotite $^{40}Ar/^{39}Ar$ ages, and even apatite and zircon fission track ages, as old as Late Cretaceous (Jacobson, 1990; Naeser et al., 1990; Wood and Saleeby, 1997; Barth et al., 2003; Grove et al., 2003; Saleeby et al., this volume). These results, combined with detrital zircon studies (Grove et al., 2003), indicate that the schist was both underthrust and exhumed earlier in the northwest than the southeast. They also imply that the synsubduction phase of exhumation caused even greater denudation in the northwest than in the southeast. In other words, middle Cenozoic extension need not have been as important in the northwest as in the southeast.

Implication of Schist Outcrop Pattern for Models of Underthrusting

The Pelona-Orocopia-Rand Schist is generally considered to underlie much of southern California (Haxel and Dillon, 1978; Magistrale and Zhou, 1996), and this is certainly a requirement of the widely held belief that the schist is a correlative of the

Franciscan Complex (Fig. 2B). Recently, however, this assumption has been challenged by Haxel et al. (2002), who argued that the subsurface extent of the schist is restricted to a narrow belt paralleling the surface distribution. In this interpretation, the schist protolith was deposited in a marine basin between North America and an outboard continental fragment. The implication is that the schist belt demarcates the suture associated with the closing of that basin. This model is based on two lines of reasoning (Haxel et al., 2002). First, some recent geophysical analyses have failed to reveal evidence that the schist is widespread in the subsurface (Langenheim, 1999; Hauksson, 2000; Fuis et al., 2001). Discussion of these studies is beyond our scope of consideration and will not be attempted here. Instead, we focus on the second point of Haxel et al. (2002, p. 122–123), which is, "The continuity and gently curvilinear shape of the Chocolate Mountains anticlinorium, over a length of >130 km, is too systematic to be accidental. If the Orocopia Schist forms an extensive layer beneath this region, we see no reason why all of its exposures should be aligned along a single tight trend." However, as already discussed, the present configuration of schist exposures in southeastern California and southwestern Arizona is largely the result of middle to late Cenozoic deformation. In fact, the alignment of schist exposures along the Chocolate Mountains anticlinorium is no more impressive than the linear distribution of core complexes to the northeast, which is clearly a middle Cenozoic feature (Fig. 1). Thus, we agree that the arrangement of schist exposures along the Chocolate Mountains anticlinorium is not accidental, but we take this as an expression of detachment faulting and subsequent folding events, not as an indicator of the subsurface extent of the schist.

SUMMARY GEOLOGIC HISTORY

The Pelona-Orocopia-Rand Schist is an important part of the tectonic framework of southern California and southwestern Arizona. Initial studies of this unit were most concerned with the mechanism of underthrusting, which is now widely agreed to have involved east-dipping, low-angle subduction. This paper focused on a second critical issue, i.e., understanding the processes of exhumation. Our results, while not resolving all questions pertaining to this debate, nonetheless imply a remarkably uniform tectonic evolution for the southeastern part of the schist terrane exposed along the Chocolate Mountains anticlinorium. Based on these results, and the work of others, we can summarize the Late Cretaceous to Cenozoic geologic evolution of this area using the Orocopia Mountains as a specific example (Fig. 17):

1. During the Late Cretaceous, arc magmatism swept into the region from the west as a consequence of decreasing angle of subduction of the Farallon plate (Fig. 17A). This event is represented in the Orocopia Mountains by the 76 Ma leucogranite. The host rocks to the Cretaceous intrusions include several late Early to Middle Proterozoic plutonic-metamorphic complexes and a well-developed magmatic arc of Jurassic age (Barth et al., 2001; Powell, 1981, 1993; Tosdal et al., 1989).

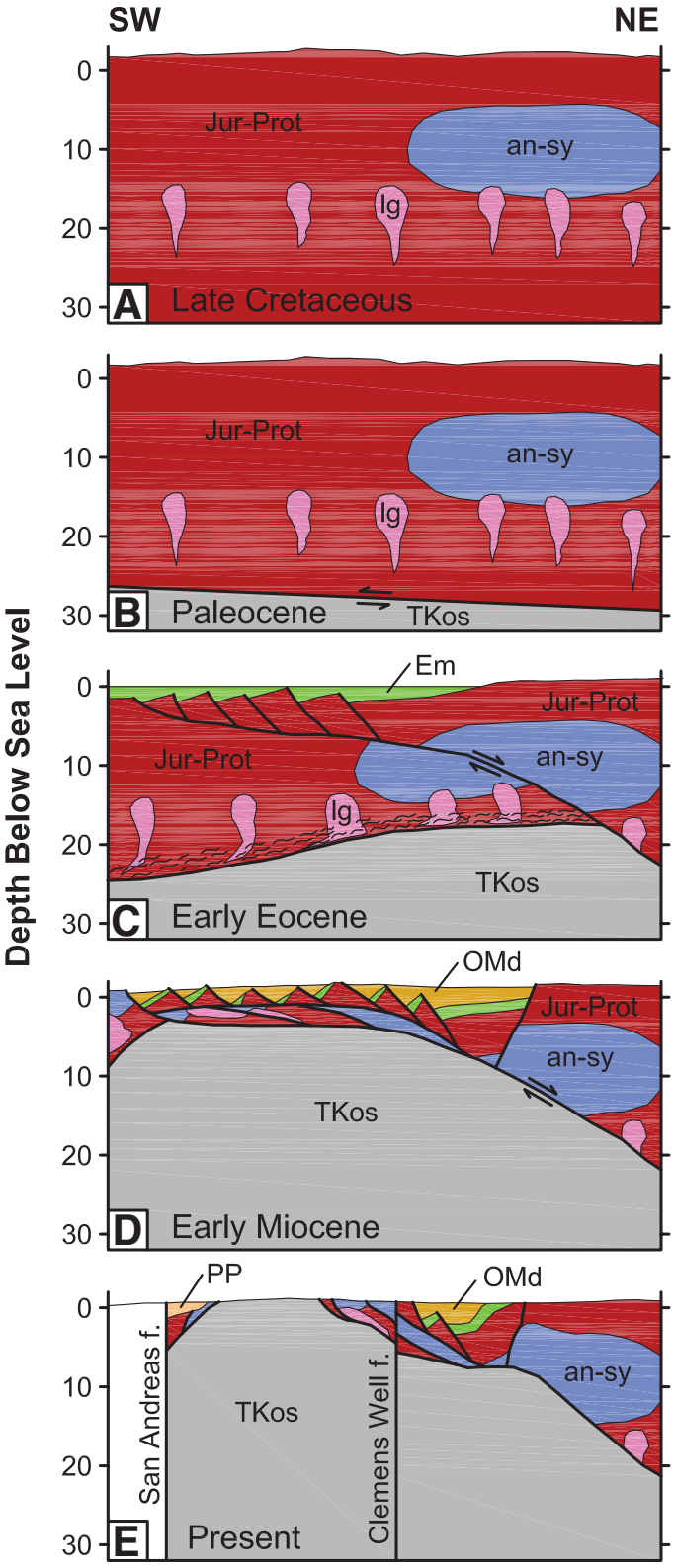

Figure 17. Geologic evolution of the Orocopia Mountains. See text for explanation. an-sy—anorthosite-syenite; Em—Maniobra Formation; Jur-Prot—Jurassic to Proterozoic crystalline rocks; lg—leucogranite; OMd—Diligencia Formation; PP—sedimentary rocks of Mecca Hills; TKos—Orocopia Schist.

2. As the angle of subduction continued to decrease, encroachment of the Farallon plate at depth led to tectonic removal of lowermost North American crust and underlying continental lithosphere and extinction of arc magmatism at this longitude. Continentally derived clastic sediment deposited in the trench in latest Cretaceous to Paleocene time was carried far beneath the continental margin, where it was accreted along with minor amounts of basaltic oceanic crust and pelagic sediment as the Orocopia Schist (Fig. 17B). Metamorphism of the schist was presumably caused at least in part by conductive heating from the recently active arc.

3. Ongoing flat subduction through Paleocene and early Eocene time resulted in the accumulation of a substantial thickness of schist beneath the North American continent (Fig. 17C). Isostatically driven surface uplift due to underplating of the buoyant schist may have given rise to a component of erosional unroofing. The same buoyancy forces may also have triggered ductile thinning of the lower crust and/or development of throughgoing normal faults (Fig. 17C). The Chocolate Mountains fault of the Gavilan Hills and a postulated equivalent fault in the Orocopia Mountains are envisioned as having formed in this manner. Note that, whereas tectonic denudation is featured prominently in Figure 17C, erosional exhumation is also implied for the right-hand side of the panel. Similarly, deposition of the Maniobra Formation is illustrated as representing both transgression of a marine embayment over crust thinned by extension (left side) and sedimentation adjacent to a topographic high above the schist (right side). In this context, it is important to consider that, although the Maniobra Formation currently lies northeast of the schist now exposed in the Orocopia Mountains (Fig. 3), that relation was likely reversed during Eocene time (but with the schist in the subsurface). This conclusion can be justified based solely upon the amount of horizontal extension inferred for early Miocene time (above and Fig. 17D), irrespective of any additional early Cenozoic normal faulting. The importance of this observation is that, even if a substantial amount of early Cenozoic denudation of the schist were due to erosion, we see no reason to envision a "moat" of Maniobra Formation surrounding a topographic high cored by the schist (compare Fig. 17C to Fig. 2C of this paper and Fig. 3 of Yin, 2002). Finally, note that the events postulated in Figure 17C would have occurred concurrently with the first phase of rapid cooling exhibited by the schist (Fig. 16B). This cooling was likely induced by a combination of denudation (tectonic and/or erosional) and subduction refrigeration.

4. Although our reconstruction for Eocene time (Fig. 17C) is subject to a high degree of uncertainty, there can be little doubt that this region was affected by a major phase of extension in the latest Oligocene to early Miocene (Fig. 17D). We concur with Robinson and Frost (1989, 1991, 1996) that the Diligencia Formation was deposited as a direct result of this event. By comparison to the classic belt of core complexes and detachment faults to the northeast (Fig. 1), we infer that the highest structural levels would have included a series of tilted fault blocks. The crystalline rocks exposed immediately east of the Clemens Well fault (Fig. 3) may represent the tops of such features (Fig. 17E), but for the most part, the postulated fault blocks either have been removed by erosion from above the antiform of the western Orocopia Mountains or are buried beneath the Diligencia basin to the east. The anorthosite-syenite and leucogranite-gneiss units that currently sit above the schist are interpreted as slices brought up from mid-crustal levels along the anastomosing Orocopia Mountains detachment system (Fig. 17D). Slight variations of structural depth within these slices are indicated by the cooling histories of the deep versus shallow K-feldspars (Fig. 16B) and by the few anomalously old biotite and hornblende ages (Fig. 13), assuming the latter are not the result of $^{40}Ar_E$. Movement on the Orocopia Mountains detachment system appears to have excised the Eocene normal fault system postulated in Figure 17C. The geometry of Figure 17D implies that the Chocolate Mountains anticlinorium is to a large degree the product of the middle Cenozoic extensional event.

5. Neogene transpression led to development of the San Andreas fault and associated branches, such as the Clemens Well fault (Fig. 17E; note that we assume that strike-slip displacement on the Clemens Well fault is on the order of 10–20 km or less). Deformation at this time may have led to tightening of the Chocolate Mountains anticlinorium and folding within the Diligencia basin.

The above history, while constructed to match the detailed character of the Orocopia Mountains, is broadly representative of the tectonic evolution along the Chocolate Mountains anticlinorium as a whole. A minor variation, however, is that, in many of the ranges along the anticlinorium, the middle Cenozoic detachment fault (e.g., the Gatuna fault) appears to sole into the deep levels of the upper plate rather than into the schist. In these cases, the early Cenozoic ductile contact between the schist and the upper plate (e.g., the Chocolate Mountains fault) is preserved beneath the middle Cenozoic brittle fault. Finally, the sequence of Figure 17 is probably representative, at least to a first order, of events throughout the Pelona-Orocopia-Rand Schist belt, although underplating clearly occurred earlier in the northwest (Grove et al., 2003), and the proportion of synsubduction exhumation may have been even greater in that area than in the regions emphasized here.

APPENDIX 1: U-Pb AND $^{40}Ar/^{39}Ar$ ANALYTICAL METHODS

Ion Microprobe U-Pb Zircon Dating

The crystallization age of the leucogranite was inferred by U-Pb dating of zircon using the UCLA (University of California, Los Angeles) Cameca ims 1270 ion microprobe. The technique was identical to that employed by Vućić (2002) and Grove et al. (2003) and is described here only in summary fashion. The spot size generated by the primary $^{16}O^-$ beam was 30–35 μm. Ten to 15 cycles of measurements were taken for $^{94}Zr_2{}^{16}O$, ^{204}Pb, ^{206}Pb, ^{207}Pb, ^{208}Pb, ^{232}Th, ^{238}U, and $^{238}U^{16}O$. Common Pb was corrected using ^{208}Pb as a proxy for grains younger than 1.0 Ga (Compston et al., 1984). Grains older than 1.0 Ga were corrected using the ^{204}Pb method. To minimize the impact of common Pb signals derived from surficial contamination, we presputtered the sample sur-

face for 3–4 min before taking measurements. Relative sensitivities for Pb and U were determined on reference zircon AS-3 (Paces and Miller, 1993) using a modified calibration technique described in Compston et al. (1984). Assuming that analytical error alone is the main source of the observed variations, we estimate that the reproducibility of our $^{206}Pb/^{238}U$ apparent ages is 3%–5%. For Cretaceous zircons, which are the ones of most interest in this study, $^{207}Pb/^{235}U$ ages determined with the ion microprobe tend to be quite large, typically an order of magnitude greater than errors for $^{206}Pb/^{238}U$ ages. Complete analytical data are provided in the GSA Data Repository.

$^{40}Ar/^{39}Ar$ Thermochronology

Separates of muscovite and biotite were prepared by placing crushed and sieved material (60–80 or 80–100 mesh) on a sheet of paper and tilting the paper so that grains other than layer silicates rolled off. This mica concentrate was then processed with a Frantz magnetic separator, followed by handpicking. Because of low content of K_2O, hornblende analyses can be severely compromised by even small impurities of mica. To avoid this problem, hornblende separates were assembled grain-by-grain (30–60 mesh) under a binocular microscope, inspecting for surface impurities. The material used in this process was preconcentrated using the Frantz magnetic separator and, in some cases, conventional heavy-liquid techniques. K-feldspar separates (30–60 mesh) were prepared using heavy liquids.

Samples were irradiated in seven separate runs at the University of Michigan's Ford reactor. Isotopic analyses were conducted in the UCLA noble gas facility following methods described in Jacobson et al. (2002), Vućić (2002), and Grove et al. (2003) and briefly summarized here. J-factors were determined using Fish Canyon sanidine (27.8 ± 0.3 Ma; Cebula et al., 1986) interspersed with samples at 1 cm spacing. Correction factors for nucleogenic K- and Ca-derived argon were determined by measuring K_2SO_4 and CaF_2 salts. Incremental heating was conducted with a double-vacuum Ta furnace. The temperature was generally increased from 500 to 1350 °C in 15 min intervals. Evolved gas was transferred by expansion in a LABVIEW automated, all-stainless-steel extraction line. Argon isotopic measurements were performed using an automated VG1200S mass spectrometer equipped with a Baur-Signar ion source and an axially fitted electron multiplier (Quidelleur et al., 1997).

Apparent ages for individual steps were calculated using conventional decay constants and isotopic abundances (Steiger and Jäger, 1977). Trapped Ar was assumed to be atmospheric. Total gas ages and associated errors were determined by weighting individual steps by the quantity of ^{39}Ar released. They reflect analytical errors only and do not include uncertainties in the flux monitor, decay constants, or correction factors for interfering nuclear reactions.

Despite care in preparation of the hornblende separates, steps released at temperatures less than 950 °C typically exhibited Ca/K ratios indicative of contamination with a K-rich phase, mostly likely biotite (see McDougall and Harrison, 1999). These steps were omitted when calculating the hornblende total gas ages. Additional steps were eliminated in some samples for which the release spectra suggested the presence of $^{40}Ar_E$.

Data reduction parameters relevant to each sample and complete analytical results are provided in the GSA Data Repository.

ACKNOWLEDGMENTS

This work was supported by National Science Foundation (NSF) grants EAR-9902788 and EAR-0106123 and Department of Energy grant DE-FG-03-89ER14049. The zircon U-Pb analyses were conducted at the UCLA (University of California, Los Angeles) Keck Center for Isotope Geochemistry and Cosmochemistry, which is supported by a grant from the NSF Instrumentation and Facilities Program (EAR-0113563). Kim Rodgers and David and Mark Jacobson are thanked for helping with the mineral separations. Our understanding of the geology of the Orocopia Mountains and adjoining areas has benefited from discussions with Andy Barth, Kim Bishop, Eric Frost, Gordon Haxel, Ray Ingersoll, Bob Powell, Stephen Richard, Jason Saleeby, Dick Tosdal, and An Yin. Brad Hacker and Jason Saleeby are thanked for their constructive reviews of the manuscript.

REFERENCES CITED

Advocate, D.M., Link, M.H., and Squires, R.L., 1988, Anatomy and history of an Eocene submarine canyon: The Maniobra Formation, southern California, *in* Filewicz, M.V., and Squires, R.L., eds., Paleogene stratigraphy, West Coast of North America: Los Angeles, California, Pacific Section, SEPM (Society for Sedimentary Geology), no. 58, p. 45–58.

Anderson, J.L., 1988, Core complexes of the Mojave-Sonoran Desert: Conditions of plutonism, mylonitization, and decompression, *in* Ernst, W.G., ed., Metamorphism and crustal evolution of the western United States (Rubey Volume VII): Englewood Cliffs, New Jersey, Prentice-Hall, p. 502–525.

Applegate, J.D.R., and Hodges, K.V., 1995, Mesozoic and Cenozoic extension recorded by metamorphic rocks in the Funeral Mountains, California: Geological Society of America Bulletin, v. 107, p. 1063–1076, doi: 10.1130/0016-7606(1995)107<1063:MACERB>2.3.CO;2.

Armstrong, R.L., and Suppe, J., 1973, Potassium-argon geochronometry of Mesozoic igneous rocks in Nevada, Utah, and southern California: Geological Society of America Bulletin, v. 84, p. 1375–1392, doi: 10.1130/0016-7606(1973)84<1375:PGOMIR>2.0.CO;2.

Ballard, S.N., 1990, The Mesozoic structural evolution of the Little Maria Mountains [Ph.D. thesis]: Santa Barbara, University of California, 380 p.

Banks, C.J., and Warburton, J., 1986, "Passive-roof" duplex geometry in the frontal structures of the Kirthar and Sulaiman mountain belts, Pakistan: Journal of Structural Geology, v. 8, p. 229–238, doi: 10.1016/0191-8141(86)90045-3.

Barth, A.P., and Schneiderman, J.S., 1996, A comparison of structures in the Andean orogen of northern Chile and exhumed midcrustal structures in southern California, USA: An analogy in tectonic style: International Geology Review, v. 38, p. 1075–1085.

Barth, A.P., Wooden, J.L., Tosdal, R.M., and Morrison, J., 1995, Crustal contamination in the petrogenesis of a calc-alkalic rock series: Josephine Mountain intrusion, California: Geological Society of America Bulletin, v. 107, p. 201–211, doi: 10.1130/0016-7606(1995)107<0201:CCITPO>2.3.CO;2.

Barth, A.P., Jacobson, C.E., Coleman, D.S., and Wooden, J.L., 2001, Construction and tectonic evolution of Cordilleran continental crust: Examples from the San Gabriel and San Bernardino Mountains, *in* Dunne, G., and Cooper, J., eds., Geologic excursions in the California desert and adjacent Transverse Ranges: Pacific Section, SEPM (Society for Sedimentary Geology), Book 88, p. 17–53.

Barth, A.P., Wooden, J.L., Grove, M.G., Jacobson, C.E., and Pedrick, J.N., 2003, U-Pb zircon geochronology of rocks in the Salinas Valley region of California: A reevaluation of the crustal structure and origin of the Salinian block: Geology, v. 31, p. 517–520, doi: 10.1130/0091-7613(2003)031<0517:UZGORI>2.0.CO;2.

Bartley, J.M., Glazner, A.F., and Schermer, E.R., 1990, North-south contraction of the Mojave block and strike-slip tectonics in southern California: Science, v. 248, p. 1398–1401.

Beyene, M.A., Wells, M.L., and Spell, T.L., 2000, Late Cretaceous extension, Pinto shear zone, New York Mountains, northeastern Mojave Desert, California: Geological Society of America Abstracts with Programs, v. 32, no. 6, p. A-3.

Bishop, K.M., and Ehlig, P.L., 1990, The Pelona fault, central Transverse Ranges, southern California: An extensional detachment fault?: Geological Society of America Abstracts with Programs, v. 22, no. 3, p. 8.

Blythe, A.E., Burbank, D.W., Farley, K.A., and Fielding, E.J., 2000, Structural and topographic evolution of the central Transverse Ranges, California, from apatite fission-track, (U-Th)/He and digital elevation model analysis: Basin Research, v. 12, p. 97–114, doi: 10.1046/j.1365-2117.2000.00116.x.

Blythe, A.E., House, M.A., and Spotila, J.A., 2002, Low-temperature thermochronology of the San Gabriel and San Bernardino Mountains, southern California: Constraining structural evolution, *in* Barth, A., ed., Contributions to crustal evolution of the southwestern United States: Geological Society of America Special Paper 365, p. 231–250.

Boettcher, S.S., Mosher, S., and Tosdal, R.M., 2002, Structural and tectonic evolution of Mesozoic basement-involved fold nappes and thrust faults in the Dome Rock Mountains, Arizona, *in* Barth, A., ed., Contributions to crustal evolution of the southwestern United States: Geological Society of America Special Paper 365, p. 73–97.

Bohannon, R.G., 1975, Mid-Tertiary conglomerates and their bearing on Transverse Range tectonics, southern California, *in* Crowell, J.C., ed., San Andreas fault in southern California: A guide to San Andreas fault from Mexico to Carrizo Plain: California Division of Mines and Geology Special Report 118, p. 75–82.

Boyer, S.E., and Elliot, D., 1982, Thrust systems: American Association of Petroleum Geologists Bulletin, v. 66, p. 1196–1230.

Burchfiel, B.C., and Davis, G.A., 1981, Mojave Desert and environs, *in* Ernst, W.G., ed., The geotectonic development of California (Rubey Volume I): Englewood Cliffs, New Jersey, Prentice-Hall, p. 217–252.

Carl, B.S., Miller, C.F., and Foster, D.A., 1991, Western Old Woman Mountains shear zone: Evidence for late ductile extension in the Cordilleran orogenic belt: Geology, v. 19, p. 893–896, doi: 10.1130/0091-7613(1991)019<0893:WOWMSZ>2.3.CO;2.

Carter, B.A., 1980, Structure and petrology of the San Gabriel anorthosite-syenite body, Los Angeles County, California [Ph.D. thesis]: Pasadena, California Institute of Technology, 393 p.

Carter, B.A., 1987, The San Gabriel anorthosite-syenite-gabbro-body, San Gabriel Mountains, California, *in* Hill, M.L., ed., Centennial field guide, volume 1: Boulder, Colorado, Geological Society of America, p. 203–206.

Carter, J.N., Luyendyk, B.P., and Terres, R.R., 1987, Neogene clockwise tectonic rotation of the eastern Transverse Ranges, California, suggested by paleomagnetic vectors: Geological Society of America Bulletin, v. 98, p. 199–206, doi: 10.1130/0016-7606(1987)98<199:NCTROT>2.0.CO;2.

Cebula, G.T., Kunk, M.J., Mehnert, H.H., Naeser, C.W., Obradovich, J.D., and Sutter, J.F., 1986, The Fish Canyon Tuff, a potential standard for the ^{40}Ar-^{39}Ar and fission-track dating methods: Terra Cognita, v. 6, p. 139–140.

Chemenda, A.I., Burg, J.-P., and Mattauer, M., 2000, Evolutionary model of the Himalaya-Tibet system: Geopoem based on new modeling, geological and geophysical data: Earth and Planetary Science Letters, v. 174, p. 397–409, doi: 10.1016/S0012-821X(99)00277-0.

Clark, M.K., and Royden, L.H., 2000, Topographic ooze: Building the eastern margin of Tibet by lower crustal flow: Geology, v. 28, p. 703–706, doi: 10.1130/0091-7613(2000)028<0703:TOBTEM>2.3.CO;2.

Cloos, M., 1982, Flow mélanges: Numerical modeling and geological constraints on their origin in the Franciscan subduction complex: Geological Society of America Bulletin, v. 93, p. 330–345, doi: 10.1130/0016-7606(1982)93<330:FMNMAG>2.0.CO;2.

Cloos, M., and Shreve, R.L., 1988, Subduction-channel model of prism accretion, mélange formation, sediment subduction, and subduction erosion at convergent plate margins, 2: Implications and discussion: Pure and Applied Geophysics, v. 128, p. 501–545, doi: 10.1007/BF00874549.

Compston, W., Williams, I.S., and Meyer, C.E., 1984, U-Pb geochronology of zircons from lunar breccia 73217 using a sensitive high mass-resolution ion microprobe: Journal of Geophysical Research, B, Solid Earth and Planets, v. 89, supplement, p. 525–534.

Coney, P.J., and Reynolds, S.J., 1977, Cordilleran Benioff zones: Nature, v. 270, p. 403–406, doi: 10.1038/270403a0.

Crowell, J.C., 1962, Displacement along the San Andreas fault, California: Geological Society of America Special Paper 71, 61 p.

Crowell, J.C., 1968, Movement histories of faults in the Transverse Ranges and speculations on the tectonic history of California, *in* Dickinson, W.R., and Grantz, A., eds., Proceedings of Conference on Geologic Problems of San Andreas Fault System: Stanford, California, Stanford University Publications in the Geological Sciences, v. 11, p. 323–341.

Crowell, J.C., 1975, Geologic sketch of the Orocopia Mountains, southeastern California, *in* Crowell, J.C., ed., San Andreas fault in southern California: A guide to San Andreas fault from Mexico to Carrizo Plain: California Division of Mines and Geology Special Report 118, p. 99–110.

Crowell, J.C., 1981, An outline of the tectonic history of southeastern California, *in* Ernst, W.G., ed., The geotectonic development of California (Rubey Volume I): Englewood Cliffs, New Jersey, Prentice-Hall, p. 583–600.

Crowell, J.C., and Susuki, T., 1959, Eocene stratigraphy and paleontology, Orocopia Mountains, southeastern California: Geological Society of America Bulletin, v. 70, p. 581–592.

Crowell, J.C., and Walker, J.W.R., 1962, Anorthosite and related rocks along the San Andreas fault, southern California: University of California Publications in Geological Sciences, v. 40, p. 219–288.

Davis, G.A., Lister, G.S., and Reynolds, S.J., 1986, Structural evolution of the Whipple and South Mountains shear zones, southwestern United States: Geology, v. 14, p. 7–10, doi: 10.1130/0091-7613(1986)14<7:SEOTWA>2.0.CO;2.

Davis, G.H., and Coney, P.J., 1979, Geologic development of the Cordilleran metamorphic core complexes: Geology, v. 7, p. 120–124, doi: 10.1130/0091-7613(1979)7<120:GDOTCM>2.0.CO;2.

Dawson, M.R., 1987, Geochemistry and origin of mafic schists from the Pelona, Orocopia, and Rand Schists: Structure and metamorphism of the Orocopia Schist, southern California [Ph.D. thesis]: Ames, Iowa State University, 136 p.

Dickinson, W.R., 1981, Plate tectonics and the continental margin of California, *in* Ernst, W.G., ed., The geotectonic development of California (Rubey Volume I): Englewood Cliffs, New Jersey, Prentice-Hall, p. 1–28.

Dickinson, W.R., 1991, Tectonic setting of faulted Tertiary strata associated with the Catalina core complex in southern Arizona: Geological Society of America Special Paper 264, 106 p.

Dickinson, W.R., 1996, Kinematics of transrotational tectonism in the California Transverse Ranges and its contribution to cumulative slip along the San Andreas transform fault system: Geological Society of America Special Paper 305, 46 p.

Dickinson, W.R., and Snyder, W.S., 1978, Plate tectonics of the Laramide orogeny, *in* Matthews, V., III, ed., Laramide folding associated with basement block faulting in the western United States: Geological Society of America Memoir 151, p. 355–366.

Dillon, J.T., 1976, Geology of the Chocolate and Cargo Muchacho Mountains, southeasternmost California, California [Ph.D. thesis]: Santa Barbara, University of California, 405 p.

Dillon, J.T., Haxel, G.B., and Tosdal, R.M., 1990, Structural evidence for northeastward movement on the Chocolate Mountains thrust, southeasternmost California: Journal of Geophysical Research, v. 95, p. 19,953–19,971.

Drobeck, P.A., Hillemeyer, F.L., Frost, E.G., and Liebler, G.S., 1986, The Picacho mine: A gold mineralized detachment in southeastern California, *in* Beatty, B., and Wilkinson, P.A.K., eds., Frontiers in geology and ore deposits of Arizona and the Southwest: Arizona Geological Society Digest, v. 16, p. 187–221.

Dumitru, T.A., Gans, P.B., Foster, D.A., and Miller, E.L., 1991, Refrigeration of the western Cordilleran lithosphere during Laramide shallow-angle subduction: Geology, v. 19, p. 1145–1148, doi: 10.1130/0091-7613(1991)019<1145:ROTWCL>2.3.CO;2.

Ebert, K.A., 2004, Exhumational history of the Orocopia Schist and development of hanging-wall structures of the Orocopia fault, southeastern California [M.S. thesis]: Los Angeles, University of California, 124 p.

Ebert, K.A., and Yin, A., 2004, A new structural model for the development of the Clemens Well fault in the San Andreas fault system: Geological Society of America Abstracts with Programs, v. 36, no. 5, p. 501.

Ebert, K.A., Yin, A., and Grove, M., 2003, Exhumational history of the Pelona-Orocopia Schist and development of the upper-plate structures of the Orocopia fault, southeastern California: Geological Society of America Abstracts with Programs, v. 35, no. 6, p. 303.

Ehlig, P.L., 1958, The geology of the Mount Baldy region of the San Gabriel Mountains, California, California [Ph.D. thesis]: Los Angeles, University of California, 195 p.

Ehlig, P.L., 1968, Causes of distribution of Pelona, Rand, and Orocopia Schists along the San Andreas and Garlock faults, *in* Dickinson, W.R., and Grantz, A., eds., Proceedings of Conference on Geologic Problems of San Andreas Fault System: Stanford, California, Stanford University Publications in the Geological Sciences, v. 11, p. 294–306.

Ehlig, P.L., 1981, Origin and tectonic history of the basement terrane of the San Gabriel Mountains, central Transverse Ranges, *in* Ernst, W.G., ed.,

The geotectonic development of California (Rubey Volume I): Englewood Cliffs, New Jersey, Prentice-Hall, p. 253–283.

Ehlig, P.L., and Crowell, J.C., 1975, Field trip guide to the San Andreas fault in southern California, *in* Crowell, J.C., ed., San Andreas fault in southern California: A guide to San Andreas fault from Mexico to Carrizo Plain: California Division of Mines and Geology Special Report 118, p. 253–272.

Ehlig, P.L., Ehlert, K.W., and Crowe, B.M., 1975, Offset of the upper Miocene Caliente and Mint Canyon Formations along the San Gabriel and San Andreas faults, *in* Crowell, J.C., ed., San Andreas fault in southern California: A guide to San Andreas fault from Mexico to Carrizo Plain: California Division of Mines and Geology Special Report 118, p. 83–92.

Ernst, W.G., 1963, Significance of phengitic micas from low-grade schists: American Mineralogist, v. 48, p. 1357–1373.

Evernden, J.F., and Kistler, R.W., 1970, Chronology of emplacement of Mesozoic batholithic complexes in California and western Nevada: U.S. Geological Survey Professional Paper 623, 42 p.

Foster, D.A., and John, B.E., 1999, Quantifying tectonic exhumation in an extensional orogen with thermochronology: Examples from the southern Basin and Range province, *in* Ring, U., et al., eds., Exhumation processes: Normal faulting, ductile flow and erosion: Geological Society [London] Special Publication 154, p. 343–364.

Foster, D.A., Miller, C.F., Harrison, T.M., and Hoisch, T.D., 1992, $^{40}Ar/^{39}Ar$ thermochronology and thermobarometry of metamorphism, plutonism, and tectonic denudation in the Old Woman Mountains area, California: Geological Society of America Bulletin, v. 104, p. 176–191, doi: 10.1130/0016-7606(1992)104<0176:AATATO>2.3.CO;2.

Frizzell, V.A., Jr., and Weigand, P.W., 1993, Whole-rock K-Ar ages and geochemical data from middle Cenozoic volcanic rocks, southern California: A test of correlations across the San Andreas fault, *in* Powell, R.E., et al., eds., The San Andreas fault system: Displacement, palinspastic reconstruction, and geologic evolution: Geological Society of America Memoir 178, p. 273–288.

Frost, E.G., and Martin, D.L., 1983, Overprint of Tertiary detachment deformation on the Mesozoic Orocopia Schist and Chocolate Mtns. thrust: Geological Society of America Abstracts with Programs, v. 15, no. 6, p. 577.

Frost, E.G., Cameron, T.E., Krummenacher, D., and Martin, D.L., 1981, Possible regional interaction of mid-Tertiary detachment faulting with the San Andreas fault and the Vincent-Orocopia thrust system, Arizona and California: Geological Society of America Abstracts with Programs, v. 13, no. 7, p. 455.

Frost, E.G., Martin, D.L., and Krummenacher, D., 1982, Mid-Tertiary detachment faulting in southwestern Arizona and California and its overprint on the Vincent thrust system: Geological Society of America Abstracts with Programs, v. 14, no. 4, p. 164.

Frost, E.G., Martin, D.M., and Houser, C.E., 1989, Mid-Tertiary ductile deformation below the Trigo Mountains detachment fault, southwestern Arizona: Geological Society of America Abstracts with Programs, v. 21, no. 5, p. 81.

Fuis, G.S., Ryberg, T., Godfrey, N.J., Okaya, D.A., and Murphy, J.M., 2001, Crustal structure and tectonics from the Los Angeles basin to the Mojave Desert, southern California: Geology, v. 29, p. 15–18, doi: 10.1130/0091-7613(2001)029<0015:CSATFT>2.0.CO;2.

Gaber, L.J., Foland, K.A., and Corbato, C.E., 1988, On the significance of argon release from biotite and amphibole during $^{40}Ar/^{39}Ar$ vacuum heating: Geochimica et Cosmochimica Acta, v. 52, p. 2457–2465, doi: 10.1016/0016-7037(88)90304-3.

Girty, G.H., Nielsen, J.L., Gasca, C., Rowland-Smith, A., Gray, R., Lovering, K., and Campbell, K., 2005, Structure and chemistry of Tertiary volcanics Picacho State Recreation Area: Implications for the transfer of Baja to the Pacific plate: Geological Society of America Abstracts with Programs, v. 37, no. 4, p. 63.

Glazner, A.F., Walker, J.D., Bartley, J.M., and Fletcher, J.M., 2002, Cenozoic evolution of the Mojave block of southern California, *in* Glazner, A.F., et al., eds., Geologic evolution of the Mojave Desert and southwestern Basin and Range: Geological Society of America Memoir 195, p. 19–41.

Goodmacher, J., Barnett, L., Buckner, G., Ouachrif, L., Vidigal, A., and Frost, E., 1989, The Clemens Well fault in the Orocopia Mountains of southern California: A strike-slip or normal fault structure?: Geological Society of America Abstracts with Programs, v. 21, no. 5, p. 85.

Goodman, E.D., and Malin, P.E., 1992, Evolution of the southern San Joaquin basin and mid-Tertiary transitional tectonics, central California: Tectonics, v. 11, p. 478–498.

Graham, C.M., and England, P.C., 1976, Thermal regimes and regional metamorphism in the vicinity of overthrust faults: An example of shear heating and inverted metamorphic zonation from southern California: Earth and Planetary Science Letters, v. 31, p. 142–152, doi: 10.1016/0012-821X(76)90105-9.

Graham, C.M., and Powell, R., 1984, A garnet-hornblende geothermometer: Calibration, testing, and application to the Pelona Schist, southern California: Journal of Metamorphic Geology, v. 2, p. 13–31.

Grove, K., 1993, Latest Cretaceous basin formation within the Salinian terrane of west-central California: Geological Society of America Bulletin, v. 105, p. 447–463, doi: 10.1130/0016-7606(1993)105<0447:LCBFWT>2.3.CO;2.

Grove, M., and Lovera, O.M., 1996, Slip history of the Vincent thrust: Role of denudation during shallow subduction, *in* Bebout, G.E., et al., eds., Subduction top to bottom: American Geophysical Union Geophysical Monograph 96, p. 163–170.

Grove, M., Jacobson, C.E., Barth, A.P., and Vućić, A., 2003, Temporal and spatial trends of Late Cretaceous–early Tertiary underplating of Pelona and related schist beneath southern California and southwestern Arizona, *in* Johnson, S.E., et al., eds., Tectonic evolution of northwestern Mexico and southwestern USA: Geological Society of America Special Paper 374, p. 381–406.

Hamilton, W., 1987, Mesozoic geology and tectonics of the Big Maria Mountains region, southeastern California, *in* Dickinson, W.R., and Klute, M.A., eds., Mesozoic rocks of southern Arizona and adjacent areas: Arizona Geological Society Digest, v. 18, p. 33–47.

Hamilton, W., 1988, Tectonic setting and variations with depth of some Cretaceous and Cenozoic structural and magmatic systems of the western United States, *in* Ernst, W.G., ed., Metamorphism and crustal evolution of the western United States (Rubey Volume VII): Englewood Cliffs, New Jersey, Prentice-Hall, p. 1–40.

Harrison, T.M., Heizler, M.T., Lovera, O.M., Chen, W., and Grove, M., 1994, A chlorine disinfectant for excess argon released from K-feldspar during step heating: Earth and Planetary Science Letters, v. 123, p. 95–104, doi: 10.1016/0012-821X(94)90260-7.

Hauksson, E., 2000, Crustal structure and seismicity distribution adjacent to the Pacific and North America plate boundary in southern California: Journal of Geophysical Research, v. 105, p. 13,875–13,903, doi: 10.1029/2000JB900016.

Haxel, G.B., 1977, The Orocopia Schist and the Chocolate Mountain thrust, Picacho–Peter Kane Mountain area, southeasternmost California [Ph.D. thesis]: Santa Barbara, University of California, 277 p.

Haxel, G.B., and Dillon, J.T., 1978, The Pelona-Orocopia Schist and Vincent–Chocolate Mountain thrust system, southern California, *in* Howell, D.G., and McDougall, K.A., eds., Mesozoic paleogeography of the western United States: Pacific Coast Paleogeography Symposium, volume 2: Pacific Section, Society of Economic Paleontologists and Mineralogists, p. 453–469.

Haxel, G.B., Tosdal, R.M., and Dillon, J.T., 1985, Tectonic setting and lithology of the Winterhaven Formation: A new Mesozoic stratigraphic unit in southeasternmost California and southwestern Arizona: U.S. Geological Survey Bulletin 1599, 19 p.

Haxel, G.B., Jacobson, C.E., Richard, S.M., Tosdal, R.M., and Grubensky, M.J., 2002, The Orocopia Schist in southwest Arizona: Early Tertiary oceanic rocks trapped or transported far inland, *in* Barth, A., ed., Contributions to crustal evolution of the southwestern United States: Geological Society of America Special Paper 365, p. 99–128.

Hendrix, E.D., 1993, Soledad basin, central Transverse Ranges, California, *in* Sherrod, D.R., and Nielson, J.E., eds., Tertiary stratigraphy of highly extended terranes, California, Arizona, and Nevada: U.S. Geological Survey Bulletin 2053, p. 243–250.

Hoisch, T.D., Miller, C.F., Heizler, M.T., Harrison, T.M., and Stoddard, E.F., 1988, Late Cretaceous regional metamorphism in southeastern California, *in* Ernst, W.G., ed., Metamorphism and crustal evolution of the western United States (Rubey Volume VII): Englewood Cliffs, New Jersey, Prentice-Hall, p. 538–571.

Hughes, K.M., 1993, The conglomerate of Bear Canyon (Miocene), Chocolate Mountains, southeastern California, *in* Sherrod, D.R., and Nielsen, J.E., eds., Tertiary stratigraphy of highly extended terranes, California, Arizona, and Nevada: U.S. Geological Survey Bulletin 2053, p. 213–216.

Jacobson, C.E., 1983a, Relationship of deformation and metamorphism of the Pelona Schist to movement on the Vincent thrust, San Gabriel Mountains, southern California: American Journal of Science, v. 283, p. 587–604.

Jacobson, C.E., 1983b, Structural geology of the Pelona Schist and Vincent thrust, San Gabriel Mountains, California: Geological Society of America Bulletin, v. 94, p. 753–767, doi: 10.1130/0016-7606(1983)94<753:SGOTPS>2.0.CO;2.

Jacobson, C.E., 1990, The $^{40}Ar/^{39}Ar$ geochronology of the Pelona Schist and related rocks, southern California: Journal of Geophysical Research, v. 95, p. 509–528.

Jacobson, C.E., 1995, Qualitative thermobarometry of inverted metamorphism in the Pelona and Rand Schists, southern California, using calciferous amphibole in mafic schist: Journal of Metamorphic Geology, v. 13, p. 79–92.

Jacobson, C.E., 1997, Metamorphic convergence of the upper and lower plates of the Vincent thrust, San Gabriel Mountains, southern California: Journal of Metamorphic Geology, v. 15, p. 155–165, doi: 10.1111/j.1525-1314.1997.00009.x.

Jacobson, C.E., and Dawson, M.R., 1995, Structural and metamorphic evolution of the Orocopia Schist and related rocks, southern California: Evidence for late movement on the Orocopia fault: Tectonics, v. 14, p. 933–944, doi: 10.1029/95TC01446.

Jacobson, C.E., Dawson, M.R., and Postlethwaite, C.E., 1987, Evidence for late-stage normal slip on the Orocopia thrust and implications for the Vincent–Chocolate Mountains thrust problem: Geological Society of America Abstracts with Programs, v. 19, no. 7, p. 714.

Jacobson, C.E., Dawson, M.R., and Postlethwaite, C.E., 1988, Structure, metamorphism, and tectonic significance of the Pelona, Orocopia, and Rand Schists, southern California, *in* Ernst, W.G., ed., Metamorphism and crustal evolution of the western United States (Rubey Volume VII): Englewood Cliffs, New Jersey, Prentice-Hall, p. 976–997.

Jacobson, C.E., Oyarzabal, F.R., and Haxel, G.B., 1996, Subduction and exhumation of the Pelona-Orocopia-Rand Schists, southern California: Geology, v. 24, p. 547–550, doi: 10.1130/0091-7613(1996)024<0547:SAEOTP>2.3.CO;2.

Jacobson, C.E., Barth, A.P., and Grove, M., 2000, Late Cretaceous protolith age and provenance of the Pelona and Orocopia Schists, southern California: Implications for evolution of the Cordilleran margin: Geology, v. 28, p. 219–222, doi: 10.1130/0091-7613(2000)028<0219:LCPAAP>2.3.CO;2.

Jacobson, C.E., Grove, M., Stamp, M.M., Vućić, A., Oyarzabal, F.R., Haxel, G.B., Tosdal, R.M., and Sherrod, D.R., 2002, Exhumation history of the Orocopia Schist and related rocks in the Gavilan Hills area of southeasternmost California, *in* Barth, A., ed., Contributions to crustal evolution of the southwestern United States: Geological Society of America Special Paper 365, p. 129–154.

Jayko, A.S., Blake, M.C., Jr., and Harms, T., 1987, Attenuation of the Coast Range ophiolite by extensional faulting and the nature of the Coast Range "thrust," California: Tectonics, v. 6, p. 475–488.

Jennings, C.W., editor, 1977, Geologic map of California: California Division of Mines and Geology, scale 1:750,000, 1 sheet.

Keith, S.B., and Wilt, J.C., 1986, Laramide orogeny in Arizona and adjacent regions: A strato-tectonic synthesis, *in* Beatty, B., and Wilkinson, P.A.K., eds., Frontiers in geology and ore deposits of Arizona and the Southwest: Arizona Geological Society Digest, v. 16, p. 502–554.

Ketcham, R.A., 1996, Distribution of heat-producing elements in the upper and middle crust of southern and west-central Arizona: Evidence from the core complexes: Journal of Geophysical Research, v. 101, p. 13,611–13,632, doi: 10.1029/96JB00664.

Kooser, M., 1982, Stratigraphy and sedimentology of the type San Francisquito Formation, southern California, *in* Crowell, J.C., and Link, M.H., eds., Geologic history of Ridge basin, southern California: Pacific Section, Society of Economic Paleontologists and Mineralogists, p. 53–61.

Langenheim, V.E., 1999, Gravity and aeromagnetic models along the Los Angles Region Seismic Experiment (Line 1), California: U.S. Geological Survey Open-File Report 99-388, 22 p.

Law, R.D., Eriksson, K., and Davisson, C., 2001, Formation, evolution, and inversion of the middle Tertiary Diligencia basin, Orocopia Mountains, southern California: Geological Society of America Bulletin, v. 113, p. 196–221, doi: 10.1130/0016-7606(2001)113<0196:FEAIOT>2.0.CO;2.

Lee, J.K.W., Onstott, T.C., Cashman, K.V., Cumbest, R.J., and Johnson, D., 1991, Incremental heating of hornblende in vacuo: Implications for $^{40}Ar/^{39}Ar$ geochronology and the interpretation of thermal histories: Geology, v. 19, p. 872–876, doi: 10.1130/0091-7613(1991)019<0872:IHOHIV>2.3.CO;2.

Livaccari, R.F., and Perry, F.V., 1993, Isotopic evidence for preservation of Cordilleran lithospheric mantle during the Sevier-Laramide orogeny, western United States: Geology, v. 21, p. 719–722, doi: 10.1130/0091-7613(1993)021<0719:IEFPOC>2.3.CO;2.

Lovera, O.M., Richter, M., and Harrison, T.M., 1991, Diffusion domains determined by ^{39}Ar released during step heating: Journal of Geophysical Research, v. 96, p. 2057–2069.

Lovera, O.M., Richter, M., and Harrison, T.M., 1993, Argon diffusion domains in K-feldspar, II: Kinetic properties of MH-10: Contributions to Mineralogy and Petrology, v. 113, p. 381–393, doi: 10.1007/BF00286929.

Lovera, O.M., Grove, M., Harrison, T.M., and Mahon, K.I., 1997, Systematic analysis of K-feldspar $^{40}Ar/^{39}Ar$ step-heating experiments, I: Significance of activation energy determinations: Geochimica et Cosmochimica Acta, v. 61, p. 3171–3192, doi: 10.1016/S0016-7037(97)00147-6.

Lovera, O.M., Grove, M., and Harrison, T.M., 2002, Systematic analysis of K-feldspar $^{40}Ar/^{39}Ar$ step-heating results, II: Relevance of laboratory argon diffusion properties to nature: Geochimica et Cosmochimica Acta, v. 66, p. 1237–1255, doi: 10.1016/S0016-7037(01)00846-8.

Luyendyk, B.P., Kamerling, M.J., Terres, R.R., and Hornafius, J.S., 1985, Simple shear of southern California during Neogene time suggested by paleomagnetic declinations: Journal of Geophysical Research, v. 90, p. 12,454–12,466.

Magistrale, H., and Zhou, H., 1996, Lithologic control of the depth of earthquakes in southern California: Science, v. 273, p. 639–642.

Mahaffie, M.J., and Dokka, R.K., 1986, Thermochronologic evidence for the age and cooling history of the upper plate of the Vincent thrust, California: Geological Society of America Abstracts with Programs, v. 18, no. 2, p. 153.

Malin, P.E., Goodman, E.D., Henyey, T.L., Li, Y.G., Okaya, D.A., and Saleeby, J.B., 1995, Significance of seismic reflections beneath a tilted exposure of deep continental crust, Tehachapi Mountains, California: Journal of Geophysical Research, v. 100, p. 2069–2087, doi: 10.1029/94JB02127.

May, D.J., 1986, Amalgamation of metamorphic terranes in the southeastern San Gabriel Mountains [Ph.D. thesis]: Santa Barbara, University of California, 325 p.

McDougall, I., and Harrison, T.M., 1999, Geochronology and thermochronology by the $^{40}Ar/^{39}Ar$ method (2nd edition): New York, Oxford University Press, 269 p.

Miller, F.K., and Morton, D.M., 1980, Potassium-argon geochronology of the eastern Transverse Ranges and southern Mojave Desert, southern California: U.S. Geological Survey Professional Paper 1152, 30 p.

Miller, J.S., Glazner, A.F., Farmer, G.L., Suayah, I.B., and Keith, L.B., 2000, Middle Tertiary magmatism across the Mojave Desert and southeastern California: A Sr, Nd, and Pb isotopic study of mantle domains and crustal structure: Geological Society of America Bulletin, v. 112, p. 1264–1279, doi: 10.1130/0016-7606(2000)112<1264:ASNAPI>2.3.CO;2.

Naeser, N.D., Naeser, C.W., and McCulloh, T.H., 1990, Thermal history of rocks in southern San Joaquin Valley, California: Evidence from fission-track analysis: American Association of Petroleum Geologists Bulletin, v. 74, p. 13–29.

Nourse, J.A., 1989, Geologic evolution of two crustal scale shear zones [Ph.D. thesis]: Pasadena, California Institute of Technology, 394 p.

Oyarzabal, F.R., 1996, Metamorphic history and structural evolution of the Orocopia Schist in the Gavilan Hills, S.E. California [Ph.D. thesis]: Ames, Iowa State University, 103 p.

Oyarzabal, F.R., Jacobson, C.E., and Haxel, G.B., 1997, Extensional reactivation of the Chocolate Mountains subduction thrust in the Gavilan Hills of southeastern California: Tectonics, v. 16, p. 650–661, doi: 10.1029/97TC01415.

Paces, J.B., and Miller, J.D., 1993, Precise U-Pb age of Duluth Complex and related mafic intrusions, northeastern Minnesota: Geochronological insights into physical, petrogenetic, paleomagnetic, and tectonomagmatic processes associated with the 1.1 Ga midcontinent rift system: Journal of Geophysical Research, v. 98, p. 13,997–14,013.

Parsons, I., Brown, W.L., and Smith, J.V., 1999, $^{40}Ar/^{39}Ar$ thermochronology using alkali feldspars: Real thermal history or mathematical mirage of microtexture?: Contributions to Mineralogy and Petrology, v. 136, p. 92–110, doi: 10.1007/s004100050526.

Peacock, S.M., 1988, Inverted metamorphic gradients in the westernmost Cordillera, *in* Ernst, W.G., ed., Metamorphism and crustal evolution of the western United States (Rubey Volume VII): Englewood Cliffs, New Jersey, Prentice-Hall, p. 953–975.

Platt, J.P., 1986, Dynamics of orogenic wedges and the uplift of high-pressure metamorphic rocks: Geological Society of America Bulletin, v. 97, p. 1037–1053, doi: 10.1130/0016-7606(1986)97<1037:DOOWAT>2.0.CO;2.

Postlethwaite, C.E., and Jacobson, C.E., 1987, Early history and reactivation of the Rand thrust, southern California: Journal of Structural Geology, v. 9, p. 195–205, doi: 10.1016/0191-8141(87)90025-3.

Powell, R.E., 1981, Geology of the crystalline basement complex, eastern Transverse Ranges, southern California [Ph.D. thesis]: Pasadena, California Institute of Technology, 441 p.

Powell, R.E., 1993, Balanced palinspastic reconstruction of pre–late Cenozoic paleogeology, southern California, *in* Powell, R.E., et al., eds., The San Andreas fault system: Displacement, palinspastic reconstruction, and geologic evolution: Geological Society of America Memoir 178, p. 1–106.

Quidelleur, X., Grove, M., Lovera, O.M., Harrison, T.M., Yin, A., and Ryerson, F.J., 1997, The thermal evolution and slip history of the Renbu Zedong thrust, southeastern Tibet: Journal of Geophysical Research, v. 102, p. 2659–2679, doi: 10.1029/96JD02483.

Raleigh, C.B., 1958, Structure and petrology of a part of the Orocopia Schists [M.S. thesis]: Claremont, California, Claremont Graduate School, 64 p.

Reynolds, S.J., Richard, S.M., Haxel, G.B., Tosdal, R.M., and Laubach, S.E., 1988, Geologic setting of Mesozoic and Cenozoic metamorphism in Arizona, *in* Ernst, W.G., ed., Metamorphism and crustal evolution of the western United States (Rubey Volume VII): Englewood Cliffs, New Jersey, Prentice-Hall, p. 466–501.

Richard, S.M., 1989, The Chocolate Mountains anticlinorium in the Middle Mountains, SW Arizona: Geological Society of America Abstracts with Programs, v. 21, no. 6, p. A64.

Richard, S.M., and Haxel, G.B., 1991, Progressive exhumation of the Orocopia and Pelona Schists along a composite normal fault system, southeastern California and southwestern Arizona: Geological Society of America Abstracts with Programs, v. 23, no. 2, p. 92.

Richter, F.M., Lovera, O.M., Harrison, T.M., and Copeland, P., 1991, Tibetan tectonics from $^{40}Ar/^{39}Ar$ analysis of a single K-feldspar sample: Earth and Planetary Science Letters, v. 105, p. 266–278, doi: 10.1016/0012-821X(91)90136-6.

Ring, U., Brandon, M.T., Willett, S.D., and Lister, G.S., 1999, Exhumation processes, *in* Ring, U., et al., eds., Exhumation processes: Normal faulting, ductile flow and erosion: Geological Society [London] Special Publication 154, p. 1–27.

Robinson, K.L., and Frost, E.G., 1989, Orocopia Mountains detachment system: Progressive ductile to brittle development of a tilted crustal slab during regional extension: Geological Society of America Abstracts with Programs, v. 21, no. 5, p. 135.

Robinson, K.L., and Frost, E.G., 1991, Tertiary extension and basin development in southern California: The temporal similarity, style of deformation and crustal geometry in the Orocopia Mountains and the San Joaquin Hills: Geological Society of America Abstracts with Programs, v. 23, no. 5, p. A132–A133.

Robinson, K.L., and Frost, E.G., 1996, Orocopia Mountains detachment system: Progressive development of a tilted crustal slab and a half-graben sedimentary basin during regional extension, *in* Abbott, P.L., and Cooper, J.D., eds., American Association of Petroleum Geologists Field Conference Guide 73: Bakersfield, California, Pacific Section, American Association of Petroleum Geologists, p. 277–284.

Rubatto, D., and Hermann, J., 2001, Exhumation as fast as subduction?: Geology, v. 29, p. 3–6, doi: 10.1130/0091-7613(2001)029<0003:EAFAS>2.0.CO;2.

Saleeby, J., 2003, Segmentation of the Laramide slab—Evidence from the southern Sierra Nevada region: Geological Society of America Bulletin, v. 115, p. 655–668, doi: 10.1130/0016-7606(2003)115<0655:SOTLSF>2.0.CO;2.

Saleeby, J., Farley, K.A., Kistler, R.W., and Fleck, R., 2007, this volume, Thermal evolution and exhumation of deep-level batholithic exposures, southernmost Sierra Nevada, California, *in* Cloos, M., et al., eds., Convergent margin terranes and associated regions: A tribute to W.G. Ernst: Geological Society of America Special Paper 419, doi: 10.1130/2006.2419(01).

Sedlock, R.L., 1999, Evaluation of exhumation mechanisms for coherent blueschists in western Baja California, Mexico, *in* Ring, U., et al., eds., Exhumation processes: Normal faulting, ductile flow and erosion: Geological Society [London] Special Publication 154, p. 29–54.

Sherrod, D.R., and Tosdal, R.M., 1991, Geologic setting and Tertiary structural evolution of southwestern Arizona and southeastern California: Journal of Geophysical Research, v. 96, p. 12,407–12,423.

Sibson, R.H., 1982, Fault zone models, heat flow, and depth distribution of earthquakes in the continental crust of the United States: Seismological Society of America Bulletin, v. 72, p. 151–163.

Silver, L.T., and Nourse, J.A., 1986, The Rand Mountains "thrust" complex in comparison with the Vincent thrust–Pelona Schist relationship, southern California: Geological Society of America Abstracts with Programs, v. 18, no. 2, p. 185.

Silver, L.T., McKinney, C.R., Deutsch, S., and Bolinger, J., 1963, Precambrian age determinations in the western San Gabriel Mountains, California: Journal of Geology, v. 71, p. 196–214.

Simpson, C., 1986, Microstructural evidence for northeastward movement on the Vincent–Orocopia–Chocolate Mountains thrust system: Geological Society of America Abstracts with Programs, v. 18, no. 2, p. 185.

Simpson, C., 1990, Microstructural evidence for northeastward movement on the Chocolate Mountains fault zone, southeastern California: Journal of Geophysical Research, v. 95, p. 529–537.

Spencer, J.E., 1982, Origin of folds of Tertiary low-angle fault surfaces, southeastern California and western Arizona, *in* Frost, E.G., and Martin, D.L., eds., Mesozoic-Cenozoic tectonics of the lower Colorado River region, California, Arizona, and Nevada: San Diego, California, Cordilleran Publishers, p. 123–134.

Spencer, J.E., 1984, Role of tectonic denudation in uplift and warping of low-angle normal faults: Geology, v. 12, p. 95–98, doi: 10.1130/0091-7613(1984)12<95:ROTDIW>2.0.CO;2.

Spencer, J.E., and Reynolds, S.J., 1990, Relationship between Mesozoic and Cenozoic tectonic features in west-central Arizona and adjacent southeastern California: Journal of Geophysical Research, v. 95, p. 539–555.

Spencer, J.E., and Reynolds, S.J., 1991, Tectonics of mid-Tertiary extension along a transect through west-central Arizona: Tectonics, v. 10, p. 1204–1221.

Spencer, J.E., Richard, S.M., Reynolds, S.J., Miller, R.J., Shafiqullah, M., Gilbert, W.G., and Grubensky, M.J., 1995, Spatial and temporal relationships between mid-Tertiary magmatism and extension in southwestern Arizona: Journal of Geophysical Research, v. 100, p. 10,321–10,351, doi: 10.1029/94JB02817.

Spittler, T.E., and Arthur, M.A., 1982, The lower Miocene Diligencia Formation of the Orocopia Mountains, southern California: Stratigraphy, petrology, sedimentology and structure, *in* Ingersoll, R.V., and Woodburne, M.O., eds., Cenozoic nonmarine deposits of California and Arizona: Los Angeles, California, Pacific Section, Society of Economic Paleontologists and Mineralogists, p. 83–99.

Spotila, J.A., Farley, K.A., and Sieh, K., 1998, Uplift and erosion of the San Bernardino Mountains associated with transpression along the San Andreas fault, California, as constrained by radiogenic helium thermochronometry: Tectonics, v. 17, p. 360–378, doi: 10.1029/98TC00378.

Squires, R.L., and Advocate, D.M., 1982, Sedimentary facies of the nonmarine lower Miocene Diligencia Formation, Canyon Spring area, Orocopia Mountains, southern California, *in* Ingersoll, R.V., and Woodburne, M.O., eds., Cenozoic nonmarine deposits of California and Arizona: Los Angeles, California, Pacific Section, Society of Economic Paleontologists and Mineralogists, p. 101–106.

Steiger, R.H., and Jäger, E., 1977, Subcommission on geochronology: Convention on the use of decay constants in geo- and cosmochronology: Earth and Planetary Science Letters, v. 36, p. 359–362, doi: 10.1016/0012-821X(77)90060-7.

Sylvester, A.G., and Smith, R.R., 1975, Structure section across the San Andreas fault zone, Mecca Hills, *in* Crowell, J.C., ed., San Andreas fault in southern California: A guide to San Andreas fault from Mexico to Carrizo Plain: California Division of Mines and Geology Special Report 118, p. 111–118.

Sylvester, A.G., and Smith, R.R., 1976, Tectonic transpression and basement-controlled deformation in San Andreas fault zone, Salton Trough, California: American Association of Petroleum Geologists Bulletin, v. 60, p. 2081–2102.

Tosdal, R.M., Haxel, G.B., and Wright, J.E., 1989, Jurassic geology of the Sonoran Desert region, southern Arizona, southeastern California, and northernmost Sonora: Construction of a continental-margin magmatic arc, *in* Jenney, J.P., and Reynolds, S.J., eds., Geologic evolution of Arizona: Arizona Geological Society Digest, v. 17, p. 397–434.

Uselding, J.E., Jacobson, C.E., and Haxel, G.B., 2001, Tertiary structural development of Orocopia Schist and related lithologies in the Peter Kane Mountain area of SE California: Geological Society of America Abstracts with Programs, v. 33, no. 6, p. 74.

Vedder, W., and Wilkins, R.W.T., 1969, Dehydroxylation and rehydroxylation, oxidation and reduction of micas: American Mineralogist, v. 54, p. 482–509.

Vućić, A., 2002, Multi-stage exhumation history of the Orocopia Schist in the Orocopia Mountains of southeast California [M.S. thesis]: Ames, Iowa State University, 102 p.

Wells, M.L., Spell, T.L., and Grove, M., 2002, Late Cretaceous intrusion and extensional exhumation of the Cadiz Valley batholith, Iron Mountains, southeastern California: Geological Society of America Abstracts with Programs, v. 34, no. 6, p. 178.

Wells, M.L., Beyene, M.A., Spell, T.L., Kula, J.L., Miller, D.M., and Zanetti, K.A., 2005, The Pinto shear zone: A Laramide synconvergent extensional shear zone in the Mojave Desert region of the southwestern United States: Journal of Structural Geology, v. 27, p. 1697–1720.

Wheeler, J., and Butler, R.W.H., 1994, Criteria for identifying structures related to true crustal extension in orogens: Journal of Structural Geology, v. 16, p. 1023–1027, doi: 10.1016/0191-8141(94)90083-3.

Wong, M.S., and Gans, P.B., 2003, Tectonic implications of early Miocene extensional unroofing of the Sierra Mazatán metamorphic core complex, Sonora, Mexico: Geology, v. 31, p. 953–956, doi: 10.1130/G19843.1.

Wood, D.J., and Saleeby, J.B., 1997, Late Cretaceous–Paleocene extensional collapse and disaggregation of the southernmost Sierra Nevada batholith: International Geology Review, v. 39, p. 973–1009.

Yeats, R.S., 1968, Southern California structure, seafloor spreading, and history of the Pacific basin: Geological Society of America Bulletin, v. 79, p. 1693–1702.

Yin, A., 2002, Passive-roof thrust model for the emplacement of the Pelona-Orocopia Schist in southern California, United States: Geology, v. 30, p. 183–186, doi: 10.1130/0091-7613(2002)030<0183:PRTMFT>2.0.CO;2.

Manuscript Accepted by the Society 13 July 2006